UNIVERSITÀ
DEGLI STUDI
FIRENZE

Dottorato di Ricerca in Ingegneria Industriale

Ciclo xxvi

Analysis of the stability of motorcycles during braking maneuvers

Settore Scientifico Disciplinare ING/IND 14

Candidato
Dott. Federico Giovannini

Tutore
Prof. Marco Pierini

Controrelatore
Prof. Sergio M. Savaresi

Coordinatore del Dottorato
Prof. Maurizio De Lucia

Anni 2011/2013

Department of Industrial Engineering
Via di Santa Marta, 3, 50139 Firenze, Italy

ISBN XXX-XX-XXXX-XXX-X

D/XXXX/XXXX/XX

"*Education is an admirable thing, but it is well to remember from time to time that nothing that is worth knowing can be taught.*"

Oscar Wilde, *The Instruction Of The Over-Educated, 1894.*

Ai miei Genitori Guglielmo e Grazia e a mio Fratello Riccardo
che mi hanno sempre supportato (e sopportato)
con forza e amore incondizionato

A mia Nonna Angela
che non perde mai un momento
per dimostrami il suo affetto

A mia Nonna Maria
che porto ogni giorno nel cuore

Ai miei Nonni Armando, Loris e Piero
che vegliano sempre su di me

A chi mi vuole bene

Preface

The research described in this manuscript is part of a doctoral course running from January 2011 to December 2013. The activity has been carried out at the Department of Industrial Engineering (DIEF) of the University of Florence, Italy and it has been integrated with an internship period of 6 months at Yamaha Motor Company, at the Advanced System & Safety Technology Research Division in Iwata Japan.

Abstract

The decreasing number of road accidents in Europe is correlated to the massive application of active safety systems on the vehicles. The evolution of advanced safety technologies, unfortunately does not apply also to Powered Two-Wheelers (PTWs). The raising trend of PTWs circulation in the streets has not been followed by an equal development of innovative active safety systems for those vehicles. The complex dynamics of PTWs slows down the design of new technologies and limits the possibility to find relevant solutions to address crucial aspects for road safety, as the vehicle stability under emergency situations. That points out the necessity to develop new advanced riding assistance systems able to enhance the riders and PTWs safety.

Accordingly, the present work studies the potentialities of the current braking systems for PTWs application and describes the design of a new braking system. Relevant issues related to the development of the advanced braking system, as the real-time estimation of the vehicle speed and tire-road friction, are addressed. Fall detection parameters, used to control the stability of the vehicle during emergency maneuvers, are defined and verified by virtual and experimental data. The analysis of different aspects correlated to the braking dynamics of PTWs gave the possibility to define a new concept of braking force modulation applicable in case of loss of stability. Rationales, benefits and limitations of this new safety function, named Active Braking Control (ABC), are presented in detail. The virtual tests carried out to assess the potentialities of the system, demonstrated the effectiveness of the new braking force modulation strategy, in terms of improvement of vehicle stability and control.

Table of Contents

List of Figures

List of Tables

List of Symbols

Chapter 2

BST	Brake Steer Torque
F	Braking force in BST computation
Fx	Longitudinal tire force
Fy	Lateral tire force
Fz	Vertical tire force
S_{tot}	Total braking force
a_y	Lateral vehicle acceleration
a	Longitudinal distance between the center of gravity and the center of the front wheel
b	Distance between the steering axle and the contact point between the tire and the road surface
g	Acceleration of gravity
h	Height of the center of gravity
l	Motorcycle wheelbase
l_h	Longitudinal distance between the center of gravity and the center of the rear wheel
n	Motorcycle trail
α	Tire sideslip angle
β	Vehicle sideslip angle
φ	Vehicle roll angle
λ	Longitudinal slip
μ	Tire-road friction coefficient
ρ_{xid}	Ideal braking force distribution between the front and the rear wheels

Chapter 3

L	Swingarm length

$M_{drive/brake\ torque}$	Moment on the swingarm due to driving/braking torque
$M_{load\ transfer}$	Moment on the swingarm due to load transfer
M_{trim}	Torque given by the chain in case of driving or engine brake
M_v	Sum of the moments acting on the swingarm
N_{tr}	Load transfer
R_r	Rear wheel radius
S	Traction force (or braking force in case of braking action)
T	Chain traction force
k_d	Derivative gain of the PID controller
k_i	Integral gain of the PID controller
k_p	Proportional gain of the PID controller
r_c	Radius of the sprocket on the rear wheel
η	Inclination angle of the chain
ϕ	Swingarm inclination angle
φ_{actual}	Actual roll angle of the vehicle
φ_{ref}	Reference roll angle
τ_s	Steering torque given by the PID controller

Chapter 4

A_n	Root mean square (RMS) amplitude of the noise of the input signal from the sensor
A_s	Root mean square (RMS) amplitude of the input signal from the sensor
Ax_{SM}	Longitudinal acceleration of the PTW
Ax_{sens}	Longitudinal acceleration given by the IMU
Ay_{SM}	Lateral acceleration of the PTW
Ay_{sens}	Lateral acceleration given by the IMU
Az_{SM}	Vertical acceleration of the PTW
Az_{sens}	Vertical acceleration given by the IMU
B	Deceleration threshold to identity the braking status
Cu	Curvature of the trajectory
D	Acceleration threshold to identify the acceleration status
F_{aer}	Aerodynamic force
Fx_f	Longitudinal force on the front tire
Fx_r	Longitudinal force on the rear tire

Fy_f	Lateral force on the front tire
Fy_r	Lateral force on the rear tire
Fz_f	Vertical force on the front tire
Fz_r	Vertical force on the rear tire
I_{wy_f}	Angular inertia of the front wheel
I_{wy_r}	Angular inertia of the rear wheel
M	Number of back-propagation samples (initialization)
M_{Gyros}	Torque due to the gyroscopic moments of the wheels
Mx_f	Rolling resistance torque of the front tire
Mx_r	Rolling resistance torque of the rear tire
My_{Bk_f}	Braking torque on the front wheel
My_{Bk_r}	Braking torque on the rear wheel
My_{DR}	Driving torque on the rear wheel
Mz_f	Aligning torque of the front tire
Mz_r	Aligning torque of the rear tire
R	Curvature radius of the trajectory
$Ry(\zeta)$	Rotation matrix around the y-axis by the angle ζ
$Ry''(\eta)$	Rotation matrix around the y"-axis by the angle η
$Rz'(\varphi)$	Rotation matrix around the z'-axis by the angle φ
S	Running Status
V_m	Mean vehicle longitudinal speed
Vx	Longitudinal speed of the PTW
Vx_f	Longitudinal peripheral speed of front tire
Vx_r	Longitudinal peripheral speed of rear tire
Vy	Lateral speed of the PTW
m_t	Total mass of the PTW
a	Longitudinal distance between the center of gravity and the center of the front wheel
a_i	Coefficients of the equation representing the tire-road friction curve
b	Longitudinal distance between the center of gravity and the center of the front wheel
b_j	Coefficients of the equation representing the tire-road friction curve
d_{fo}	Flip over deceleration
d_{max}	Maximum deceleration of the PTW
h	Relative threshold used for computing V_m
h_a	Hysteresis threshold for accel./decel. status
h_v	Hysteresis threshold for low speed status
h_φ	Height of the center of gravity, function of the roll angle and the tire crown radius

h_{φ_d}	Vertical distance between the center of pressure of F_{aer} and the line of intersection of the wheels with the ground
k_f	Ratio between the front braking pressure and the front braking torque
k_r	Ratio between the rear braking pressure and the rear braking torque
l	Wheelbase $(a + b = l)$
r_{φ_f}	Rolling radius of the front tire, function of the roll angle
r_{φ_r}	Rolling radius of the rear tire, function of the roll angle
v	Threshold for checking speed consistency while braking
v_1	Threshold used to detect the outliers
v_{min}	Velocity threshold to identify low speed status
α_f	Sideslip angle of the front tire
α_r	Sideslip angle of the rear tire
δ	Kinematic steering angle
$\Delta\alpha$	Difference between the front sideslip angle and rear sideslip angle
η	Pitch angle due to braking
φ	Vehicle roll angle
ϕ	Vehicle pitch angle
κ_f	Longitudinal slip of the front tire
κ_r	Longitudinal slip of the rear tire
ψ	Yaw angle (Body fixed system of reference)
ψ_a	Yaw angle (Absolute system of reference)
ω_f	Angular speed of the front wheel
$\dot{\omega_f}$	Angular acceleration of the front wheel
ω_r	Angular speed of the rear wheel
$\dot{\omega_r}$	Angular acceleration of the rear wheel
μ_{max}	Maximum tire-road friction coefficient
μ_f	Actual front tire-road friction coefficient
μ_r	Actual rear tire-road friction coefficient
ζ	Ground slope angle

Chapter 5

F	Ratio between $\dot{\phi} \cdot (Vx_f - Vx_r)$ and Ax_{SM}

K_{4ii}	Coefficients of the $RISK_{iT}$ equations
L_{sw}	Last second swerving maneuver
$RISK_i$	Parameter addressing the potential risk of fall
$RISK_{iT}$	Threshold of the parameter addressing the potential risk of fall
TRH_{4i}	Coefficients of the $RISK_{iT}$ equations
$\dot{\delta}$	Steering rate
$\dot{\varphi}_{sens}$	Roll rate sensed by the IMU
$\dot{\phi}_{sens}$	Pitch rate sensed by the IMU
$\dot{\psi}_{sens}$	Yaw rate sensed by the IMU

Chapter 6

Fx_T	Total longitudinal force
Izz	Yaw inertia of the PTW
P_{sr}	Power of the reference signal
P_{si}	Power of the signal under investigation
R_{dB}	Attenuation of signal under investigation respect to the reference signal
ϵ_y	Coefficient representing the time evolution of the variables in the equations of the torques balance around the yaw axis
ϵ_r	Coefficient representing the time evolution of the variables in the equations of the torques balance around the roll axis
$\sum(Mz_i)$	Aggregate of all the moments (except those one function of ρ_x) addressing the torques balance around the yaw axis, in body fixed system of reference
ρ_c	Correction of the braking force distribution between the front and the rear wheels
ρ_x	Braking force distribution between the front and the rear wheels

Glossary

Chapter 2

ABS	Anti-lock Braking System
AEB	Autonomous Emergency Brake
BSTAM	Brake Steer Torque Avoidance Mechanism
CBS	Combined Braking System
HMI	Human Machine Interface
KIBS	Kawasaki Integral Brake System
MAEB	Motorcycle Autonomous Emergency Brake
MAIS	Maximum Abbreviated Injury Scale
MIB	Motorcycle Integral Brake
MSC	Motorcycle Stability Control
PFW	Powered Four Wheeler
PTW	Powered Two Wheeler

Chapter 4

IMU	Inertial Measurement Unit
SNR	Signal-to-Noise Ratio

Chapter 6

ABC	Active Braking Control
PSD	Power Spectral Density

Chapter 1

Introduction

Road safety is a high priority issue in Europe. The European Community has been making a great effort to reduce the road accidents and make the European transportation safer for all users. One of the most challenging goals posed by the EC policy is the drastic reduction of road fatalities by 2020, by the 50% of the current number. Looking back to 20 years ago, it is possible to see the relevant results brought by the road safety evolution: the number of fatalities recorded in Europe in 1991 was over 85000 and in 2012 was below 30000. Following this trend the 2020 target is not far to be achieved [1].

Those numbers refer to a general evaluation on road safety, thus considering all road users. Addressing in particular powered two-wheeler (PTW) users, including motorcyclists and moped users, some specific considerations should be drawn.

The number of circulating PTWs is increasing year by year, in particular in urban areas, where PTWs are considered the most efficient mean of transport, able to move nimbly through the traffic at reasonable costs (looking at maintenance and fuel consumption). From 2001 to 2007 the number of motorcycles in Europe increased by the 34%. Unfortunately, the evolution of PTWs number did not cope with an evolution of PTW safety as well. For example in 2008, the fatalities concerning PTWs resulted to be the 17% of all the road fatalities in Europe. Taking into consideration that PTW riders are the 2% of the road users, it is clear that they can be included in the group of the most Vulnerable Road Users (VRUs).

This aspect points out that the descending trend of road fatalities described for cars does not completely apply for PTWs.

PTWs are less stable then cars and less visible, they have a minimal user protection and the control is very demanding. Moreover, the injury severity in case of accident is much higher in PTW than in cars.

In addition, PTW safety cannot be comparable with car safety. Concerning active safety systems, the number of devices available on the market for four-wheeled vehicles is not comparable with the number of safety devices available for motorcycles. Car users can rely on efficient end validated systems such as ABS, ESC, ABC (Active Body Control), AEB (Autonomous Emergency Braking), ACC (Adaptive Cruise Control), LDW (Lane Departure Warning), etc. Concerning PTWs, the number of safety systems is limited: only ABS, CBS (Combined Braking System) and TC (Traction Control). Recently a new sophisticated version of the

aforementioned systems has been launched on the market; however, no new solution addressing innovative safety functions for PTWs, has been introduced yet.

Leaving out the issue related to the differences among PTWs and cars in terms of structures and the passive safety devices, the focus goes on the active safety devices. That is because the relevant decrease in car accidents is mainly related to the evolution and development of innovative active systems. The application of those systems, supported by massive distribution of electronics in cars, made the difference.

On the other side, the great variety of PTWs in the market does not match with a similar variety of safety systems. The reasons of lack of safety systems are many; the main one is that the design of an effective and efficient active safety system for PTW application is more complex and difficult than for cars. The two-wheeled vehicle requires the rider control, at the same time, over the trajectory and the roll (and steer) stability. The latter aspect becomes crucial and demanding in case of emergency situations: a panic braking or a sudden swerving to avoid a collision requires to the rider the best abilities in vehicle control. An unsuccessful control in such events can lead the rider (and the PTW) to fall or crash against an obstacle. Braking is the most difficult manoeuver to perform, especially in emergency situations. The rider must control the front and rear brakes separately, trying to apply the best braking forces distribution, maximizing at the same time the deceleration and stability, counterbalancing all the effects the braking maneuver introduces (e.g. steering torques).

Some manufactures dedicated their efforts to the development of innovative and sophisticated systems to support the rider braking. As example Honda proposed the eCBS, an *electronic Combined Braking System*, including also the anti-lock braking function, BMW has been working on the MIB, the *Motorcycle Integral Brake*, a sophisticated combined braking, and recently Robert Bosch GmbH introduced on the marked the first cornering ABS (Anti-lock Braking System) named MSC, *Motorcycle Stability Control*, able to optimize the anti-lock function for curve braking. Those advanced braking systems can be supported by other active devices like active suspensions or active steering dumpers, useful to enhance the stability of the vehicle and the performances of the safety systems implemented on the vehicle. Looking at the academic researches, some valuable activity addressed the design of new safety braking systems and functions as well.

Despite the interesting activities ongoing on the development of new solutions to increase the braking performances and PTW stability, the research effort on these topics is still lacking and still many aspects related to the aforementioned issues should be addressed and investigated in detail, in order to provide effective and validated solutions for the PTWs safety.

The present work aims to investigate the effects of the braking manoeuver on the stability of PTWs and to provide the outcomes to define the concept of an advanced braking system able to provide at the same time good braking performances and vehicle stability.

The analysis of the state of the art of advanced braking systems under development will provide important feedbacks about the main aspects and elements to address and to improve the potentialities of the current systems. The investigation

of the braking dynamics will go in detail, addressing not only standard dynamics but also motorcycle fall dynamics and vibrations behavior.

The findings gathered from the analyses will lead to the definition of a set of algorithms able to define clearly the most relevant parameters useful to describe accurately the real-time status of standard PTWs, and to be applicable to innovative active safety systems.

In Chapter 2, the state of the art of the braking systems will be described. The most promising motorcycle active safety systems will be presented, describing the point of strength and the limitations.

In Chapter 3 the influence of the braking manoeuver on motorcycle performances will be investigated in detail. In particular, the analysis will focus on the influence of the transmission properties on the *Chatter* mode of the vehicle, addressing how much the evolution of this mode can affect the motorcycle control and stability.

Chapter 4 describes the model and the equations, applicable to real powered two-wheelers, adopted to detect the vehicle dynamics in real-time. The main topics addressed will be the real-time identification of the tire-road friction conditions and the estimation of the PTW longitudinal speed.

Chapter 5 analyzes the dynamics of motorcycle fall and proposes a set of algorithms to detect potential motorcycle falls, or critical events for the vehicle stability.

In Chapter 6 the information collected about vehicle dynamics during a braking manoeuver are utilized to define a preliminary layout for an innovative braking system, able to increase the vehicle stability in case of emergency braking while cornering. The results of the virtual tests are presented and discussed; rationales and limitations are presented as well.

Finally the conclusions to the activity are drawn in Chapter 7.

Chapter 2

Braking dynamics of motorcycle State of the art

The state of the art of braking dynamics for powered two-wheelers (PTWs) application is composed of a first part describing the standard and new braking systems for motorcycles and scooters and a second part reporting the accidents analysis related to the braking systems and the braking dynamics.

In the first part the general details of innovative safety systems for PTWs and the corresponding research activities will be presented (§2.2); in the second part the studies about the accidentology addressing the effectiveness of active braking systems will be described (§2.3).

2.1 Dynamics of motorcycle braking

Motorcycle braking can be considered as one of the most demanding maneuvers to perform, especially among novice riders. Differently from cars, PTWs rely only on two wheels to stabilize and decelerate the vehicle, introducing a stability issue coupled to the deceleration issue. Moreover, generally speaking, the load transfer in a PTW is bigger than in a four-wheelers vehicle, thus requiring a more complex control of the braking force during the maneuvers [2].

In standard braking systems for motorcycles the front and rear brakes need to be actuated separately. Therefore, the rider has to balance the braking forces independently in order to decelerate. During the deceleration phase the rider should avoid dangerous conditions for the vehicle stability: the rear tire lifting or the tires skidding. Of course those two events happen alternatively in case of front wheel braking, according to the most restrictive condition among them. E.g. in case of low adherence between the tire and the road surface the road friction is the most limiting condition for the load transfer, thus leading, in case of front hard braking, the tire to skid instead of leading rear wheel to lift.

The ideal braking manoeuver can be performed reaching the same friction coefficient on the front and the rear wheels. This generates a better braking stability not only in straight braking but also in case of braking while cornering. The best braking distribution guarantees the possibility to reach the highest deceleration during a combined braking with high intensity. The expression to

derive the best braking force distribution (ρ_{xid}), for straight braking is the following [2]:

$$\rho_{xid} = \frac{a - \frac{h \cdot S_{tot}}{m_t \cdot g}}{l} \tag{2.1}$$

where a is the longitudinal distance between the center of gravity (CoG) of the vehicle and the center of the front wheel, h is the height of the CoG, m_t is the total vehicle mass, g is the acceleration of gravity, l is the wheel base and S_{tot} is the total braking force.

Of course the general geometrical properties of the vehicle are not the only parameters involved in the braking dynamics. The aerodynamic force, the non-linear suspensions and the tire properties play a crucial role as well. In particular the importance of the suspensions will be addressed in the following sections, pointing out the relevance of active regulations in terms of braking stability.

PTWs are intrinsically unstable, thus highlighting the influence of the braking maneuvers on the lateral dynamics. Different braking strategies deeply affect the vehicle response: for example the rear braking while cornering generates aligning and stabilizing torques on vehicle; on the contrary front braking tends to yaw the vehicle. In case of hard braking while cornering the manoeuver itself is much more demanding, and the rider must control not only the longitudinal dynamics for the best deceleration but also the lateral forces balance, thus including the steering control.

The necessity of a complex control on the vehicle in case of hard braking while cornering can be also derived by the modal analysis. Limebeer et al. [3] clearly show how the *Wobble* mode becomes less stable under braking and the stability decreases when the braking intensity increases. The effect is more intense in case of front braking maneuvers. The rear braking manoeuver does not affect the *Wobble* significantly, but it increases the *Weave* oscillations, especially if heavy braking maneuvers are performed. That points out that even if the rear braking helps to stabilize the cornering, in case of high load transfer the rear tire can slide, thus limiting the overall control of the PTW.

Addressing the sports motorcycles, the general information described above are verified as well, however some aspects related to the braking dynamics should be revised in detail. According to Corno et al. [4], concerning the sports motorcycles, an important distinction between braking strategy following the slip target or the stoppie-target should be done. The ratio between the CoG height and the wheelbase is high, thus enhancing the load transfer and increasing the importance of speed on braking dynamics: at high speeds the aerodynamics forces have high relevance, thus leading the wheel locking to be dominant in the deceleration phase; instead as soon as the speed decreases the aerodynamics force decreases as well, thus making the rear wheel lifting the most limiting conditions. Therefore in sports motorcycle in some conditions the braking strategy can be twofold.

In addition, in powerful sports motorbikes, the engine brake can be crucial in the vehicle control during the deceleration. In case the clutch is engaged during the maneuver and the rider is applying a hard rear braking, the combination of

the braking torque and the engine brake can lock the wheel. To avoid this problem current sports motorcycles have anti-hopping clutches.

The aforementioned general information about motorcycle braking dynamics highlights the complexity of the braking maneuver. It shows the importance of active and passive safety systems, able to assist the rider during the deceleration, thus reducing his effort, in terms of vehicle control, especially in case of heavy braking.

The standard and the most promising new braking systems will be described in the next pages.

2.2 Braking systems

2.2.1 Standard braking systems for motorcycle application

The first active braking system, implemented on a motorcycle was the Anti-lock Braking System (ABS). The ABS avoids the wheel locking during braking maneuvers that lead the motorcycle tire to exceed the road friction limit. Avoiding the wheel locking, the system optimizes the vehicle deceleration, reduces the braking distance and increases the overall vehicle stability.

The first ABS for motorcycle application was launched in the market by BMW in 1988, for the BMW K1000, and it was developed in cooperation with FTE automotive GmbH. The system was heavy (7 kg) and it was composed of two separated complete braking "lines" (control units and actuators) for the front and rear wheels. Later, in 2001, BMW introduced a lighter system, 4 kg, composed of a single body including actuators and controllers. Starting from years 2000 the ABS system was adopted by an increasing number of motorcycle manufactures, like Yamaha Motor, Honda, Ducati, Piaggio, and Aprilia, and started to be developed and implemented on scooters as well. The latest development of the ABS architecture was presented in 2010 by Bosch, with the ABS 9.0 (total weight lower than 2 kg, Figure 2.1).

In 1996 Honda matched the ABS system to the integral brake system, thus introducing on the market a new concept of braking system for sports motorcycles. Today the integral brake (or combined braking system, CBS) is implemented on several sports motorbikes by different manufactures.

The integral braking systems are based on the concept of braking force distribution between the front and rear wheel, able to optimize the deceleration (see [5]).

Since the origin of this system, many kinds of layout were presented, from the simplest one, with the single combined braking distribution, to the sophisticated eCBS (electronic Combined Braking System) with *Brake by Wire*.

Honda, which introduced the first CBS system in 1976, applies different integral braking systems on various motorcycle and scooter models: single CBS, dual CBS and *Brake by Wire* systems. All these systems, in the latest motorcycle models are combined with the ABS [6].

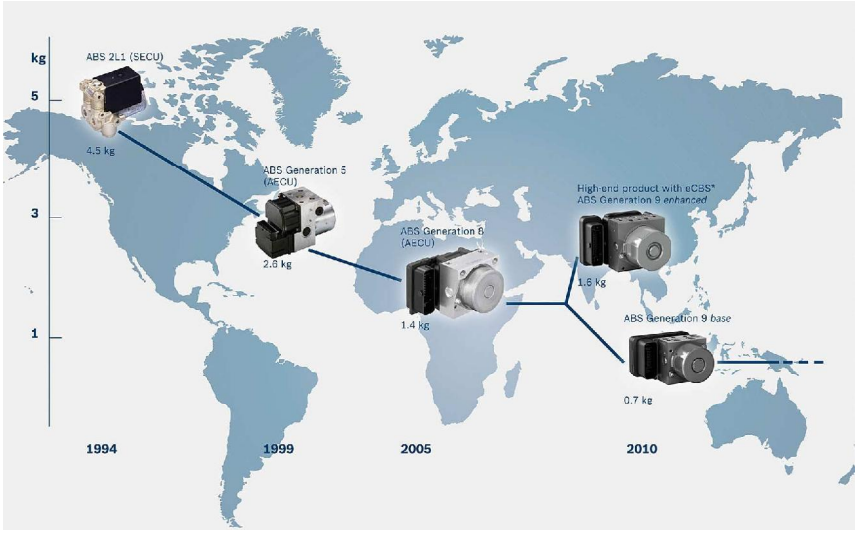

Figure 2.1: Evolution of ABS for motorcycle application by Bosch

The single CBS, mechanical or hydraulic, redistributes the braking force only in case of rear braking, thanks to an equalizer case, and it is adopted mainly for scooters and mid-size touring motorbikes.

The dual CBS performs the braking force distribution on both wheels in case of both front wheel braking and rear wheel braking. In the standard CBS systems the distribution is carried out by a hydraulic valve, thus leading the force distribution close to the best braking configuration, but still not optimized (Figure 2.2, [6]). The braking force redistribution operated by a mechanical device is characterized by a static behavior, and the system is not able to adjust the forces combination for different load configurations (e.g. the rider plus the passenger) and pitch movements.

To address the optimal braking distribution, Honda presented in 2008 the *Brake by Wire* system. In the system, a sensor detects the rider's brake inputs and an actuator regulates the pressure on the brake calipers electronically [6]. Then the brake levers actuation is "physically" separated from the brake calipers actuation.

Differently from the braking distribution actuated by hydraulic vales, the electronic actuation helps the rider to perform the optimal braking manoeuver, adjusting the hydraulic pressures as function of the load transfer and the pitch angle. This system increases the braking performances also in terms of braking smoothness, in particular whether integrated with the ABS system. Generally, standard Anti-lock Braking Systems generate pulsations to the brake levers due to pressure fluctuation during the operation, caused by the imprecise control of the hydraulic pressure by the valves. In case of electronic control of the pressure, the ABS operation is much more precise, thus reducing the pulses to the brake levers.

Concerning BMW, the ABS system is available for almost every motorcycle

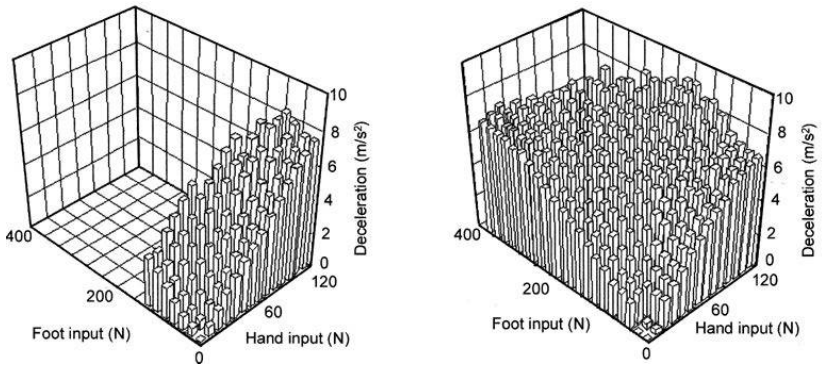

(a) Decelerations carried out by a Standard braking system

(b) Decelerations carried out by a dual CBS

Figure 2.2: Comparison of decelerations achievable by a standard braking system and a dual Combined Braking System (CBS) [6]

of the fleet and starting from 2013 all the new models have the ABS as standard equipment (according to EU law, ABS for newly registered motorcycles will not be mandatory until 2016). In some BMW motorcycle the ABS system is combined with a combined braking system, named Motorcycle Integral Braking system (MIB)[1]. The braking force modulation is not performed by a mechanical valve but by an electronic unit. Then the force combination is given by the control logic, instead of a valve displacement.

Kawasaki, on its top level motorcycles, differently from Honda, did not merge the ABS with the combined braking, but focused on the development of an advanced Anti-lock Braking System. The Kawasaki Intelligent anti-lock Braking Systems (KIBS) is a smart evolution of the standard ABS, aiming to increase the rider's confidence during braking, thus optimizing the stopping distances and reducing the pitching phenomena. The Kawasaki's system integrates a quite high number of sensors for different inputs: wheel speed, braking pressure, throttle position, engine speed, clutch actuation, gear position, etc. Thanks to an accurate control system the operation is really smooth, thus minimizing the kickback to the brake lever and the motorcycle pitching movement.

Recently some manufacturers introduced the ABS and simple CBS on their scooter lines, such as Yamaha Motor on *T-Max*, Honda on *SH*, Piaggio on *Beverly*, and so on. It is worth noting that the active braking systems for scooters are simpler than the motorcycle application. Huang and Shih [7] show that the number of components of ABS for scooters is limited and the overall system cost as well. The anti-locking function is played directly by a hydraulic valve and the pressure balancing (made by electro-pumps in standard ABS) does not need an expansion

[1] There is also the semi-integral version of MIB system

reservoir[2].

2.2.2 Innovative braking systems

The effectiveness of ABS and CBS is proved for braking on straight paths and for a limited number of accident scenarios. In order to increase the rider safety, a number of research activities addressed the design and the development of innovative active systems aiming to maximize the braking performances of the powered two-wheelers in different running conditions and facing various critical events.

In the following paragraphs the most interesting pioneering researches on innovative active braking systems will be presented. The description will be divided in two sections according to the studies addressing active braking systems mainly verified on straight path and studies addressing also braking on curve.

Braking in a straight path

A new promising and innovative braking system was proposed within the European project PISa [8, 9]. The project goal was to develop new integrated safety systems for powered two-wheelers (PTW) application, able to reduce significantly the road accidents involving PTWs.

The final device the PISa consortium developed was the *Motorcycle Autonomous Emergency Braking* (MAEB). The MAEB system is able to mitigate/prevent collisions by applying an autonomous braking force: the control logic is able to apply and modulate the braking force regardless the braking action the rider could perform.

The logic algorithm for the control of the autonomous braking activation was developed at the University of Florence, by Savino et al. [10, 11].

The system was developed following the hypotheses below:

- complete integration of the system in the vehicle body;
- feasibility of the safety function the system provides;
- innovative concept of the safety system, in order to increase the level of safety already provided by others devices.

The MAEB was developed to avoid the collision or, at least, mitigate the injuries in case of no rider reaction in emergency situations. For such autonomous devices, it is fundamental that the algorithms for the control of the system operate correctly the activation of the autonomous braking force, thus inhibiting the system in those scenarios where the effectiveness of the system itself is not certain or there could be some possibility to increase the risk of injuries. Accordingly, the activation logic and the solutions to the system false triggering were the main issues the system designers addressed (see [10, 12, 13, 14, 15] for more details).

It is worth noting that the device is subjected to the rider acceptability: the final decision on the activation of the autonomous braking is given by the rider.

[2]The expansion phase is carried out by the valve itself.

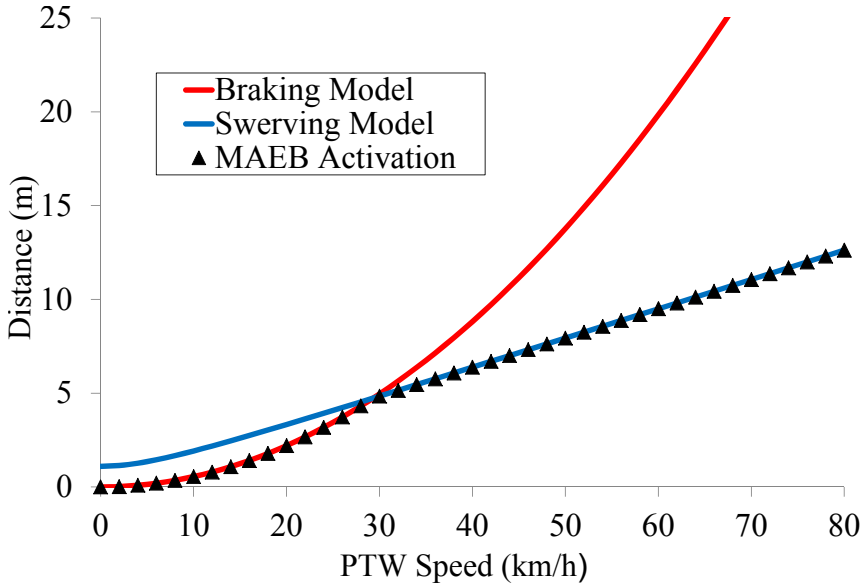

Figure 2.3: Comparison between the curve representing the minimum distance to avoid a fixed obstacle by a braking manoeuver and the curve representing the minimum distance to avoid a fixed obstacle by swerving. The comparison of these curves defines the criteria for the activation of the MAEB [15, 11]

Summing up the main features of the MAEB system:

- it detects the scenarios potentially dangerous for the rider safety;
- it detects the potential collisions;
- it slows down the vehicle speed;
- it is activated in case of no reaction from the rider.

The MAEB system was developed to increase the rider safety and assist the braking manoeuver, but it does not substitute the rider braking maneuver. It is important to underline that the autonomous braking is activated only when the collision is no more avoidable, by a braking maneuver performed by the rider or by a swerving maneuver ([13, 14, 15], Figure 2.3).

An additional safety function integrated in the system is the *Enhanced Braking* (EB) function, that can be associated to a brake assist. The EB function helps the rider to brake in case the rider applies a braking force before the collision. In this situation the rider is fully aware of the oncoming danger, therefore the system can support the rider braking manoeuver increasing the braking force. Only in such condition the MAEB system produces a full braking action. It is expected that the rider is concentrated on the manoeuver, and then he is able to control a hard braking maneuver.

Figure 2.4: Instrumented scooter for the investigation of MAEB technology [10]

The MAEB system (Figure 2.4) includes a number of sensors for the vehicle dynamic state computation: an IMU (inertial measurement unit), brake pressure sensors, a laser-scanner for obstacles detection and a group of control units to manage the system software. Moreover an HMI device (visual) is installed on the vehicle in order to warn the rider when a dangerous event is detected and the system is going to be activated.

The system was validated with an experimental campaign conducted by the Transportation Research Laboratory (TRL) at Crowthorne House, Berkshire (United Kingdom). The PTW was ridden towards a lightweight test object positioned in a clear space at approximately constant speed of 25, 35, 45 and 55 km/h. Moreover the detection effectiveness of the system was validated by testing the device in car following and crossing scenarios and by simulating standard urban traffic conditions (Figure 2.5).

This preliminary validation tests showed good results in terms of obstacle detection (the percentage of the positive runs in terms of proper detection of the obstacle is 97%) and MEAB positive activation (proper activation by 98%, 149/151 runs).

Further evaluations of the system effectiveness in different scenarios are presented in §2.3.

Figure 2.5: Experimental test of the first prototype of MAEB system [10]

The technology introduced by Savino et al. is at the starting phase of its development process and it requires further investigations and tests aiming to create a device able to merge perfectly the rider actions and reactions and the activation of autonomous safety systems. It is important to say that the implementation of autonomous systems on PTWs it is not easy as for cars, due to the PTW complex dynamics. Anyhow, the motorcycle active braking system is an interesting solution for PTW safety. Looking at car safety systems, AEB (Autonomous Emergency Braking) is becoming a standard technology for many vehicles, showing undeniable benefits for road safety; accordingly, it is expected that in the future the same technology applied on PTWs could produce similar benefits for riders.

Braking in a curve

Curve braking is one of the most demanding maneuvers for the riders, in terms of concentration, confidence and control. Differently from braking on a straight path, during the braking maneuver in a curve, the positions of the contact point between the tires and the road surface generates a torque on the steering axle, function of the roll angle. This torque, if it is not promptly compensated by the rider, leads to modification in the motorcycle roll angle, thus a change in the vehicle trajectory.

The stabilization of the motorcycle by active control systems, similar to active systems for cars, is more complicated due to the motorcycle roll dynamics. At different speeds the motorcycle stability is influenced mainly by different effects: at high running speeds the gyroscopic effect is the main aspect influencing the motorcycle dynamics, then at low speed the stability is mainly under the control of steering torques. It is worth noting that both aspects are directly connected to friction properties of the tires. In order to keep the motorcycle on a specific turning condition the tires must always provide enough lateral adherence, always below the friction limit (maximum friction coefficient).

Due to the aforementioned consideration it is clear how difficult is to maintain the motorcycle in stable position in a curve, in case of unsteady state maneuvers, as braking or acceleration, or low friction conditions.

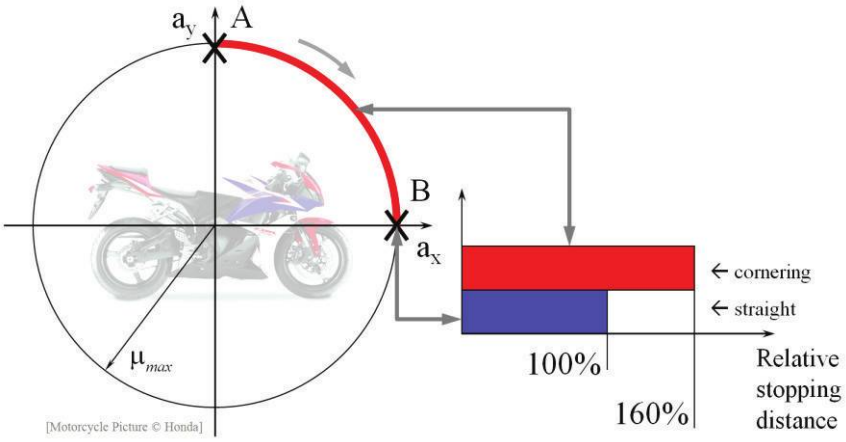

Figure 2.6: Representation of the Kamm's circles that graphically shows the correlation between the lateral and longitudinal accelerations, in order to point out the differences between the motorcycle braking performances on a straight path and during cornering [16]

The standard ABS and CBS have a limited working range. Their effectiveness is proved on straight paths and for limited roll angles. In case of large roll angles and large lateral tire slips, the aforementioned systems can help the motorcycle stability avoiding the wheel locking and providing a better braking force balance but they slightly influence the motorcycle trajectory.

Schröter et al. [16] showed that a leaning motorcycle (at max roll angle), running at 30 km/h, during a braking maneuver needs 60% more space to stop than the same motorcycle running at the same speed on a straight path (Figure 2.6).

Besides the aspect described above, the curve braking introduces additional effects on the vehicle dynamics. In case of front braking, the tire forces generate a steer torque (BST) that can be computed by the following equation:

$$BST = F \cdot b \tag{2.2}$$

where F is the braking force and b is the distance between the steering axle and the contact point between the tire and the road surface. The BST can be minimized with different techniques:

1. reducing the braking force on the front wheel and redistributes it on the rear wheel [17];
2. reducing the offset b [16];
3. using a steering damper [18];
4. using an active counter-steering system [19, 20].

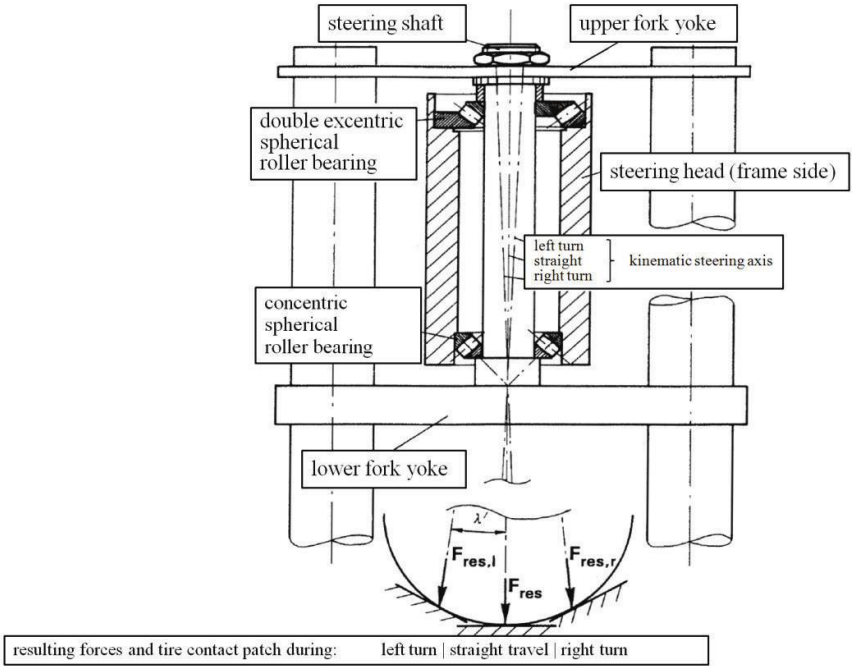

Figure 2.7: BSTAM system [16]

A number of studies show the development of new promising technologies for the stabilization of the motorcycle, addressing the aforementioned safety functions.

Let's consider the second option (the others will be analyzed later on). Schröter et al. [16] addressed the offset modification by an adjustable steering axle[3], named BSTAM (Brake Steer Torque Avoidance Mechanism). Looking at Figures 2.7 and 2.8 it is possible to see that the steering axle is between a taper roller bearing (lower part) and an eccentric, taper roller bearing, electronically adjustable. This architecture allows the movement of the steering axles respect to the standard configuration, in order to locate the kinematic steering axle on the plane passing through the tire-road contact point, thus reducing the distance between the steering axle and the contact point between the tire and the road surface.

The BSTAM solution involves many issues to consider and solve, as the compensation of the front suspension. In any case the authors proved that this solution helps the motorcycle control reducing the steering torque the rider should apply to perform a curve. It is worth noting that in order to obtain the best performances from this system, an active control of the steering position is needed, able to adjust the steering axle orientation as a function of the roll angle.

Considering the possibility to modulate the braking forces in order to control the motorcycle stability, Tanelli et al. [17] studied the improvement of an ABS

[3]The project takes inspiration from a mechanism designed by Honda

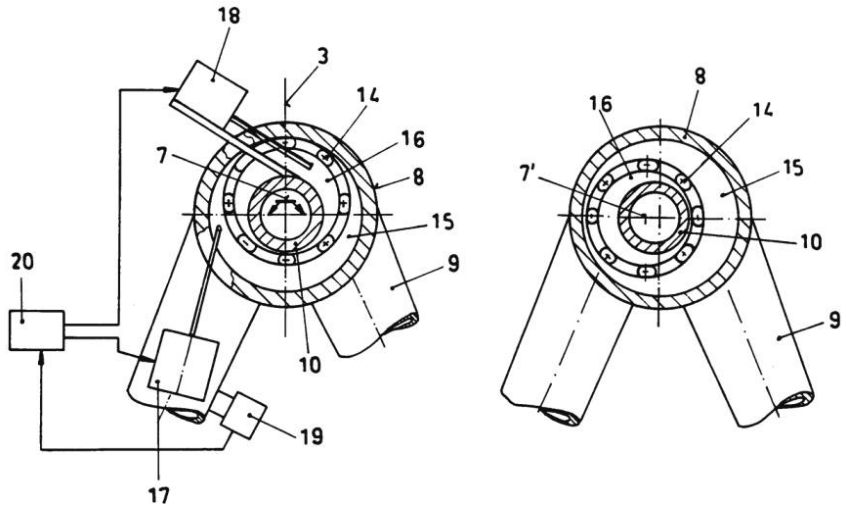

Figure 2.8: Detailed representation of the BSTAM system. For more information about the components please see [16]

system to optimize curve braking.

For motorcycle application a number of studies [4, 21, 22, 23, 24, 25, 26] demonstrated the effectiveness of the ABS in avoiding accidents involving motorcycle braking on straight paths. On the other side it has not yet proved the effectiveness of standard ABS in case of panic braking in a curve. The current systems can guarantee good braking performances only for limited roll angles. The applicability of the ABS only on straight braking is related to the low "flexibility" of the system.

As a matter of fact the activation of the ABS is function of wheels deceleration, not considering the lateral and roll dynamics. Therefore, the support given by the ABS to the rider in order to increase the braking performance, decreases as much as the roll angle increases.

In [17], Tanelli et al. propose a different control of the ABS system, based on a modulation of point of activation as function of the roll angle.

From a preliminary study the authors show that the longitudinal slip at which the friction coefficient reaches the maximum value ($\lambda_{\mu_{max}}$[4] changes as function of the roll angle). More precisely, as long as the roll angle increases $\lambda_{\mu_{max}}$ increases as well.

The proposed braking algorithm assumes that the tires slip and the roll angle are available. For real vehicle application, the aforementioned elements must be usually estimated (or measured with expensive sensors). The estimation process is not easy, especially because of the complex dynamics of powered two wheelers. For more detail see [27, 28] and §4.2.

As Figure 2.9 shows, it is important to maximize the longitudinal friction coefficient in accordance to the lateral friction coefficient values. For high roll

[4]Only referring to the work by Tanelli et al. the longitudinal tire slip is defined as λ. In the remaining part of the thesis it will be addressed as κ.

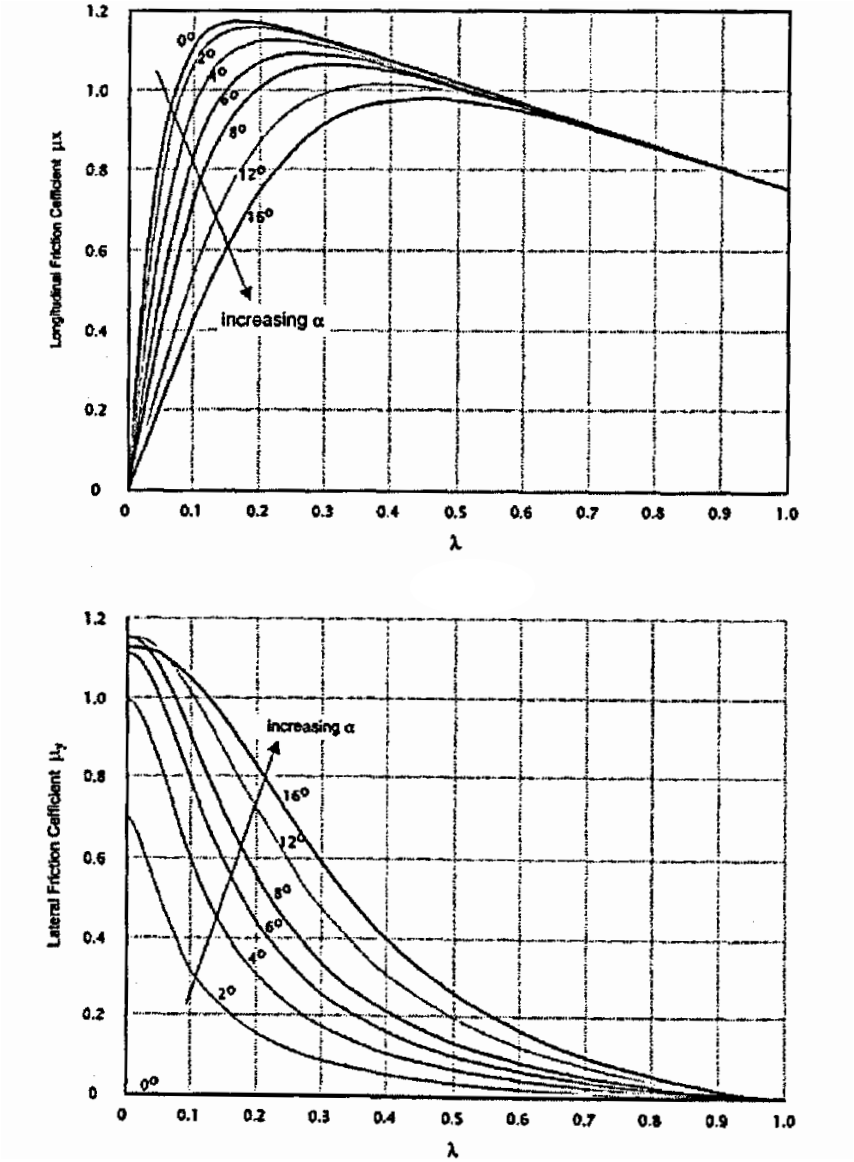

Figure 2.9: Variation of the longitudinal and lateral friction coefficients as function of the longitudinal slip and the sideslip [28]

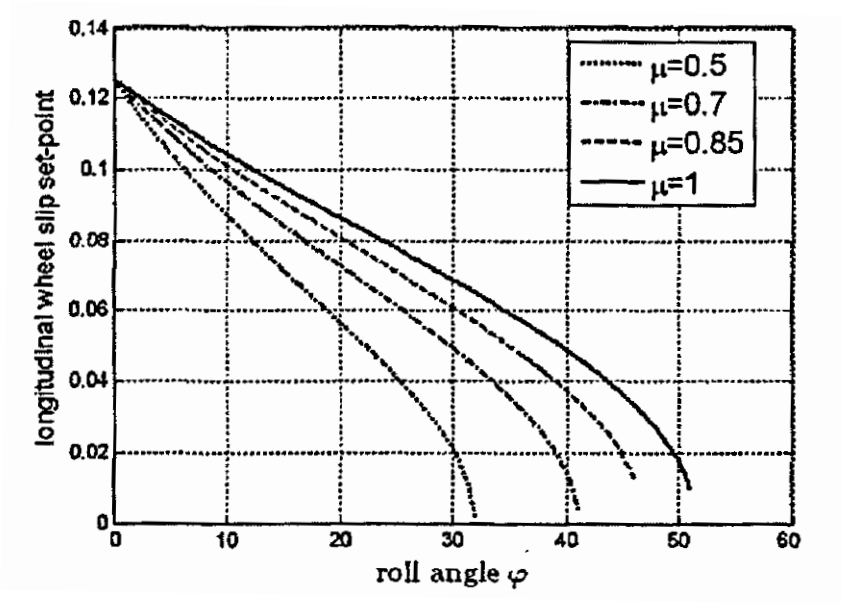

Figure 2.10: Representation of the longitudinal wheel slip set-point change, $\bar{\lambda}$, as function of the roll angle for different friction conditions [28]

angles (and for high sideslip angles, α) the best longitudinal friction conditions are located at high longitudinal slip values (λ). On the other side for increasing longitudinal slips the lateral friction condition decreases. To modulate the roll angle while cornering it is necessary to find the best compromise between the longitudinal and lateral friction conditions.

The resulting best values of λ, named $\bar{\lambda}$, have been mapped by the authors following the conditions below:

$$\bar{\lambda} = argmax_{\lambda}[Fx(\lambda, \varphi, Fz)] \quad subjected \quad to \quad Fy(\bar{\lambda}) \geq Fz \cdot tan(\varphi) \tag{2.3}$$

where Fx is the longitudinal force, φ is the roll angle and Fz is the vertical force. The complete range of the set-point values $\bar{\lambda}$ as a function of the roll angle can be observed in Figure 2.10

As soon as the roll angle increases in each friction condition the longitudinal wheel slip set-point decreases, tending to zero.

The authors assumed the road condition to be known. For practical application if it is not possible to know this detail, it would be better to assume a fixed road condition, e.g. the worst one (in the figure is $\mu = 0.5$). It is worth noting that making the aforementioned assumption the braking performances are not optimized.

The ABS algorithm has been validated by virtual simulations, using Bikesim®. The outcomes show that the system is theoretically applicable but, with the current technology, not easily feasible nowadays. The authors underline the necessity to go

further in the identification of the complete vehicle dynamics and the activation criteria in order to implement and test the system on real powered two-wheelers.

A recent work by De Filippi et al. [29, 30] shows the last updates of the activity for the development of a braking system able to assist the rider to control the motorcycle suability. De Filippi et al. proposed a methodology to increase the motorcycle stability, reducing the roll oscillations, in case of acceleration or braking. In the system presented, the input variables used for control logic are the braking forces and the driving forces. It is assumed that this advanced stability system is associated to a Brake By Wire and a Ride by Wire system, in order to control the braking forces and the driving forces independently from the rider. By a number of simulations using Bikesim®software the authors investigated the motorcycle dynamics in order to define how to control the wheel torques: it was observed that the front braking torque has the major influence on roll dynamics and both wheels have similar influence on the acceleration/deceleration. The authors set up a MIMO controller (Multi Input Multi Output) able to control at the same time the vehicle stability and the vehicle acceleration (in a previous work by De Filippi et al. [31] the controller was able to address only the stability and not the acceleration). To control the longitudinal acceleration the system modulates only the torque on the rear wheel, and to control the roll rate the system modulates the braking forces in order to achieve maximum contribution, on roll dynamics, from the front wheel.

The authors validated the control logic with different experiments:

- perturbing the motorcycle motion, during a steady state cornering (30°) at high speed (130 km/h), with a front braking torque;
- double disturbance on the front and rear wheels, simulating the motorcycle passage over a bump, again in curve at high speed;
- double disturbance on the front and rear wheels, simulating the motorcycle passage over a bump, during straight running.

Figure 2.11 reports the effects of the stability controller in case of a braking torque of 100 Nm on the front wheel. That level of torque can be associated with a low-medium intensity braking maneuver (as a matter of fact the deceleration is below 0.3 g). The results clearly highlight how the new system can sensitively reduce the fluctuations of the roll rate, thus limiting the influence of the maneuver on the roll angle. Moreover the intervention of the system does not influence the longitudinal deceleration, thus maximizing the braking performances.

Usually, in case of panic braking while cornering a standard braking system cannot avoid the motorcycle fall. On the other side the stability controller is able to enhance the vehicle stability and for some condition it can avoid completely the motorcycle fall. E.g. in Figure 2.12, for a braking torque of 300 Nm the, in case of cornering at 30°the vehicle is successfully supported by the stability controller, that avoids completely the fall.

At the end of 2012 Robert Bosch GmbH revealed a new promising ABS system, named *Motorcycle Stability Control* system (MSC, Figure 2.13). The MSC system

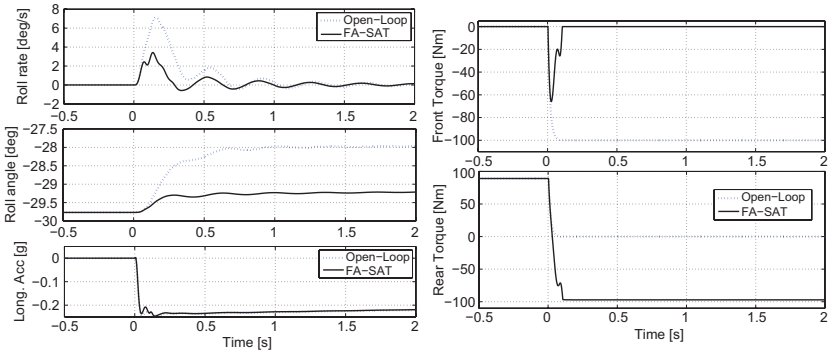

Figure 2.11: Controller response for a 100 Nm perturbation (braking torque) of the front wheel, during steady cornering at 30°. Comparison by the new control algorithm and the standard braking actuation [30]

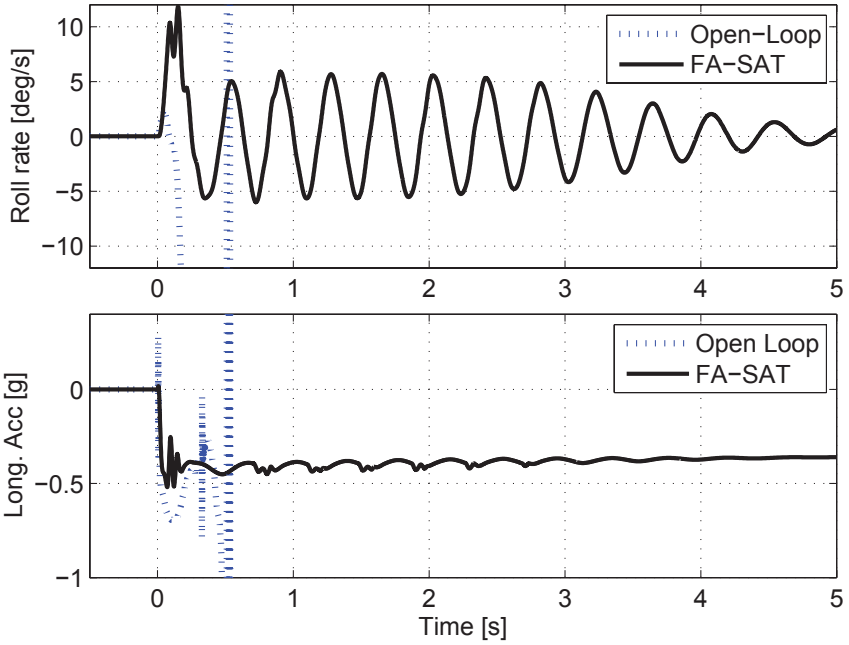

Figure 2.12: Controller response for a 300 Nm perturbation (braking torque) of the front wheel, during steady cornering at 30°. That represents a hard braking manoeuver. Comparison by the new control algorithm and the standard braking actuation [30]

Figure 2.13: New Motorcycle Stability Control system (MSC) by Bosch. The picture depicts the main elements of the system: the ABS unit and the inertial measurement unit

includes an extensive array of sensors (roll angle sensors, gyroscopes, accelerometers, etc.) and sophisticated software.

The main functions offered by the system are the following:

- it reduces the motorcycle's tendency to return to an upright position, thus limiting the possibility to leave the lane;
- it reduces the risk of low-side falls. The system counteracts this phenomenon by detecting low-side fall risk and limiting the maximum brake force;
- the eCBS (electronic Combined Braking System) function, implemented in the MSC system, always performs the optimal braking force distribution, even in curve.

Those main functions are associated with the Traction Control (TC), wheelie mitigation and rear-wheel lift-up mitigation. In conclusion, Robert Bosch GmbH claims that the MSC system can ensure optimal braking and accelerating maneuvers in straight path and curve, thus reducing the risk of accident and improving road safety.

The system has gone in series production in 2013 and the first motorcycle equipped with MSC, KTM 1190, was presented in summer 2013.

The MSC represents an important evolution of motorcycle ABS. It will be very interesting to verify its influence on motorcycle accidents in comparison with the standard ABS systems.

The roll angle can be theoretically stabilized also by a direct control on the steering toque. Implementing an active steering control system, it is possible to influence the roll angle by a variation of the steering angle. Addressing the option to assist the rider control by an active counter-steering system, prof. Marumo et al. [19, 20] proposed a collision avoidance system for motorcycle by automated steering control. The authors presented the last update on the steering system control,

showing promising results in terms of avoidance performance. In any case this technology with such level of automation applied on the motorcycle steering bar needs to be further investigated in detail, in particular addressing the issues related to the rider's acceptance and rider reaction, to the automatic steering movements.

Addressing the stabilization of the motorcycle *Weave* and *Wobble* vibrations, De Filippi et al. [18] proposed an innovative semi-active steering damper. The system adjusts the control strategy, switching between two control methods, according to a frequency range selector. The semi-active damper has been evaluated via virtual simulations and experimental tests. The findings showed that the system is able to increase the motorcycle stability during cornering, thus limiting the vibration on the front frame and increasing the rider confidence while bending.

In case of motorcycle running in steady state conditions, without acceleration either deceleration, the stability control of the motorcycle is more complicated if compared to the scenarios described in the paragraphs above. In steady state running it is not possible to change the stability by the simple control of the longitudinal dynamics.

A number of research activities were conducted by Seiniger, Gail et al. [32, 33, 34, 35, 16] on this topic, aiming to control the vehicle stability in real-time, detect potential dangerous events and correct the motorcycle dynamic state without the application driving/braking forces.

In [33] the authors proposed a criterion to estimate the stability of leaning vehicles based on the motorcycle slip angle β. Due to the necessity to estimate to values of β and $\dot{\beta}$ a simple estimation methodology is presented.

The motorcycle instability detection is given by the comparison between $\dot{\beta}$, computed from the vehicle lateral dynamics and a reference parameter $\dot{\beta}_{ref}$, computed from the steering dynamics:

$$\dot{\beta} = \dot{\psi} - \frac{a_y}{\dot{x}} \tag{2.4}$$

$$\dot{\beta}_{ref} = -\dot{\delta}_{eff} \cdot (\frac{l_h}{l} + \frac{n}{l}) \tag{2.5}$$

The aforementioned equations refer to the motorcycle model represented in Figure 2.14, where $\dot{\psi}$ is the yaw rate, a_y is the lateral acceleration of the CoG, $\dot{x}$ is the vehicle longitudinal speed, δ_{eff} is the steering angle, l_h is the longitudinal distance between the CoG and the center of the rear wheel, n is the trail, and l is the wheelbase.

Comparing the Eqs. 2.5 and 2.4, and defining a value of uncertainty ($\dot{\beta}_{un}$), it is possible to detect the vehicle instability when the following equation is verified:

$$|(\dot{\psi} - \frac{a_y}{\dot{x}}) - (\dot{\delta}_{eff} \cdot (\frac{l_h}{l} + \frac{l_h}{l}))| \geq \dot{\beta}_{un} \tag{2.6}$$

The authors tested the aforementioned methodology in two different real scenarios:

- sudden road friction coefficient variation, during a steady state curve;

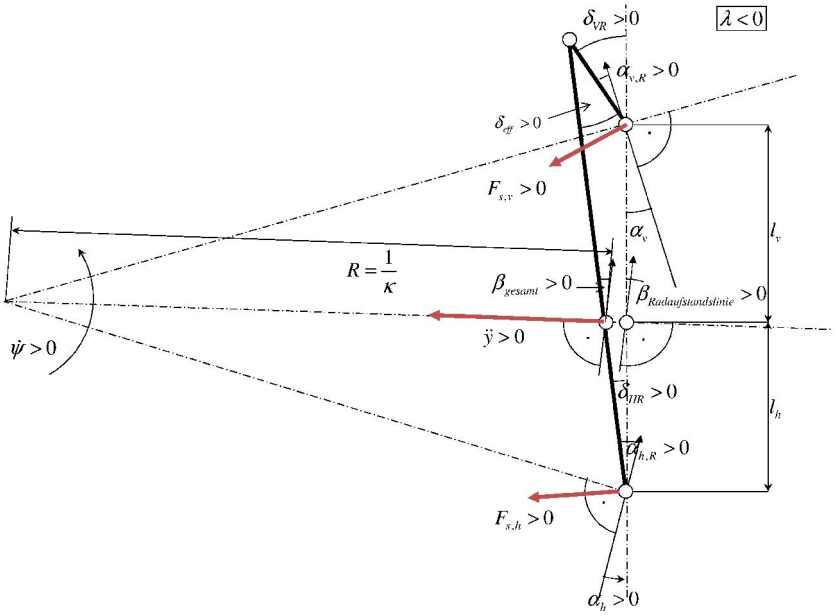

Figure 2.14: Motorcycle model adopted by [33] to investigate the criteria for critical events (for stability) detection

- curve running, exceeding the lateral friction conditions.

In every run, the methodology was able to detect correctly the critical situation, without false positives.

In addition to the aforementioned fall detection criteria, the authors proposed also the investigation of potential systems for the roll stabilization by active suspensions [32].

The roll angle is influenced by the momentum generated by the gravity force and the centrifugal forces around the roll axis, and the tires lateral forces.

Going more in detail on motorcycle lateral dynamics, taking into account the rear wheel, considering good friction conditions (longitudinal slip under 0.1-0.2, for standard asphalt), it is interesting to notice that a modification of the lateral slip angle could compensate the lack of adherence in the front wheel, thus increasing the stability of the vehicle. Anyhow, the modification of the slip angle would need a rear active steering system with a fast actuation (lower than 0.1s), that is not feasible (or very difficult) with the current technologies. In case the friction conditions on the rear wheel exceed the limit the roll correction it is not feasible at all. In accordance with the aforementioned considerations, Seiniger et al. [32, 33, 34, 35] stated that, for motorcycle applications, it is not possible to develop an ESC system, able to assist the motorcycle motion in case of loss of stability while cornering in steady state conditions (not in the braking phase nor during the acceleration phase) with the same peculiarities of car ESC. The authors demonstrated that, even with

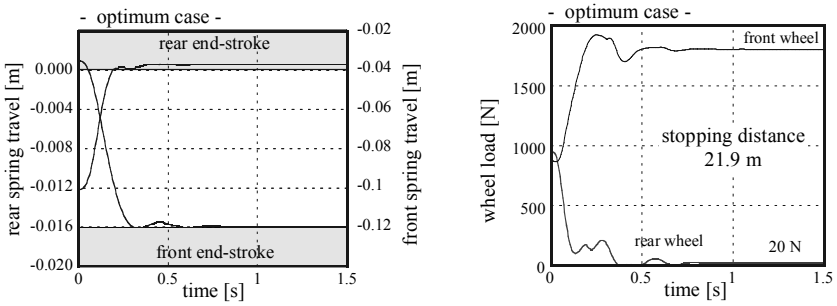

Figure 2.15: Spring travel and wheel load in case of optimal suspension set-up [36]

active suspensions, it is not possible to influence the adherence coefficient in order to increase the roll stability.

The only possibility to increase the motorcycle stability by active suspensions is to change the target of stabilization, from the roll angle to the yaw angle. Active systems able to modify the sideslip angles, the camber angle and the longitudinal slip could help to change the yaw momentum of the motorcycle and stabilize the yaw movements. This methodology is technologically feasible, however the authors claim that a system with similar stability devices would be effective only in a small range of accidents scenarios.

Finally, addressing again the influence of motorcycle suspensions on the vehicle stability, Doria et al. [36] and Corno et al. [4] investigated the correlation between the braking distance and the suspensions set-up. Doria et al. analyze how much the braking distance on a straight path can be influenced by different suspension calibrations. The results show that in case the friction coefficient is the most restrictive aspect to consider, compared to the rear wheel lift-up condition, it is not possible to find relevant differences among different suspensions set-up, in terms of stopping distances. In this case the suspension working range is stable and limited.

In case of high friction coefficients (the rear wheel lift-up condition is more restrictive), different braking performances can be found for different suspension set-up.

Aiming to find the best configuration for front and rear suspension at the same time, the solution is different from the combination of the best set-up of the front and rear suspensions separately. It was found that the best theoretical configuration is at the end-stroke of both suspensions (Figure 2.15).

In [4] the authors investigated the influence of the braking toque oscillation on the braking distances. First of all it was found that the longitudinal slip pulse is equal to the braking torque pulse. This means the implementation of an active braking system, like the ABS or CBS, with a high frequency of activation would minimize the fluctuations of the braking torque, thus limiting the slip and pitch oscillations. In accordance with the results presented by Doria et al., the authors show the minor influence of the suspensions set-up on braking performances in case of slippery surfaces. The only clear difference between the configurations is the

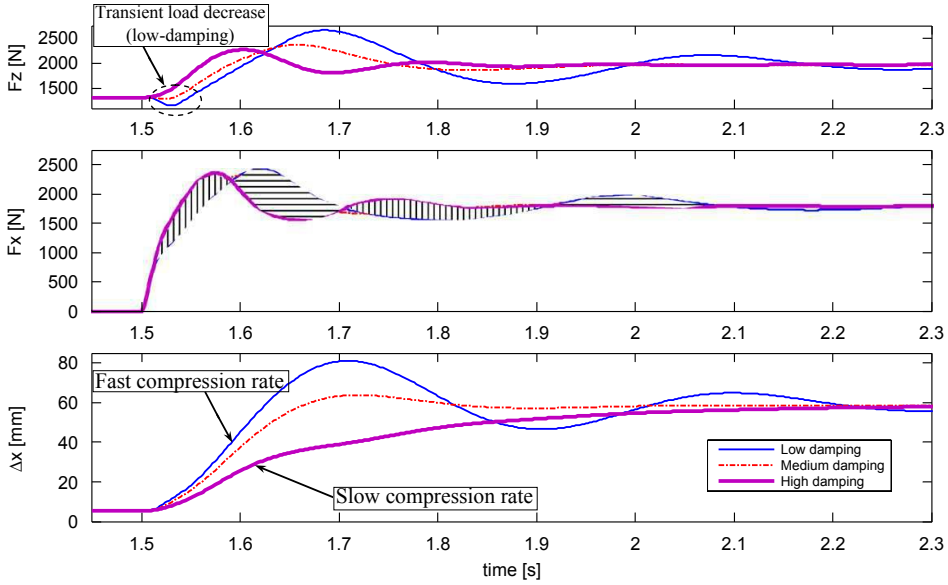

Figure 2.16: Responses of different suspensions set-up, in terms of longitudinal and vertical forces and fork elongation, in case of front braking [4]

different time response of the systems, thus the load transfer dynamics: with a low damped suspension the load transfer is fast, while with a high damped suspension the load transfer is slower. On the other side the suspension oscillations in the second configuration are highly decreased.

Accordingly, only adaptive suspensions provide the highest benefits to the braking manoeuvers [37].

2.3 Accidents analysis

The objective of the accident analyses related to the motorcycle braking is to find out the most relevant correlations between the motorcycle braking maneuver, the riders injuries, and the potential effectiveness of the current braking systems in terms of users injury reduction or mitigation.

The risk and the severity of rider injuries are influenced by the collision dynamics (impact speed, impact angle, etc. [38]) and by the rider fall dynamics. In particular the latter element, the possibility to fall, to hit the ground or other obstacles, increases the severity of injuries and it affects the type of injury suffered.

Sporner et al. [39, 40] investigated the consequences of rider fall after braking and the possibility of damages, analyzing more than 600 car/motorcycle accidents, obtained from the databases of German car insures from 1990 to 1999. The authors found out that in 65% of the accidents the rider performed a braking maneuver before the collision (Figure 2.17). Considering this percentage, in the 19% of the investigated cases the riders fell down before the collision against the obstacle/car.

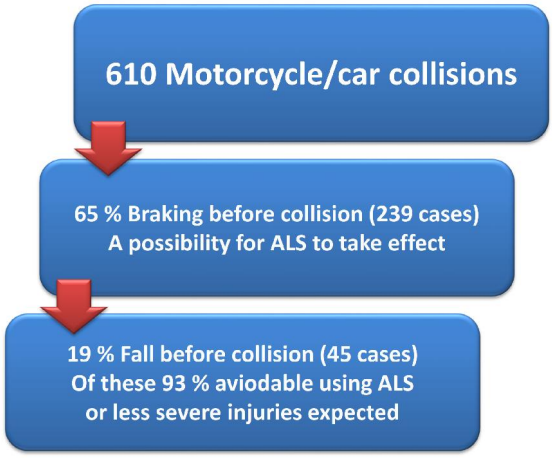

Figure 2.17: Details of the car/motorcycle collisions, with an explicit reference to the potential benefits of Anti-Lock Systems (ALS) [39]

In all these cases, the rider fall can be related to the braking maneuver that caused the motorcycle loss of stability (due to different reasons, e.g. fast swerving, wheel looking, etc.). Assuming the application of brakes in a controlled manner at the same reaction point, without falling, the author find out that the 93% of accidents could be avoided or, at least, minor injuries could be suffered. Figure 2.18 depicts how much the fall of the rider increases the injury severity.

In particular, the effect of fall down is clearly visible for severe injuries (MAIS 4+). The percentage of severe damages is the double respect to the accidents without a fall. On the other side, taking into account minor injuries it is possible to see that for medium severity the percentage of accidents with and without a fall is almost the same, and in case of low severity the number of accidents not involving a rider fall are clearly in greater number.

Even if the author did not showed any other explicit correlations between the vehicle dynamics and the investigated accidents it is not possible to draw other conclusions on data depicted in Figure 2.18. However it is possible to hypothesize that: the accidents showing major injuries are related to higher running speeds, thus leading the vehicle to higher instability in case of sudden braking; the minor injuries are related to lower running speeds, due to the possibility, for the rider, to control more easily the braking maneuver and the motorcycle stability. Following these considerations it could be possible to partially explain the high number of accidents without a fall in case of low level injuries.

Sporner et al. concluded that the motorcycle fall increases the level of damages the rider can suffer in an accident. From this point of view, safety systems that prevent the rider to fall down after a sudden braking maneuver, thus increasing the vehicle stability and control, will definitely reduce the number of accidents, or, at least, the injury severity.

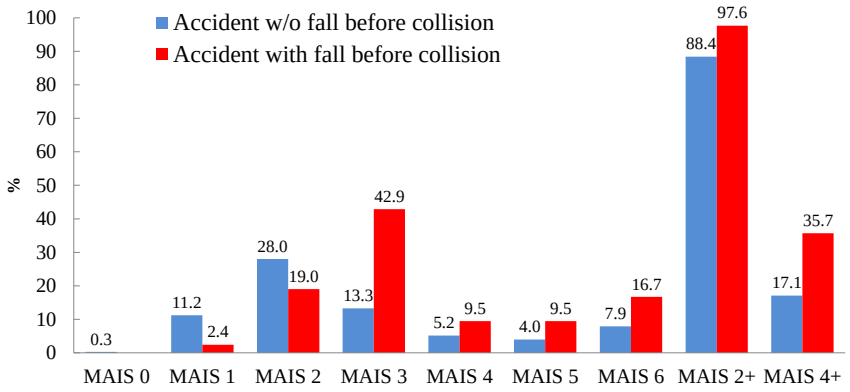

Figure 2.18: Influence of motorcycle fall before collision, addressing the rider injuries [39]

As already said in §2.2, as the motorcycle market concerns, the primary safety systems available for high-end models are the ABS, the combined braking system (CBS) and the traction control (TC). In the literature a number of studies were conducted to investigate the benefits coming from the aforementioned systems; in particular, several authors evaluated the ABS effectiveness in real world crashes.

Roll et al. [41] studied the ABS effectiveness in case of frontal collisions with other obstacles. 51 accidents, from DEKRA accident database, were investigated. All the cases were divided mainly in two accident scenarios: a U-turn of the leading vehicle and a crossing scenario. The authors studied the potential benefits of conventional braking systems, standard ABS systems[5], and advanced braking system (ABS matched with combined braking, collision detection and automatic brake pre-fill) on the aforementioned 51 scenarios.

An example of application of different braking systems on the same accident scenario is depicted in Figure 2.19.

The collision speed and the time to collisions are the main terms of comparison to analyze the braking systems effectiveness. The main results are summarized in Figure 2.20.

The authors reported the number of avoidable accidents and the number of accident in which the injury due to the collision could be reduced due to a decrement of the impact speed.

As expected, the braking system with the highest level of technology could be the most effective system compared with the remaining system. It is worth noting that even with the simplest ABS technology available, almost 1/4 of the accidents could be avoided. The ABS allows a higher deceleration (maximizing the friction coefficient) and provides a better driving stability for the maneuver performed. Moreover, ADAS systems (ABS system with automatic pre-fill) would help to save time in the braking application, thus decreasing the braking distance, then the

[5]The ABS systems were divided in three categories: ABS only on front wheel, full ABS and C-ABS (combined braking matched with ABS)

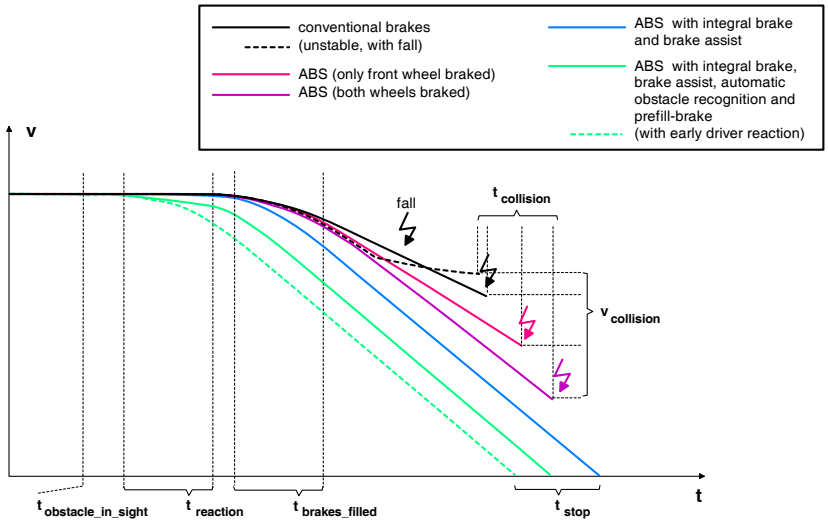

Figure 2.19: Effectiveness of different brake controls in case of panic braking on a straight path [41]

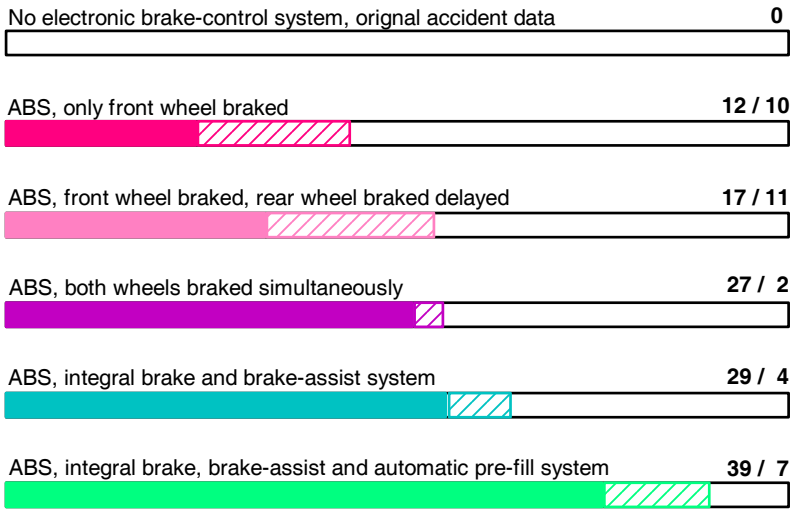

Figure 2.20: Theoretical number of collisions totally avoided and highly mitigated by different braking systems [41]

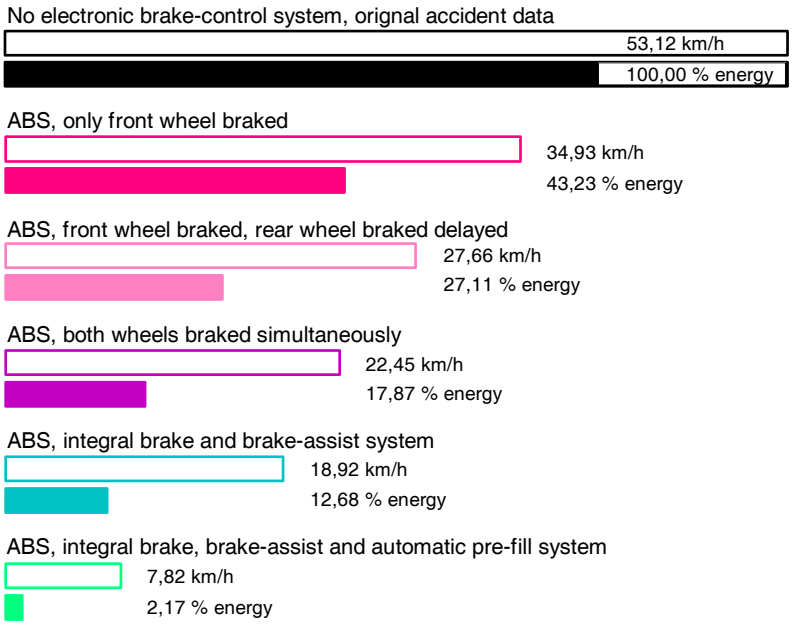

Figure 2.21: Medium collision speeds and percentile crash energy depending on different brake control systems [41]

number of accidents avoided[6]. A larger time interval before the collision would give the rider the possibility to avoid the collision with other evasive maneuvers, e.g. by a sudden swerving maneuver [15].

Another aspect related with the impact speed decrease is the impact energy reduction. Looking at Figure 2.21 it is possible to see that even with only the simplest ABS configuration (ABS on the front wheel) the total impact energy is drastically reduced (in the example the front ABS reduces the impact energy by 20%).

The effectiveness of different braking systems on straight running and on a curve is also presented by Gail et al. [35]. The authors analyzed the braking performances of nine riders on the same motorcycle with changeable braking systems (standard, standard ABS, CBS, CBS+ABS only on the hand lever, full CBS+ABS). The riders were asked to reach high decelerations during braking, in both straight running and curve running.

The first crucial aspect that the research activity shows is the time the motorcycle (and the rider) takes to fall, in case of wheel locking: the tests highlight that the vehicle falls only after less than 0.5 s (Figure 2.22).

That interval is so small that it is quite impossible for the rider to react

[6]The aforementioned considerations are drawn in theoretical braking conditions. In case of autonomous braking systems, as reported in [11], the rider acceptance and the rider possibility to control the vehicle during the automatic braking are two fundamentals issues to consider

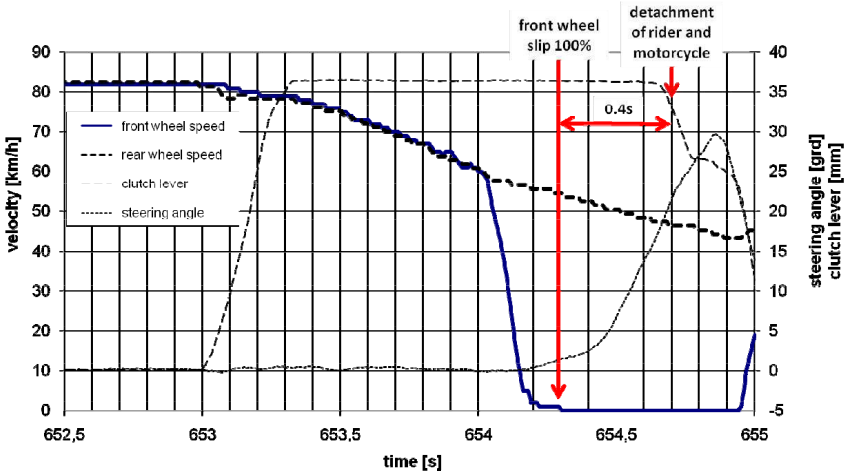

Figure 2.22: Time evolution of rider fall in case of motorcycle wheel locking, due to a hard braking [35]

promptly and correct the motorcycle position. In those scenarios, active systems, characterized by calculation and actuation times below 0.1 s can help the rider to manage the maneuver.

The second main aspect related to advanced braking systems is the physical effort. The authors demonstrated that the presence of the ABS on the motorcycle increases the rider confidence and reduces the physical strain. In particular, during braking on a curve.

Focusing only on ABS, several studies addressed the importance and the effectiveness of that system on different road scenarios (e.g. [21, 22, 23, 24, 25, 26]). The ABS system gives the rider the possibility to increase the braking performances, thus applying the braking force up to the tire-road friction limits [21, 22, 23, 24].

Teoh [25] investigates the motorcycle fatal accidents from the Fatality Analysis Reporting System (FARS)[7] per 10000 registered vehicles during 2003-2008, comparing the accidents for 13 motorcycles, considering the same models with and without ABS. The results of his analysis shows that the ABS is effective in reducing significantly the fatal crashes by the 37% and it would avoid the accident by the 21% of the cases.

Rizzi et al. [26] comes to similar conclusions investigating all the fatal accidents involving motorcycles, in Sweden, between 2005 and 2008. Rizzi adopted a scale from 1 to 5 to evaluate the influence of ABS on fatal crashes:

1. ABS would definitely not have influenced the crash;

2. ABS would perhaps have influenced the crash;

[7]Fatality Analysis Reporting System (FARS), a national census of fatal crashes occurring on public roads that is maintained by the National Highway Traffic Safety Administration of the US Department of Transportation.

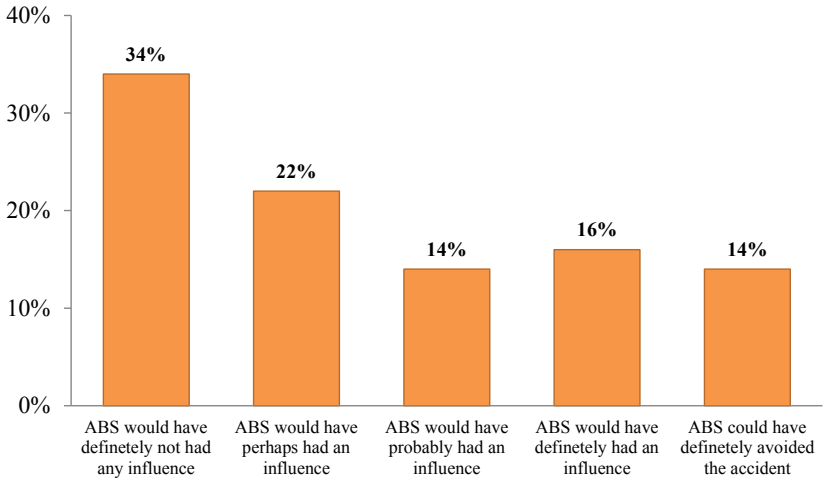

Figure 2.23: ABS effectiveness evaluation [26]

3. ABS would probably have influenced the crash;
4. ABS would definitely have influenced the crash;
5. ABS could definitely have avoided the crash.

The accidents available were investigated in detail, and all the information were used to derive the potential effectiveness of the ABS on those scenarios.

The results show that the ABS was effective mainly in head-on collisions and collisions at the intersection (in those cases that could be clearly affected by the system). In 30% of all the cases the system would have definitely had an influence on the collision or could have avoided the collision at all, and in 66% of all the ABS could have the possibility to influence the accident (Figure 2.23).

Moving to economical and societal considerations about the ABS, Gail et al. [35] take into account the future time interval between 2015 and 2020 for the analysis. Considering as drawbacks the development costs and the production costs and as benefits the expenses avoided, like medical costs, insurance costs and repair costs of the vehicle, in case of avoided accident the benefits results 4.7 times higher than the drawbacks. In terms of money, the latter result means hundreds of million Euros saved.

It is worth noting that even if the aforementioned study reports clearly the benefits from the ABS implementation on the motorcycles, a number of limitations should be considered, like the impossibility to quantify the influence of other factors on the accident rate, the geographical restriction of the databases, the small sample of ABS motorcycle, the lack of information on pre-crash events, and so on. Accordingly, more broad and international studies are needed to draw general robust conclusions on ABS effectiveness.

In addition to the standard and advanced braking systems currently on the market, in §2.2 the further steps forward an integrated safety for motorcycles were presented. Considering the MAEB system [11] a number of accident analyses were carried out to provide a preliminary evaluation of the potential benefits and limitation of the system [8, 42, 43, 44]. Savino et al. in [44] studied the potential effectiveness of the MAEB system over a representative, though small, in-depth crash database (55 PTW cases representing European crash configuration). The authors proved the beneficial effects of the system in the car-following scenario and in the crossing scenarios with a mean impact speed reduction of 2 m/s by the 67% of the cases (this value represents the estimated applicability of MAEB over all the accident scenarios). Then, in [43] it was proposed a complementary analysis to the previous one, assessing the potential benefits of MAEB using detailed crash reconstruction. 7 relevant fatal accidents involving a motorcycle and a car in rear-end collision were selected from the Swedish national in-depth fatal crash database and reconstructed in a virtual environment (PreScan®and Bikesim®). The accidents dynamics were simulated and investigated comparing the same scenarios with and without the implementation of the advanced braking system. The MAEB system turned out to be applicable and useful in the majority of the cases with benefits. In no case, the activation of the autonomous braking led to a reduction of vehicle stability or to an increase of collision risk. In particular the Enhanced Braking function (EB) (integrated in the MAEB logic) turned out to be the most interesting and useful element of the system, especially in those scenarios characterized by poor (and not sufficient) braking maneuvers performed by the rider.

MAEB represents an innovative solution for motorcycle safety and the results are encouraging. Nevertheless, this technology is still not ready to be applied on commercial PTWs. Deeper investigations on the effect of the autonomous braking on vehicle and rider dynamics should be addressed. In addition, the validity of the results must be extended to a higher number of scenarios, addressing different counties and communities, thus requiring further analyses with larger, representative databases.

These study demonstrated the potential benefits of the application of the autonomous braking in the described scenarios. The indications obtained from the presented analyses will help the next steps of MAEB development. In particular, they will be crucial for the development of the system deployment and inhibition criteria in order to avoid any false triggering as well as promptly activate the MAEB when a collision becomes unavoidable.

Chapter 3

Influence of braking on motorcycle Chatter

It is well known that motorcycle vibrations have a relevant influence on motorcycle stability and handling. Within several categories of powered two wheelers, these vibration modes and their characteristics can change significantly, and turn into disturbing motions for the rider. Some vibration mode can become unstable and make the vehicle control very complicated, thus leading to poor riding performances and increasing the risk of crash. It is possible to find the basic modes in all the PTWs, of course with different characteristics depending on the structural and dynamical features of the vehicles.

In case of braking, the vibrational behaviors of the motorcycles change significantly (for some running conditions some vibration modes can be exited and turn into unstable). The investigation of the modes that most affect the vehicle dynamics during braking is fundamental to understand their influence on the PTW dynamics for different braking scenarios and to point out their effect, in general terms, on vehicle stability.

In the next paragraphs, the influence of vibration modes on PTW dynamics will be addressed. In particular the attention will focus on the relation between the rear frame instability and the *Transmission* mode in case of emergency braking involving a high performance motorcycle.

3.1 Motorcycle behavior during a braking maneuver

In terms of stability, the motorcycle is strongly affected by a number of vibration modes that can influence the steering stability, the suspension movements, the chassis movements and so on. The vibration modes most investigated are the well known *Wobble*, *Weave*, *Rear Hop* and *Front Hop* [45, 46, 47]. Those modes have a direct influence on the handling and maneuverability of the vehicle and their vibration frequency range is usually less than 10 Hz and the damping ratios are limited (depending on the running conditions). They have a relevant influence on control and stability of the vehicle because, in case of unstable conditions, they affect directly the steering axle and the mainframe oscillations (in *Weave* these movements

are coupled). *Front Hop* and *Rear Hop* that possess high vibration frequencies and safer damping ratios (negative Real part of the eigenvalues) influence the motorcycle pitch behavior (directly related to the suspensions dynamics). In recent years another vibration phenomenon named *Chatter* has been studied. This mode is usually observed during racing competitions and it mainly concerns sports-racing motorcycles. It is a vibration mode that it is possible to find (by modal analysis) not in all the motorcycles. *Chatter*, differently from *Wobble* and *Weave*, is a structural mode and, to be observed, it requires a vehicle model with specific features of the transmission assembly and specific properties (stiffness and damping) of the chassis and the front and rear frames (front fork, front head, swingarm, etc.). The *Chatter* vibration, differently from *Wobble* and *Weave*, is characterized by high-level frequencies, over 20 Hz; it involves all vehicle body, and depending on the *Chatter* subcases investigated, it can influence different parts of the vehicle assembly.

The studies on this topic are quite few due to the complex analysis of this vibration mode, though recently there is growing interest about *Chatter*, since the phenomenon occurred in MotoGP races involving different competitors.

Cossalter et al. in [48] presented a detailed analysis of the *Chatter* vibration, using simulations and experimental data, investigating the motorcycle dynamics under straight running conditions and braking along a straight path, and while cornering, and gave a physical interpretation to the phenomenon.

The *Chatter* highlighted by the authors has a vibration frequency around 20 Hz and the origin of the mode can be found in the flexibility of the transmission system. Therefore, this *Chatter* subcase has been named *Transmission*. According to authors, the *Chatter* characterizes the motorcycle vibration mainly at the beginning of a curve (involving braking) but the rider can clearly perceive it while cornering.

Massaro et al. [49, 50] in 2011 showed the relation between the transmission properties and the *Chatter* vibration, thus highlighting the influence of different drive transmission characteristics on the vibration behaviors of the motorcycle, focusing in particular on the *Transmission* mode response.

In [51], Cossalter et al. carried out a virtual analysis of the *Chatter* vibration presenting the continuation of the research activity presented above. The authors investigated in depth the correlation between the *Transmission* mode instability and the drive transmission properties, thus pointing out the influence on *Chatter* of the transmission components, such as the sprocket absorber, the gear ratio, the braking conditions and the presence of the engine brake.

According to Cossalter, Massaro et al. the general *Chatter* phenomenon is expected to be influenced also by structural properties of the vehicle and some modifications to the body structure could potentially change the *Chatter* influence on vehicle dynamics.

Sharp and Watanabe in [52] indicate how much the *Chatter* behavior can be influenced by the motorcycle structure design and the test conditions. The authors focused the analysis only on *Chatter* response to different chassis flexibility properties, considering a sports motorcycle running on steady cornering. The authors do not address the *Chatter* mode influenced by the transmission components, but they focus the attention on the subcase of the mode influenced by the torsional

front head flexibility and fork lateral bending. Differently from the *Transmission* mode, this mode investigated by Sharp has an oscillation frequency around 25 Hz (the other is around 20 Hz). The study highlights how much the *Chatter* mode reduces its stability as soon as the running conditions proceed through larger roll angles at higher speed.

In [53] Massaro et al. extended all the previous research activities on *Chatter* introducing a more detailed new analytical vehicle model to analyze. The authors find out the *Chatter* subcases previously described, due to transmission and torsional stiffness of the chassis, and also describe a third mode caused by the fork longitudinal bending, characterized by a vibrational frequently over 30 Hz. The three different subcases of *Chatter* are named *Chatter1* (the mode previously named *Transmission*), *Chatter2* (due to torsional properties of the chassis) and *Chatter3* (due to longitudinal fork compliance), to highlight the temporal order in which these modes have been studied.

The aforementioned works show that an advanced multi-body motorcycle model is needed to investigate in detail the *Chatter* vibration in different running conditions. In particular, the definition and the accuracy of the non-rigid elements of the vehicle, such as the suspensions, the tires and the drive transmission assembly play a key role in the characterization of the phenomenon.

The relevance of *Chatter* in emergency (hard) braking manoeuvres requires an in-depth study in order to develop appropriate design and real-time control solutions to limit the instabilities the vibrational phenomenon can introduce on the vehicle.

Accordingly, during the research activity the *Chatter1* was investigated using a detailed motorcycle model reproduced in SimMechanics, focusing the attention on the vehicle dynamics during hard braking maneuvers along a straight path and on steady cornering. The influence of different braking torques and distributions on the vehicle vibrations by modal and time-domain analyses was investigated, thus highlighting the differences between normal and hard (emergency) braking conditions in terms of motorcycle dynamics and braking performances. Finally the influence of the frame flexibility on the *Chatter1* mode is pointed out by comparing the dynamic response of different chassis designs, in case of straight braking.

3.2 Motorcycle multibody model for Chatter analysis

The virtual motorcycle model used for the *Chatter* investigation was built in Matlab/SimMechanics virtual environment. The motorcycle represented is a large touring motorcycle 1300cc, comparable to the vehicles used for the simulations by Fujii et al. [54] and Teerhuis et al. [55].

The vehicle reproduced in SimMechanics, has been build according to the geometrical, inertial and mass characteristics of the real motorcycle during other research activities [55], and each part of the real vehicle was measured and reproduced in virtual environment.

The virtual model of the motorcycle in (Figure 3.1, [54]) consists of 10 rigid bodies representing the main frame (chassis), the upper part of the front fork, the lower part of the front fork, the rear swing arm, the arm relay, the engine, the

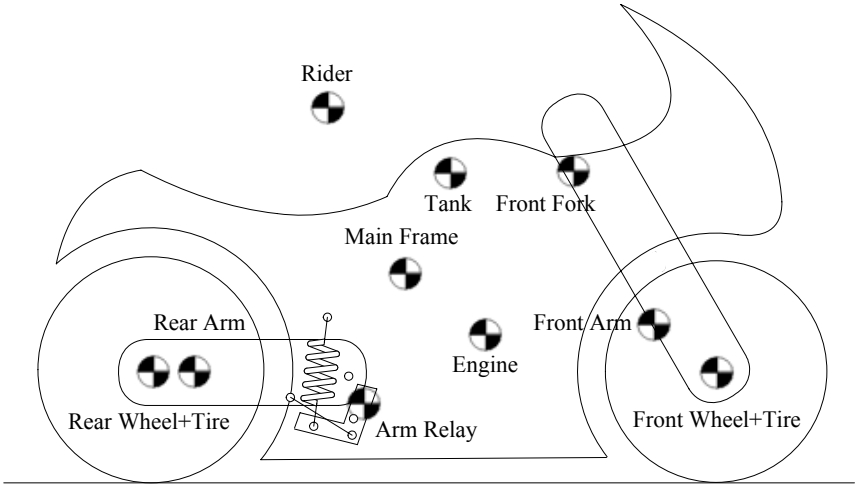

Figure 3.1: Representation of the different bodies composing the motorcycle multibody model

tank, the rider, and the front and rear wheels. The bodies are interconnected by joints (rotational and prismatic) and in total, the system has 13 degrees of freedom (DoF).

The front and rear wheels are characterized by the MF-Tyre provided by TNO. The standard features of the front and rear tires of the real bike were implemented on the vehicle, thus giving the possibility to investigate the vehicle behaviors with the support of a validated tire model.

The tire properties used during the research activity were:

- Tire side: symmetric
- Contact method: smooth road
- Dynamics: relaxation behavior
- Slip forces: combined

MF-Tyre developed by TNO represents the tire dynamics by the implementation of the Pacejka's *Magic Formula*, including also a number of aspects such as the effects of inflation pressure and estimation of combined slip behavior. By that tire model, it is possible to simulated validated steady state and transient behavior up to 8 Hz, making it the ideal tire model for handling and control prototyping analyses. The good correspondence between this virtual model under investigation and the real vehicle is demonstrated by a number of publications [56, 45, 57, 55] involving the same virtual motorcycle model.

Finally, the last remarkable properties of the virtual motorcycle are the following: the front and rear suspensions have non-linear behaviors, the rider body is rigidly connected to the main frame and the aerodynamic forces acting on the vehicle are taken into account.

In the first part of the analysis no flexibility properties of the chassis, of the front assembly or of the swingarm were considered. As already stated at the beginning of the chapter the flexibility properties of the vehicle are fundamental to reach an in depth investigation of the *Chatter* behaviors, in particular for *Chatter2* and *3*. However it was decided to focus mainly on the effects coming from the transmission components and *Chatter1* to study the first and most evident "component" of the *Chatter* and to give solid basis to set up, in future activities, the analysis of the other subcases of the *Chatter* mode.

Controller

The vehicle shown in the previous paragraph is controlled by a system composed of a PID (Proportional-Integral-Derivative) controller for the steering torque and a PI controller for the driving torque. The inputs to the PID/PI controllers are function of the simulation set-up. The main control parameters are the target roll angle and the target speed to follow during the test. Concerning the steering torque control, it is possible to generalize the PID action with the following equation:

$$\tau_s = k_p \cdot (\varphi_{actual} - \varphi_{ref}) + k_d \cdot \dot{\varphi}_{act} + \int k_i \cdot (\varphi_{act} - \varphi_{ref}) dt \tag{3.1}$$

where τ_s is the steering torque given to the controller, φ_{actual} is the actual roll angle, φ_{ref} is the reference roll angle and k_p, k_d and k_i are the proportional, integral and derivative gains of the controller.

More in detail k_p and k_d are function of the speed, according to the following equation (preliminary tuned with Ziegler-Nichols approach[1] then finally derived experimentally with trial and error methodology during the controller tuning process):

$$k_p = 47.7 \tag{3.2}$$

$$k_d = k_p \cdot 0.165 \cdot C_f \tag{3.3}$$

$$C_f = -8.7 \cdot log(Vx) + 34.5 \tag{3.4}$$

In addition, to provide a further stability to the control system a fixed small Integral gain, k_i was added to the final control architecture. The value k_i was kept small in order to reduce the fluctuation of the control.

As example, the final layout of the steering torque controller is schematized in Figure 3.2.

[1]The Ziegler-Nichols (Z-N) methodology is a classic method used for PID tuning in automotive applications. This heuristic method is widely used for controllers tuning due to its easy application. In fact, it does not require a mathematical model of the system under control. The method is based on the evaluation of the best system response (in closed loop) using a step input (k): starting from safe PID values (stable response, no oscillations, but slow), from the system response analysis the critical gain k_p (from safe PID configuration) and the parameters a and T can be evaluated (see [58]). It is important to underline that the Ziegler-Nichols methodology is effective on simple dynamic systems with few degrees of freedom. In motorcycle model under investigation

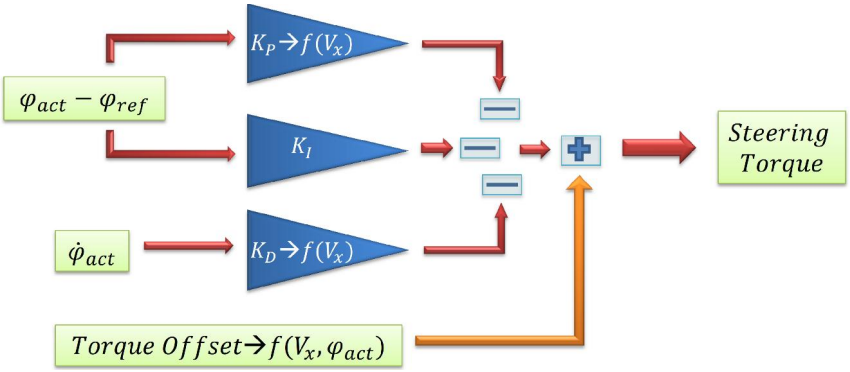

Figure 3.2: Layout of the PID steering torque controller

To reach the reference input values of speed and roll angle, fix offset values are added to the PID output for the steering controller. The torque offsets given to steering torque controller (also to the speed controller) depend on the combination of roll angle and vehicle speed (actual values).

The entire set of torque offsets, both for drive torque offset and steering torque offset, was computed both using a trial-and-error methodology, from a set of simulations of steady state curves at different roll angles and different speeds, and deriving analytically the relations between roll, speed and toque offsets.

The offset to the steering torque controller was given to provide additional robustness to the control and fast reaction as well (to compensate the small value of k_i).

3.2.1 Transmission Model

According to Cossalter et al. [48, 51] and Massaro et al. [50] [49] [53] a drive transmission model (chain actuated) it is necessary to investigate the vehicle modal behavior during unsteady state maneuvers. The influence of the transmission compliance on the motorcycle stability is not negligible, especially for maneuvers such as braking, cornering and lane change. The transmission stiffness, the gear engaged, etc., strongly affect the in-plane vibration modes. Moreover, the effects related to the transmission model, implemented in the vehicle, influence the motorcycle handling as well.

Therefore a chain transmission system was introduced in the model described in §3.2. Since the transmission layout adopted does not respect the current configuration of the real vehicle (it is shaft driven), the work carried out on that model should be considered as a case study to get preliminary information on the possible effects of the chain transmission on vehicle dynamics.

The chain transmission model implemented on the motorcycle is composed of two

---

the assembly has 13 DoF and non-linear behaviors. For this reason it is clear that the PID controller, tuned by the Z-N algorithm, cannot be the final solution for the motorcycle control, nevertheless it can be assumed as a good starting point for the optimization process.

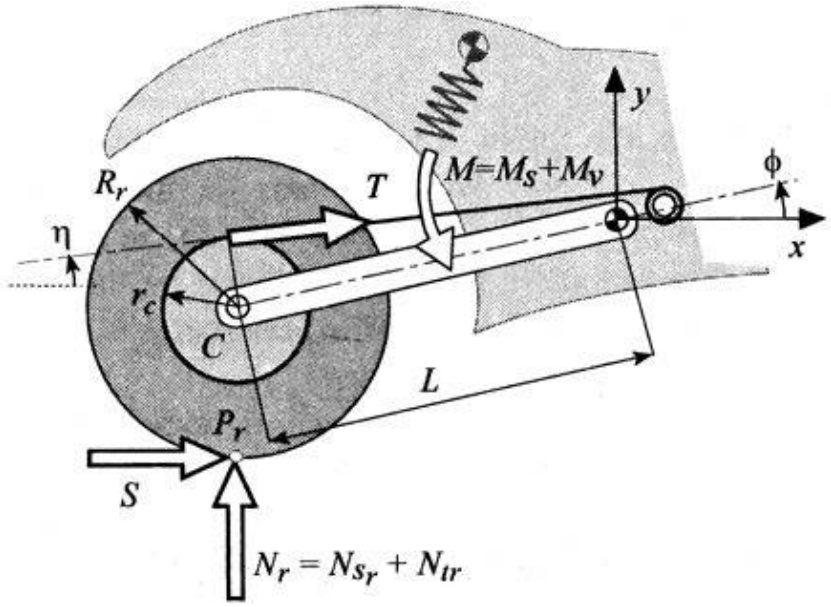

Figure 3.3: Effects of the chain transmission on the rear frame dynamics [5]

main parts, the subsystem for the computation of the transmission influence on rear swing arm and the subsystem representing the virtual model of the transmission.

The implementation of the first aforementioned subsystem was necessary due to the layout of the second subsystem. In fact, the virtual model of transmission is not directly installed on the vehicle but it is separated. Hence, an additional algorithm for the computation of the chain transmission effects on the swing arm was needed (mainly to take into account the effects related to chain force for different positions of the swingarm). The chain effects on the rear frame are depicted in Figure 3.3.

The subsystem takes into account the effect of the chain forces on the swingarm equilibrium according to Cossalter [5].

Looking at Figure 3.3, the following equation describes the equilibrium of the moments acting on the swingarm:

$$M_v = N_{tr} \cdot L \cdot cos(\phi) - S \cdot (R_r + L \cdot sin(\phi)) + T \cdot (r_c - L \cdot sin(\phi - \eta)) \quad (3.5)$$

where N_{tr} is the load transfer, L is the swingarm length, ϕ is swingarm inclination angle, S is the traction force (or braking force in case of braking action), R_r is the wheel radius, T is the chain traction force and η is the inclination angle of the chain[2]. The aforementioned equation can be summed up as follows:

$$M_v = M_{load\ transfer} - M_{drive/brake\ torque} - M_{trim} \quad (3.6)$$

[2]In the equation the static elastic moment of the suspension was neglected because it is equal to the negative moment generated by the static vertical force.

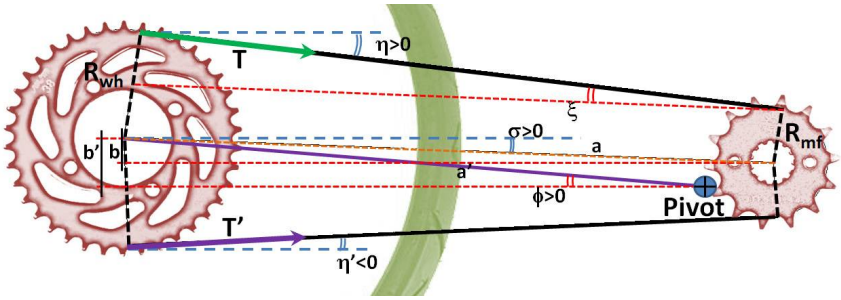

Figure 3.4: Chain transmission geometry

It is worth noting that M_{trim} must address properly the torque given by the chain in case of driving or engine brake.

In Figure 3.4 a geometrical sketch of the chain transmission is represented.

Chain transmission subsystem

The model of the chain subsystem has been implemented by SimMechanics. It is composed of the following elements:

a) Engine shaft

b) Clutch

c) Primary shaft

d) Secondary shaft

e) Gearbox

f) Chain

g) Sprocket absorber

The elements from a) to e) were built using SimMechanics toolbox, while the elements f) and g) were built using SimScape toolbox. The use of a different toolbox for the chain block was due to some limitations of the SimMechanics software. In fact, a system built using SimMechanics should be easily outlined as a set of rigid bodies and joints. Then a real chain cannot be easily implemented using only joints and bodies. Moreover, there is not any element among SimMechanics blocks that can be used to represent the chain linear flexibility. For these reasons, the Chain (and the sprocket absorber) has been implemented using SimScape. The general layout of the complete transmission is shown in Figure 3.5.

About the clutch, the engagement/disengagement phase is realized by an algebraic loop.

Finally, about the final transmission part, the chain interaction is composed by SimScape®blocks representing a sports motorcycle chain pinion on the secondary shaft, the chain sprocket on the rear wheel, the linear deformation of the chain,

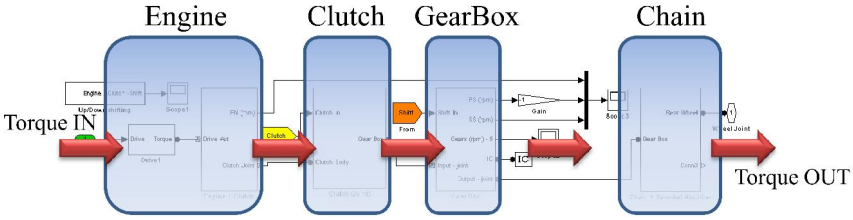

Figure 3.5: Schematization of the transmission layout

etc. The stiffness and the damping ratio selected for the model were $2 \cdot 10^7$N/m and 100 Ns/m. While the damping ratio was chosen according to Xu et al. [59], the stiffness was computed considering the chain as a double, long steel plate, with a cross section equal to the cross section of a standard sports motorcycle chain.

3.3 Analysis of Chatter during braking

The transmission model has a remarkable influence on the vehicle dynamics. From the comparison in Figure 3.6, it is possible to see that, as a consequence of the transmission compliance, the in-plane vibration modes directly influenced by the transmissions behaviors, like *Rear Spin* and *Rear Hop*, are strongly affected and their frequencies, compared to the modal graph of the motorcycle model without transmission, decrease respectively from 135-165 rad/s to 90-95 rad/s and from 88-89 rad/s to 81-82 rad/s. Moreover, real values of the *Rear Spin* increased for high speeds, thus moving the mode to less stable conditions. The remaining vibration modes, already showed in the modal analysis of the original model, are slightly influenced by the transmission compliance.

The names given to the vibration modes are in accordance with the eigenvectors analysis made on every mode (e.g. Figure 3.7).

The vibration mode over 20 Hz is the *Chatter1* mode. In the next part of the chapter this mode will be addressed as *Transmission* mode, according to [50]. Its presence is due to the non-rigid chain transmission system. It is strictly related to the interactions between the rotational elements of the transmission system and the rear wheel. As a matter of fact the eigenvector of the *Transmission* mode, in case of 150 km/h, in straight running, shows that the main element affecting the mode is the fluctuation of the rotational elements of the transmission assembly and the rear wheel.

The *Transmission*, *Rear Hop* and *Rear Spin* are the modes most influenced by the elastic properties of the new transmission model, implemented on the vehicle.

As the absorber becomes more rigid, the frequencies of the three modes increase. On the contrary, the damping ratio decreases in the *Transmission* mode and *Rear Hop* and it increases in *Rear Spin*. For a rigid transmission (including a rigid chain and a rigid sprocket absorber) the *Transmission* mode disappears.

The analysis presented in Figure 3.6 was extended to braking maneuvers to study the influence of the transmission mode on the motorcycle dynamics in case

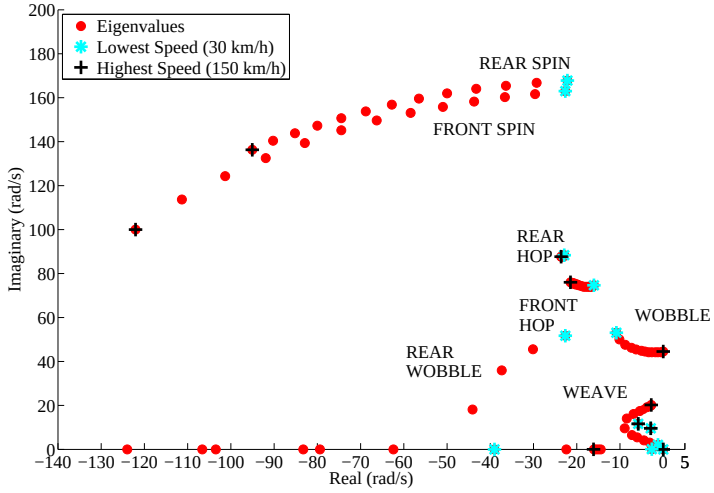

(a) Root locus of the motorcycle vibration modes, for a multibody model with a rigid transmission

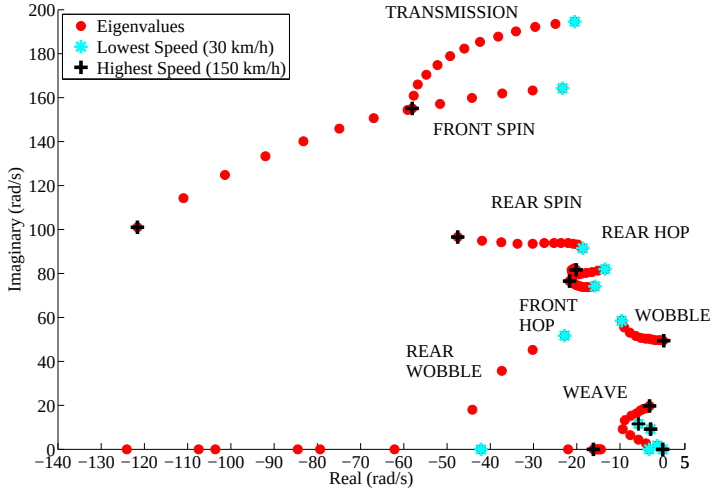

(b) Root locus of the motorcycle vibration modes, for a multibody model with a flexible transmission

Figure 3.6: Root loci of the motorcycle vibration modes, for a multibody model with and without a rigid transmission, running on a straight path. The red dots represent the eigenvalues of the different vibration modes, at different running speeds, from 30 km/h to 150 km/h. The cyan stars are the eigenvalues at the lowest speed, for each mode; the black crosses represent the eigenvalues at the highest speed, for each mode

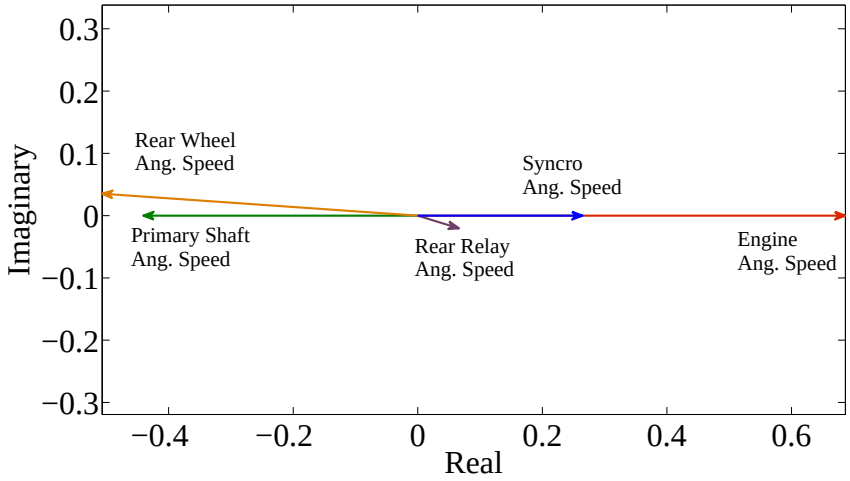

Figure 3.7: Example of eigenvector of the *Transmission* mode. Straight running at 150 km/h

of braking. The investigation aims to find out in which running condition and for which events the *Chatter* can decrease the vehicle performances, and stability as well.

The behavior of the motorcycle related to *Chatter1* has been analyzed for different braking maneuvers, considering straight running and steady state cornering. In particular, the analysis of the non-linear model is carried out using different braking torques, braking force distributions, target roll angles, target speeds and gears engaged.

For the simulations reproducing braking maneuvers along a straight path, the modal analysis is used to describe the motorcycle dynamics in common braking conditions, involving braking torques up to 500 Nm for the front brake and 380 Nm for the rear brake, leading to longitudinal decelerations up to 5 m/s^2. Then, the time-domain analysis is used to investigate hard braking maneuvers, involving braking torques over the torque limits specified above. The frequency-domain analysis is not used for hard braking maneuvers due to unsteady state conditions of the vehicle during the braking phase. Differently from the model of Massaro et al. [51], that is completely analytical, the model adopted for the analysis presented in this chapter is numerical. Therefore, it is not possible to define arbitrarily the initial conditions for the linearization, but it is necessary take the initial conditions from the final layout of the simulations under investigation. That procedure implies that the final conditions of a sequence of simulations should be coherent and related.

Summing up, the standard modal analysis method, with a numerical multi-body model, requires steady state conditions to linearize the vehicle model, however the high vibrations that arise during high decelerations generate highly unsteady conditions and the corresponding modal analysis does not shows clear results. According to Massaro, using an analytical model [51], it is possible to bypass the aforementioned problem by modeling the maneuver as steady state motion adding

specific apparent forces as inputs to the linearized vehicle model.

Notwithstanding, also with the analytical model, linearized for unsteady maneuvers, it is not possible to get detailed indications about the behaviors of such maneuvers, that are intrinsically non-linear.

Therefore, to highlight the nonlinear behavior of the motorcycle the time-domain analysis is adopted for the investigation of the hard braking maneuvers. In particular, the time-domain analysis is used to characterize the unstable behaviors of the motorcycle during different phases of the braking manoeuver.

3.3.1 Braking on straight running

Modal Analysis

The maximum braking torques of 500 Nm for the front wheel and 380 Nm for the rear wheel have been considered to evaluate the modal response of the vehicle subjected to front and rear braking on a straight path. Over those limits the non-linear behaviors of the tires and the transmission start to be relevant, thus reducing the possibility to carry out a clear modal analysis. Therefore, for higher braking torques the time-domain analysis was addressed.

It is important to point out that concerning the modal analysis, the model linearization concerns only the vehicle, without the controllers.

Below 500 Nm for the front wheel and 380 Nm for the rear wheel each maneuver has been investigated considering the same initial speed (150 km/h) and the same gear (4^{th}) engaged. The status of the motorcycle has been computed during the braking phase, after the motorcycle reached a steady deceleration, thus neglecting the initial part of the deceleration characterized by relevant unsteady oscillations of the vehicle suspensions. Therefore, the motorcycle status has been addressed between 110 km/h and 60 km/h, in each braking maneuver.

Figure 3.8 shows the root-locus of a braking manoeuver on a straight path for different braking torques applied only on the front wheel. As expected the *Front Spin* mode, the *Front Hop* and the *Wobble* are influenced by this maneuver. More precisely the influence of different torques is clearly visible on the *Front Spin* mode; *Front Hop* and *Wobble* show minor changes. Also the *Transmission* (or *Chatter*) mode is lightly influenced by the front braking, in particular for high braking speeds (the beginning of the maneuver). Looking at the *Rear Spin* mode only negligible changes are detected.

This dynamic behavior of the motorcycle under front braking is directly related to the load transfer: as soon as the load transfer and the braking force on the front wheel increase, the influence of the braking maneuver on the steering torque and on the steering bar handling increases as well. Accordingly, the vibration modes strictly related to the front frame, show more significant changes compared to the modes mainly related to the rear frame and the transmission compliance.

In Figure 3.9 the root-locus for different braking torques applied only to the rear wheel is depicted. Under these braking conditions the *Front Spin* mode (the mode mainly influenced in front braking) is not significantly affected since the braking action does not affect directly the front frame. The *Transmission* shows a decreasing stability, thus a lower damping ratio, as soon as the braking torque, thus

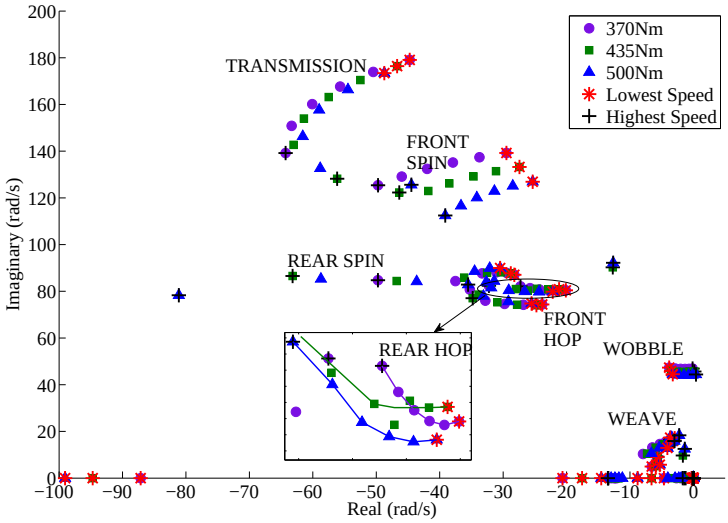

Figure 3.8: Root locus of front braking on a straight path. Braking torques: 500, 435 and 370 Nm. Gear engaged: 4^{th}. Initial speed: 150 km/h; Highest br. speed: 110 km/h; Lowest br. speed: 60 km/h. Speed step for the analysis: 10 km/h

the deceleration increases. Moreover the root locus shows that the *Transmission* mode is more stable for higher initial braking speeds, that is at the beginning of the braking maneuver. Finally, about the *Rear Spin* mode, the vibration frequency decreases as soon as the torque increases and the mode becomes more stable as well. It is supposed that for higher torques, the vibration frequency of this mode tends to zero.

In case of distribution of the braking force on front and rear brakes (Figure 3.10) the maneuver turns out to be more stable, if compared to the previous cases. Due to the concurrent application of the front and rear braking forces, the vibration modes related to the front frame and the rear frame show a limited number of changes for different torques. The variations about frequency and damping ratio remain limited, thus showing minor effects on the vehicle stability.

Time-domain Analysis

To investigate the non-linear characteristics of the motorcycle subjected to hard braking, the time-domain analysis was carried out for different braking strategies involving braking torques over the limits imposed for the modal analysis. In accordance with the modal analysis the tests considered the same initial speed of 150 km/h and the braking maneuvers were performed in 5^{th} and 4^{th} gear.

In case of hard braking, as the braking torque increases on the front wheel (Figure 3.11), the initial phase of the manoeuver is characterized by relevant non-

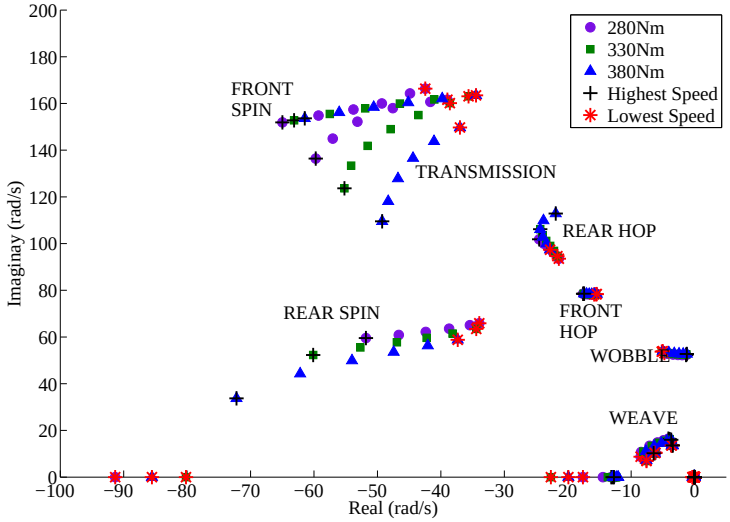

Figure 3.9: Root locus of rear braking on a straight path. Braking torques: 380, 330 and 280 Nm. Gear engaged: 4^{th}. Initial speed: 150 km/h; Highest br. speed: 110 km/h; Lowest br. speed: 60 km/h. Speed step for the analysis: 10 km/h

periodic pulses. The picture depicts the vertical accelerations, the suspensions travel, the longitudinal and vertical forces of the front and rear wheels during the braking maneuver.

In case of cornering, such pulses on the front frame would generate relevant oscillation of the vehicle, thus decreasing the vehicle stability. The steering behavior would be less stable due to high accelerations that arise on the front wheel during the first phase of the braking manoeuver and such accelerations would make the vehicle difficult to control.

Notwithstanding, the pulses on front wheel and on the rear wheel decrease as the speed decreases (only the initial phase of the braking maneuver turns out to be crucial for the vehicle control and the braking performance due to the aforementioned high wheel accelerations). According to the modal analysis, the chain transmission compliance does not affect the vehicle stability during front braking and the effects of the driving system are minor if compared to the effects due to the front tire dynamics.

The braking simulations involving only the rear brake were performed following the same procedure described at the beginning of the paragraph (with a braking torque over 380 Nm and initial speed of 150 km/h).

It is worth noting that hard braking maneuvers only on the rear wheel lead to the *Chatter* phenomenon in case of braking actions close to the friction limit. The interaction of the transmission elements added to the non-linearities of the tire induces relevant vibration on the rear frame as well as on the whole vehicle. Thus

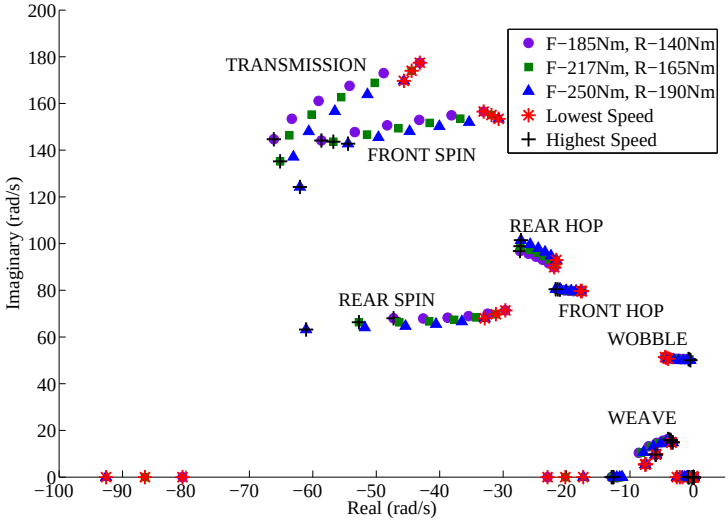

Figure 3.10: Root locus of combined braking on a straight path. Braking torques: front 250, 217 and 185 Nm - rear 190, 165 and 140 Nm. Gear engaged: 4^{th}. Initial speed: 150 km/h; Highest br. speed: 110 km/h; Lowest br. speed: 60 km/h. Speed step for the analysis: 10 km/h

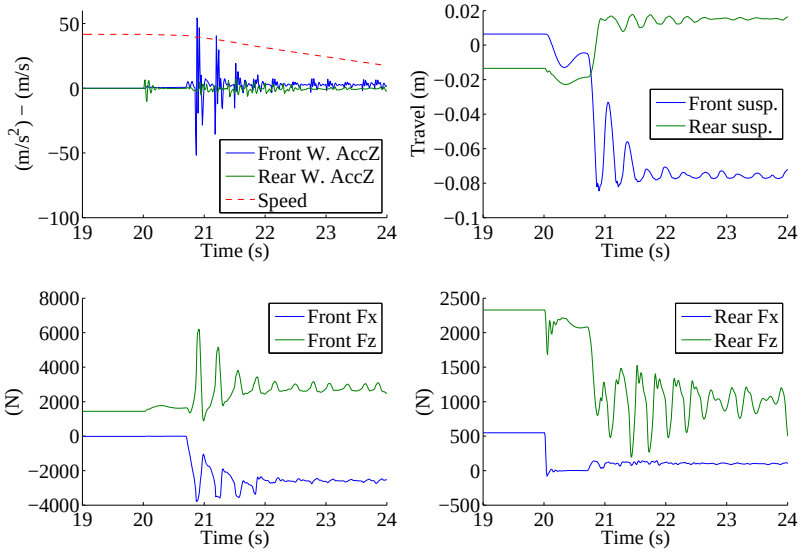

Figure 3.11: Time-domain analysis of front braking on a straight path for hard braking conditions. Braking torque: 740 Nm. Gear engaged: 5^{th}. Initial speed: 150 km/h

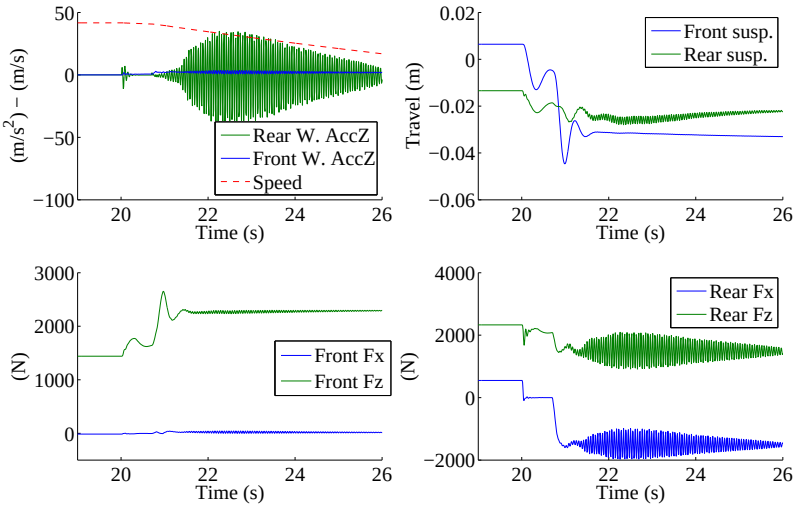

Figure 3.12: Time-domain analysis of rear braking on a straight path for hard braking conditions. Braking torque: 470 Nm. Gear engaged: 5^{th}. Initial speed: 150 km/h

pointing out the effect of *Chatter1*. Considering the motorcycle under investigation it was found that the *Transmission* mode reaches the unstable area (unstable vibration of the front and rear frames) for braking torque exceeding 425-470 Nm. Figure 3.12 shows an example of *Chatter* vibration occurring on the rear wheel.

The graph depicts a braking maneuver performed with only the rear brake, using a braking torque of 470 Nm, with the 5^{th} gear engaged during the simulation. It is possible to see that as soon as the vehicle starts to slow down its speed, the rear wheel vibrates with high amplitude, leading the wheel acceleration on the z-axis over 3 g. The graph shows the influence of the rear wheel pulses on the front frame, even if the values remain below 0.3 g. Within the aforementioned braking conditions, the vehicle is influenced by the *Chatter* mainly in the first part of the braking phase and, as the vehicle speed decreases, the *Chatter* decreases as well.

Even if these pulses do not reach relevant values, they can strongly affect the riding style and this usually results in poor riding performances.

In case of higher braking torques the *Chatter* vibration tends to get worse: for harder braking maneuvers, the *Chatter* vibrations increase as well, thus reaching high amplitudes and leading vertical wheel accelerations close to 20 g. In Figure 3.13 the vehicle response for a braking maneuver only on the rear wheel, with 560 Nm of braking torque, is shown. Considering the previous case, almost 100 Nm of difference cause significant changes in the results. The *Chatter1* occurs as well: under these braking conditions, it is more powerful and the vibrations are not damped. The amplitude of the pulses on the rear and the front wheels is twice the

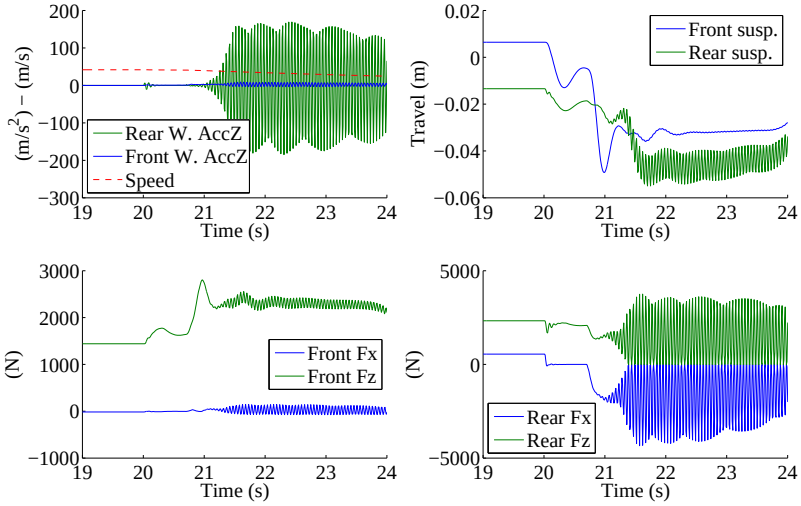

Figure 3.13: Time-domain analysis of rear braking on a straight path for hard braking conditions. Braking torque: 560 Nm. Gear engaged: 5^{th}. Initial speed: 150 km/h

amplitude of the 470 Nm case. Moreover, the braking maneuver is no more safe and stable for decreasing speed because the vibrations are no more damped and they maintain the same amplitude until the end of the simulation.

It is important to point out that, the tires friction coefficients for those hard braking conditions are close to the friction limit. The actual friction coefficient, at the beginning of the manoeuver starts to fluctuate around the maximum value and the longitudinal slip starts to diverge in the final part of the braking manoeuver (always pulsing). That introduces, in addition to the high pitch instability due to the oscillations, a secondary issue related to the friction conditions. Anyhow, the instant and impulsive loss of adherence is not so critical for the vehicle control along a straight path and skilled riders can easily control the motorcycle trajectory. However, it is expected that under cornering or at corner entry the instant loss of adherence would critically reduce the lateral stability of the motorcycle, making the vehicle difficult to handle and control even for expert/professional riders.

The gear engaged influences the amplitude of the *Chatter* vibration as well. For high gears, thus low powertrain spin inertia on the rear wheel, the *Chatter* vibration has lower amplitude and it occurs for high braking torques. A comparison between two braking maneuvers, performed in 4^{th} gear and 5^{th} gear, with 560 Nm of braking torque is depicted in Figure 3.14. The graph shows relevant differences in the front and rear wheels accelerations on the z-axis, in particular in the first part of the manoeuvre. For increasing gear ratios (lower gear engaged) the influence of the transmission compliance and the wheel acceleration amplitudes increase and

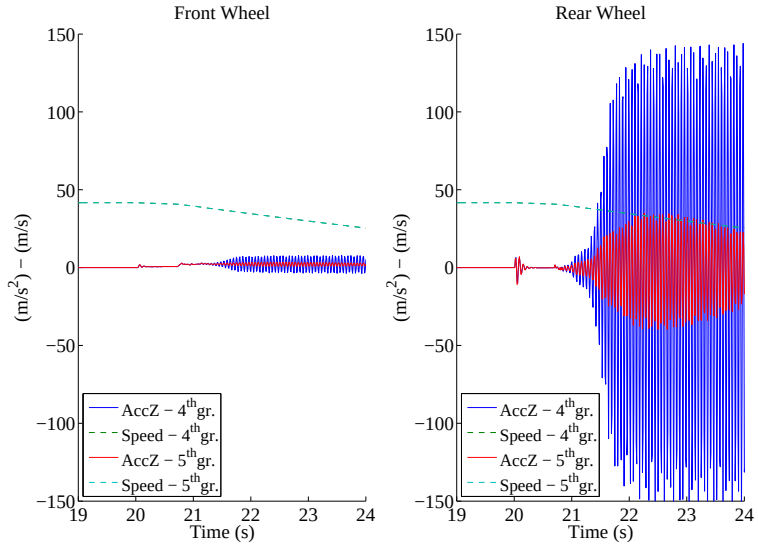

Figure 3.14: Time-domain analysis of rear braking on a straight path for hard braking conditions. Comparison between the same braking maneuver carried out in 5^{th} and 4^{th} gear. Braking torque: 560 Nm. Initial speed: 150 km/h

the time interval between the non-vibrating condition and the vibrating condition (periodical) decreases.

3.3.2 Braking on steady cornering

In the following paragraph, different braking strategies are analyzed under steady cornering. In addition to the simulation procedure adopted for the test run on straight path, the attention is focused on the influence of different initial speeds and different roll angles on the braking maneuvers and the vehicle stability as well. Also in case of steady cornering, the braking maneuvers involving only the front wheel reveal a stable *Transmission* mode in the whole simulation range. Since the front braking maneuver does not influence the unstable behavior of *Chatter1* only the tests involving rear braking are reported. The entire set of simulations was carried out as follows:

- Initial speed from 100 km/h to 150 km/h;
- Steady cornering, max roll angles: 10°, 20°, 30°and 40°;
- Braking Torques: 12 Nm-620 Nm (Front), 10 Nm-470 Nm (Rear);
- Braking distribution: only front braking, only rear braking;
- 5^{th} gear and 4^{th} gear engaged during the deceleration phase.

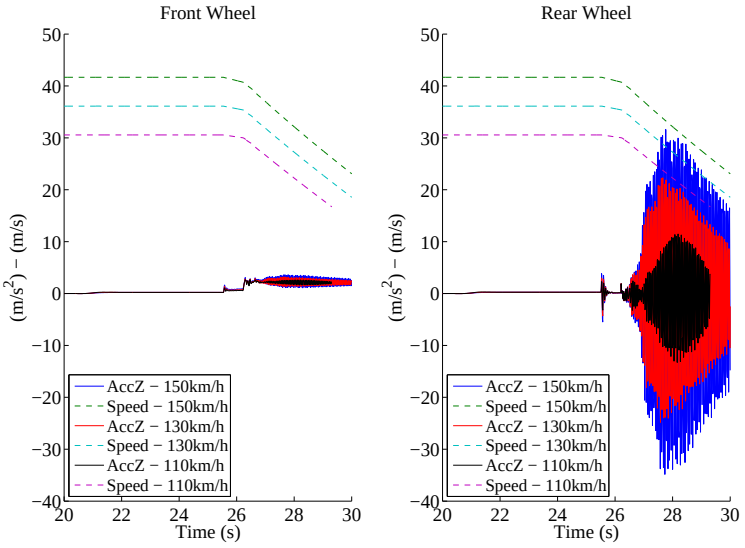

Figure 3.15: Braking on steady state cornering. Influence of initial running speed on *Chatter* behavior in case of rear braking. Roll angle: 10°. Braking torque: 470 Nm. Gear engaged: 5^{th}. Initial speed: 110 km/h - 150 km/h

The effect of different initial speeds on the vehicle dynamics during the braking manoeuver is clearly depicted in Figure 3.15. For "low" speeds, hard braking leads to restricted and damped *Chatter* behaviors (Figure 3.15). For higher speeds the *Chatter* vibration increases becoming a continuous oscillation on the front and the rear frames. Because of high vibrations during cornering, the tires friction coefficients show large variations, thus affecting the running performance of the vehicle.

The roll angle affects the rear hard braking maneuver as well. Figure 3.16 shows a comparison between hard braking maneuvers for different roll angles: it is worth noting that as the roll angle increases, the amplitude of wheels acceleration on z-axis (body-fixed system of reference) decreases and it becomes damped. Looking at Figure 3.16, it is worth noting that the variation of the *Chatter* vibration as a function of the roll angle could be influenced by the *Weave* mode: it is possible to recognize the standard *Weave* vibration frequency (up to 4 Hz for high speeds), on the front wheel. In particular, considering the vertical acceleration curve at 30°of roll angle, the oscillation frequency is approximately 1 Hz. Therefore, for larger roll angles the *Weave* mode influence on the motorcycle stability increases, thus becoming the most relevant mode.

The latter aspect becomes relevant also in terms of stability. The hard braking maneuver at 30°of roll angle introduces an oscillation motion on the vehicle that the rider cannot control. The lack of stability cannot be related directly to the *Chatter* vibration due to the low amplitude of the wheel acceleration (Figure 3.17),

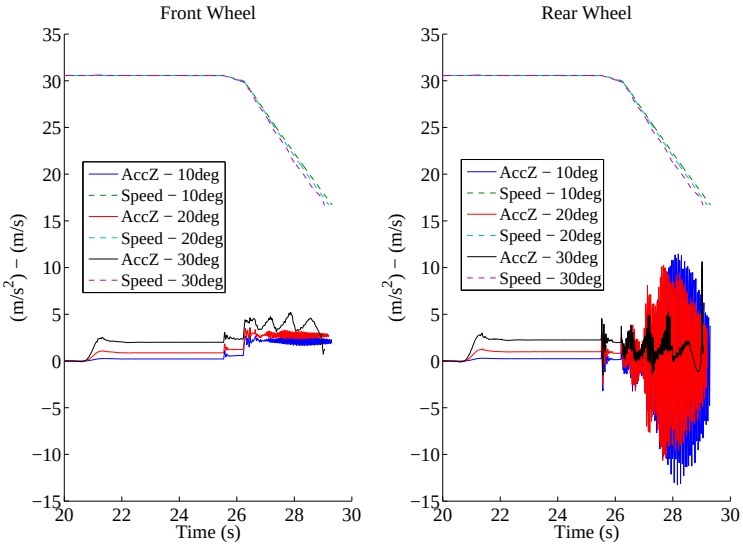

Figure 3.16: Braking on steady state cornering. Influence of roll angle on *Chatter* behavior in case of rear braking. Roll angle: 10°- 30°. Braking torque: 470 Nm. Gear engaged: 5^{th}. Initial speed: 110 km/h

however it is expected that the presence of *Chatter* would have contributed to excite the roll and yaw oscillations of the vehicle.

3.3.3 Influence of chassis properties on Chatter

According to Sharp et al. [52] and Massaro et al. [53] the studies on *Chatter* vibration should carefully consider also the influence of the motorcycle design on vehicle modal response. In particular the flexibility properties of the front frame assembly (longitudinal and lateral bending) and other flexile parts of the vehicle affect the *Chatter* (the general mode) of sports motorcycles. In addition, considering racing motorcycle, the vibration of the saddle around its connection point to the main frame should be considered for the vibration modes investigation as well. Usually in racing motorcycles, the saddle is designed as light as possible in order to reduce the total weight of the vehicle. However, the light structure characterizing the saddle frame is associated to a low stiffness, thus increasing the possibility for the riders to experience high *Chatter* vibrations coming from the saddle. Then, the relation between the *Chatter1* mode and the saddle flexibility was examined with a number of simulations, using a modified version of the SimMechanics multi-body model presented in §3.2. To simulate the saddle flexibility a new DoF was added, between the saddle and the main frame, characterized by a rotational stiffness and a rotational damping ratio. The rotation axis (y-axis) is perpendicular to the symmetry plane of the rear assembly (Figure 3.18).

The aforementioned model represents a simplified schematization of the flexi-

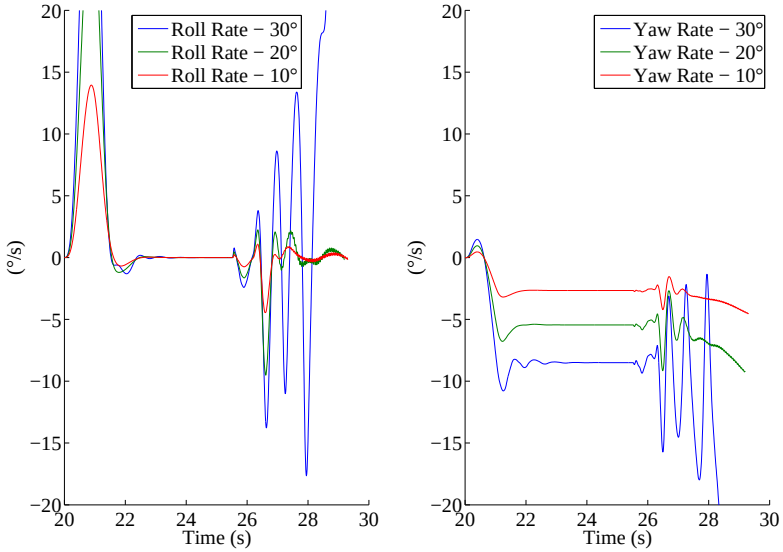

Figure 3.17: Braking on steady state cornering. Influence of roll angle on *Chatter* behavior in case of rear braking. Focus on the motorcycle roll rate and yaw rate for different roll angles. Roll angle: 10°- 30°. Braking torque: 470 Nm. Gear engaged: 5^{th}. Initial speed: 110 km/h

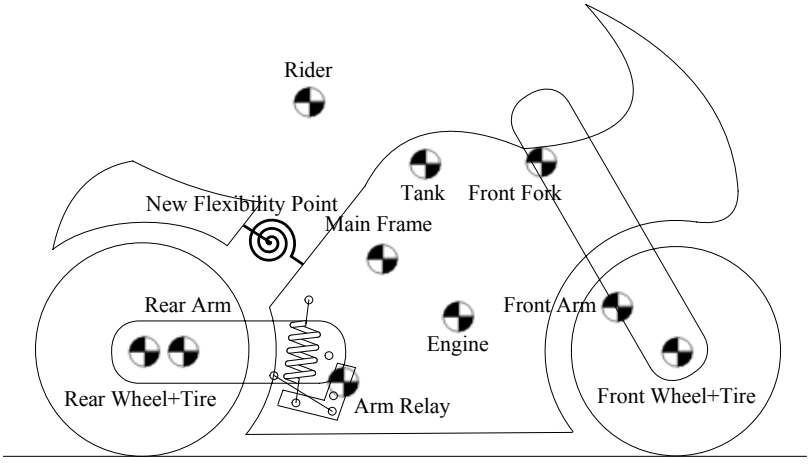

Figure 3.18: Schematization of the multibody model adopted for the investigation of the saddle vibration due to *Chatter1*

Table 3.1: Properties of flexibility of the rotational DoF representing the connection point between the saddle and the main frame

	Hard	Medium	Light
Torsional Stiffness (Nm/deg)	10^5	10^4	10^4
Damping Ratio (Nms/deg)	10^2	10^2	10^{-1}

bility properties of the saddle and it is not exhaustive. However the aim of this analysis is to obtain some general indications of the correlation between the design of the motorcycle frames and vibration of *Chatter1*, useful to derive the basis for a further study, thus involving more complex and detailed motorcycle virtual models. The investigation focuses the attention on normal and hard braking maneuvers (braking torques similar to §3.3.1), involving front and rear wheels, considering the vehicle running on a straight path at 150 km/h. The simulations performed with the original multi-body model (Standard) and the multi-body model with the flexible saddle (Flex) are compared.

Standard Model VS Flexible Model

The flexibility properties implemented during the simulations are reported in Table 3.1. The values adopted for the torsional stiffness were not directly measured on the real vehicle and they were set to perform a preliminary evaluation of the *Chatter* behavior for different flexibility steps. In comparison with the torsional stiffness of the main frame, the values assumed in Table 3.1 ranged between 20 times and 2 times those one introduced in [5].

The model with the highest value of stiffness and damping can be addresses as rigid. The modal analysis and the time domain analysis of the braking maneuvers using this flexibility features did not showed any relevant changes between the Flex Model and the Standard one. In particular, the *Transmission* mode is almost unchanged by the new flexibility point. It is worth noting the new degree of freedom in the system introduces a new vibration mode. However, since the stiffness values are tentative values and they do not refer to real vehicle properties, this new mode has not been addressed in the investigation.

Comparison of different Flexible Models

The influence of different chassis flexibility properties were investigated comparing the model configurations reported in Table 3.1. The models were compared considering different braking maneuvers during straight running, with an initial speed of 150 km/h.

The analysis of the front braking did not present any difference within the comparison. On the contrary, by the investigation of the rear braking, it was found that the influence of the flexibility properties is significant, and the vehicle dynamics is strongly affected.

Looking at the *Transmission* mode and *Rear Hop* in Figure 3.19, the modal analysis shows two main results: considering the *Transmission* mode at 380 Nm,

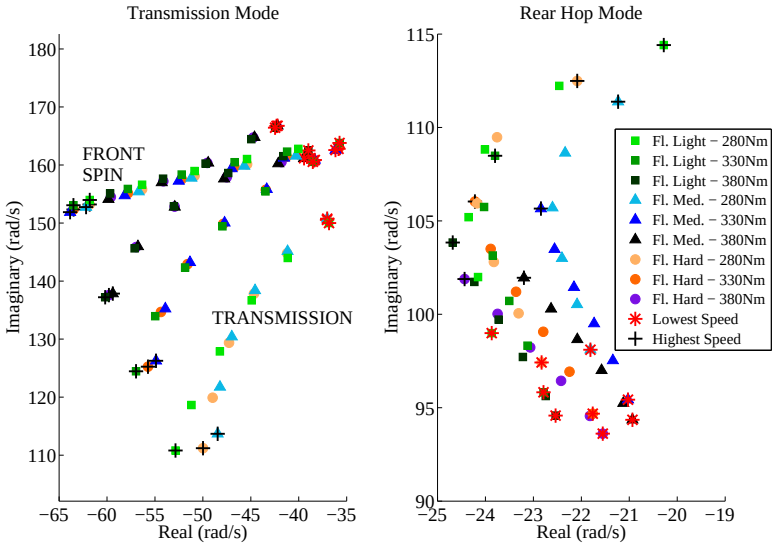

Figure 3.19: Root locus of rear braking on a straight path. Comparison between the three different flex model configurations. Zoom on *Transmission* mode and *Rear Hop* mode. Braking torque: 280 Nm, 330 Nm and 380 Nm. Gear engaged: 4^{th}. Initial speed: 150 km/h; Highest br. speed: 110 km/h; Lowest br. speed: 60 km/h. Speed step for the analysis: 10 km/h

the model *Light* (with the lowest stiffness and the lowest damping ratio) is the most stable and the model *Medium* is the least stable, in particular for high braking speed (at the beginning of the braking maneuver). Considering *Rear Hop* in low-medium braking speed range (at the end of the maneuver), *Hard* and *Medium* models are less stable than *Light* model, however for low braking speeds, the *Light* model becomes the least stable one.

The time domain-analysis gives some more indications on the differences between the non-linear behaviors of the three different flexible models.

As an example, the rear braking with braking torque of 470 Nm, 4^{th} gear, is depicted in Figure 3.20. For the flexible model *Light*, characterized by low damping ratio and low stiffness, in case of hard braking on the rear wheel, the *Chatter* vibration occurs with stronger oscillations on the front wheel, than the other models.

The graphs clearly show how much the model flexibility can influence the behavior of *Chatter1* and the vehicle dynamics for braking conditions close to the tire-road friction limit (longitudinal slip within 0.1 and 0.2).

Lower damping causes a faster increase of the *Chatter* vibrations, in particular on the front wheel. Moreover, the *Chatter* vibration becomes continuous and no more damped, both on the front wheel and on the rear wheel.

Looking the aforementioned results it is expected that different flexibility

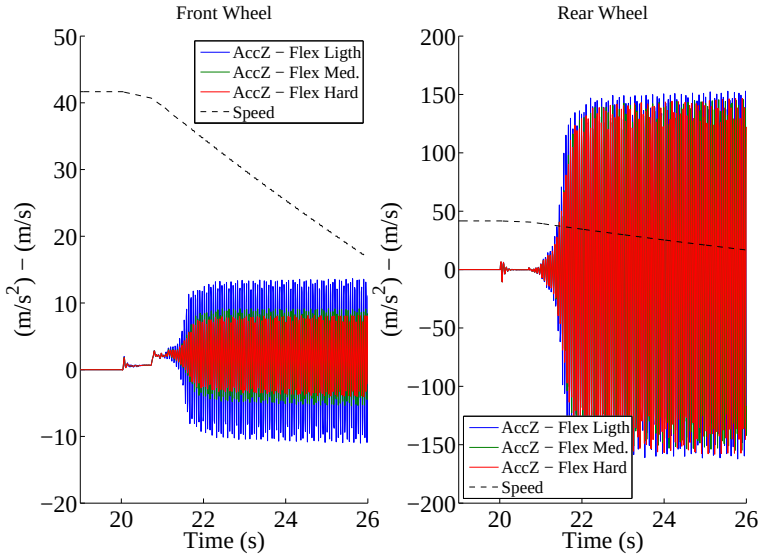

Figure 3.20: Time-domain analysis of rear braking on a straight path. Comparison between the three different flex model configurations. Braking torque: 470 Nm. Gear engaged: 4^{th}. Initial speed: 150 km/h

properties of the main frame, with respect to the one used in the simulations, could further affect the motorcycle dynamics and the riding performances, in other riding scenarios not investigated in this chapter, i.e. braking at corner entry or during the acceleration phase at the end of a curve.

3.4 Discussion

The simulations results pointed out interesting dynamic behaviors of motorcycles under hard braking maneuvers. In accordance with other valuable international research activities on motorcycle dynamics, the tests showed that the braking strategy defines the vibration behavior of the vehicle and it is crucial for the vehicle stability and the riding performances, on a straight path and while cornering. A braking maneuver involving only the front brake can lead to high decelerations and high braking performances; at the same time, it strongly affects the motorcycle steering control and, in case of high braking torques, it can cause high pulses on the front frame, thus decreasing the motorcycle handling performances. Therefore, a better force distribution (combined braking) can improve the vehicle control.

The pulses detected on the front wheel, as a consequence of full front braking, can be related to the combination of the non-linear properties of the tire and the front suspension. Accordingly, a different set-up in the front frame (e.g. active suspensions, or different suspension geometry) is expected to modify the vehicle response, in terms of vibrations, to the front braking maneuver.

In case of braking maneuver performed only using the rear brake, the braking effects on the steering control are minimized. Anyhow, the tests involving hard rear braking showed that during strong decelerations the transmission compliance (in case of clutch engaged) leads to high accelerations on the rear frame (transmitted almost simultaneously to the front). Those accelerations are characterized by high vibration frequencies and amplitude that exceeds 10 g, considering the wheels vertical axis.

This particular vibration mode, named *Chatter1* negatively influences the rider confidence and the riding performances. The analysis pointed out the influence of the vibrations on the vehicle dynamics during braking maneuvers performed in different test scenarios. In particular, the motorcycle dynamic properties most affecting the simulations are the initial longitudinal speed, the gear engaged and the target roll angle (in case of braking on steady state cornering). The results showed opposite vehicle behaviours related to the initial speed and the roll angle variations. As the vehicle speed increases the *Chatter* increases as well; on the other hand, the roll angle increase reduces the *Chatter* effects. As a drawback, the roll angle increase excites other modes, such as *Weave*, that negatively influence the motorcycle dynamics.

In addition to the running conditions, different designs can influence the vehicle *Chatter* as well. The introduction of a new degree of freedom, representing the flexibility properties of the connection area between the saddle and the main frame, showed that lower stiffness and lower damping values (typical of racing motorcycles) excite the wheels vibration, in particular the front wheel. In future activities a more detailed vehicle model, characterized by flexibility properties directly measured on the real motorcycle, would highlight more in detail the correlation between the vehicle design and the vibrations modes.

The state of the art of the studies about *Chatter* and the investigation presented in this chapter highlight the influence of the braking manoeuver on the mode evolution. The combination of transmission flexibility, suspension dynamics and tire dynamics turned out to be crucial for the excitement of the vibrating mode, reaching, for hard braking maneuvers, unstable conditions, depleting the braking performances.

It is worth noting that the analysis of the yaw movements and roll movements, in case of unstable *Chatter1* due to rear braking, revealed a direct small contribution of the vibration mode to the vehicle overall oscillation (yaw and roll). On the other side low direct influence on yaw and roll does not mean a low influence on the rider handling behaviors. The effect of *Chatter1* can influence, negatively, other motorcycle modes like *Weave*, thus exciting a fast evolution of those modes to unstable conditions. Within this activity, it has not been modeled the effect of *Chatter1* out of the motorcycle plane, then it is expected the lateral "bending" of the transmission assembly could affect the vehicle stability as well.

It is worth noting that the *Chatter* mode is characteristic of super sports motorcycles[3] and only for those vehicles it becomes, for specific running conditions,

[3]The *Transmission* mode is characteristic of all the vehicles, chain driven, shaft driven, and belt driven, however it is mainly investigated in relation with super sports motorbikes

unstable.

Even if the analysis involving *Chatter* is usually limited to certain vehicles, the investigation carried out in this chapter gives a general overview of the influence of vibrations on rider and motorcycle braking performances. Apparently the motorcycle stability is slightly affected by *Chatter1*, however even if small, its effects can aggravate the vehicle instability as a result of the interaction of the mode with other causes of destabilization, like sudden change of adherence or low tire-road friction.

As a matter of fact, considering the worst braking case investigated, the swingarm pitching movements at high frequencies, due to *Chatter1*, leads to micro slips, that means instantaneous loss of contact between the rear tire and the ground. It is worth noting that such tire dynamics can definitely influence the vehicle braking performances and stability, in particular whether the motorcycle experiences unexpected critical events (e.g the road has irregularities or the motorcycle tire faces sudden variations of road adherence passing, for example, from a dry surface to a wet surface).

Even if the present study addresses only a part of the complex *Chatter* phenomenon, it gives interesting indications about the vehicle non-linear behaviours due to the transmission vibrations. The findings can be a useful support to increase the knowledge of hard braking maneuvers for high performance motorcycles and they provide additional information to develop better solutions to enhance PTWs safety and performances.

Chapter 4

Motorcycle braking dynamics

4.1 Vehicle model

As discussed in §2.1 motorcycle dynamics is more complex to investigate than four-wheeled vehicle dynamics, mainly due to the roll dynamics and the articulated correlation between lateral dynamics and longitudinal dynamics.

Differently from a four-wheeled vehicle, the roll motion, the steering behaviors and the position of the rider on the vehicle add crucial degrees of freedom to the control of a PTW and they have a big influence on the stability. Concerning car dynamics, usually the roll angle is limited, below 10°and the sideslip angles are quite large, in particular during turning maneuvers with small curvature radii. On the other side, concerning PTWs, the aforementioned considerations are the opposite.

Summing up, the description of motorcycle dynamics is not simple, in particular in case of unsteady maneuvers, such as braking, acceleration, unsteady cornering, etc. However, by theoretical models, the dynamics of the vehicle can be fully investigated: the motorcycle behavior can be described in detail in every scenario. For example taking into account the investigation the tire forces and torques, it is possible to have a full representation of tire dynamics with different models from the literature [60, 61, 62]. The most famous one is the Pacejka's *Magic Formula* [60], presented for the first time in 1993. Pacejka proposed a semi-empiric model of the tire taking into consideration a number of tire parameters in order to provide the best description of tire dynamics, made explicit by a set of equations. Knowing the characteristics of the tire under analysis, like the cornering stiffness, the actual friction condition, the peak value of the forces, the effective tire rolling radius, etc., Pacejka's equations provide a satisfactory and realistic description of the tire behavior. Moreover, knowing the time evolution of the variables included in the equations it is possible to have, for example, the value of the longitudinal and lateral forces in real-time, in every kind of running scenario, considering at the same time the influence of the longitudinal slip and the sideslip angle.

Canudas De Wit et al. [63, 64] proposed a complex model for the identification of the tire forces. Differently from Pacejka, that developed and validated his model for linear steady state conditions only, the authors derived a dynamic friction force model, based on the Lu-Gre model. This model provides a representation of the

tire dynamics even more accurately than Pacejka's model, addressing the non-linear behaviors and the transients of the tire forces in unsteady state maneuvers. It is worth noting that the model by Canudas De Wit is more complex than Pacejka's one: it requires the tire characteristics, as the stiffness coefficient and the shape of the stress-strain curve of the tire, and it is composed of differential equations.

The aforementioned models requires many and specific information about the vehicle and most of the time, in powered two-wheelers applications, not all the parameters needed for the model's equations are available, or at least some of them cannot be directly measured. Considering for example the longitudinal speed, it cannot be directly measured easily. Then, it must be derived, indirectly, by the information coming from other detectable and measurable parameters.

In addition, equations based on parameters strictly related to a specific type of vehicle component (e.g. the tire) limit the versatility of the model itself. In case of similar components but with different characteristics, the results of the model are less accurate.

Referring to the present research the target of the motorcycle dynamics investigation, in case of braking, was the definition of a set of equations, based on a simple model, able to describe the motorcycle dynamics with a good accuracy adopting parameters easy to measure with standard sensors for PTW application, or easy to derive from other signals. It is important to define that for "standard" sensors it means those devices implemented on motorbikes currently on the market (mainly high-end vehicles). The main ones are wheel speed sensors, accelerometers, gyroscopes, rotative sensors (e.g. on the steering bar or on the throttle), and pressure sensors[1].

The model adopted for the vehicle dynamics investigation comes from the basic theory of powered two wheelers [5, 60, 33] and it is depicted in Figure 4.1.

In this representation the motorcycle moves on cornering with a roll angle φ, a steering angle δ_r, a kinematic steering angle δ, a longitudinal speed Vx and a lateral speed Vy. The lateral dynamics are described by the lateral acceleration Ay_{SM} and the Yaw rate $\dot{\psi}$ as well.

The model presented is a rigid model and it does not take into account the deformation of the elastic elements of the vehicle, as the front and rear suspensions, and the tires. The tires are considered rigid bodies and the interaction with the road surface is not addressed with tire models, like Pacejka's. In addition, the rider is considered as a fixed body on the vehicle, characterized by a specific mass and Inertia, with no degrees of freedom (DoF).

Every equation and parameter reported below is considered in SAE system of reference (z-upwards). As the figure shows, there is an absolute reference system and a body fixed reference system. In the following paragraphs, the reference

[1] In case of laboratory applications, during the design and test phases of new vehicles or new devices/systems, it is also possible to find other elements like optical sensors, GPS devices, etc. However, the definition of the model equations does not consider the possibility to have the signal coming from such expensive acquisition systems.

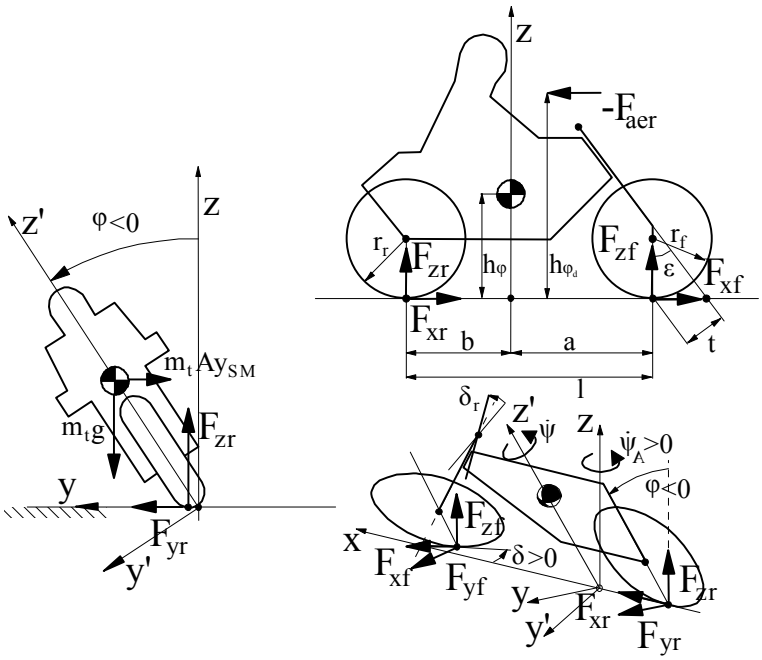

Figure 4.1: Sketch of the motorcycle model for the dynamics analysis (drawing layout modified from [60])

system used for the equations computation will be specified.

Forces

Let us consider the general configuration of a motorcycle turning, and applying a longitudinal force on the front and rear wheels. The reference system considered in the following equation is the absolute one. The equilibrium on the longitudinal axis can be assured only in case the driving force is equal to the longitudinal aerodynamic force. In case of acceleration or braking, considering a plain surface, it is not possible to speak of steady state equilibrium. According to Pacejka's motorcycle simple model [60], neglecting the influence of the lateral force on the longitudinal dynamics (function of the steering angle), the "quasi-equilibrium" in the longitudinal direction is expressed by:

$$m_t \cdot \ddot{x} = m_t \cdot Ax_{SM} = Fx_f + Fx_r + F_{aer} \tag{4.1}$$

where m_t is the total mass of the vehicle, Ax_{SM} is the vehicle longitudinal acceleration, Fx_f and Fx_r are the longitudinal forces and F_{aer} is the longitudinal aerodynamic force.

Then the equilibrium on the remaining axes is given by:

$$Fy_f + Fy_r + Fx_f \cdot \delta - m_t \cdot Ay_{SM} = 0 \tag{4.2}$$

$$Fz_f + Fz_r - m_t \cdot g = 0 \tag{4.3}$$

where Fy_f and Fy_r are the front and rear lateral forces, Fz_f and Fz_r the vertical forces, Ay_{SM} the lateral acceleration of the vehicle (parallel to the ground), δ is the kinematic steering angle and g is the gravity acceleration.

The steering angle δ is small ($sin(\delta) = \delta$, $cos(\delta) = 1$) and it is considered not affecting the lateral forces.

The equilibrium of the vehicle around the Yaw axis, Pitch axis and Roll axis is addressed by the following equations:

$$\begin{aligned} -Fx_f \cdot (h_\varphi \cdot sin(\varphi) - a \cdot \delta) - Fx_r \cdot h_\varphi \cdot sin(\varphi) + Fy_f \cdot a - Fy_r \cdot b \\ +(h_{\varphi_d} - h_\varphi) \cdot F_{aer} \cdot sin(\varphi) + Mz_f + Mz_r = 0 \end{aligned} \tag{4.4}$$

$$\begin{aligned} Fz_r \cdot b - Fz_f \cdot a - Fx_r \cdot h_\varphi \cdot cos(\varphi) - Fx_f \cdot h_\varphi \cdot cos(\varphi) \\ +(h_{\varphi_d} - h_\varphi) \cdot F_{aer} \cdot cos(\varphi) = 0 \end{aligned} \tag{4.5}$$

$$\begin{aligned} Fy_r \cdot h_\varphi \cdot cos(\varphi) + Fy_f \cdot h_\varphi \cdot cos(\varphi) - Fz_f \cdot h_\varphi \cdot sin(\varphi) \\ -Fz_r \cdot h_\varphi \cdot sin(\varphi) + Mx_f + Mx_r + M_{Gyros} + Fz_f \cdot t \cdot \delta \cdot cos(\varphi) = 0 \end{aligned} \tag{4.6}$$

The lateral and longitudinal forces can be computed with the following equations:

$$\begin{aligned} Fz_f = 1/l \cdot (b \cdot m_t \cdot g - m_t \cdot Ax_{SM} \cdot h_\varphi \cdot cos(\varphi) \\ - h_{\varphi_d} \cdot F_{aer} \cdot cos(\varphi)) \end{aligned} \tag{4.7}$$

$$\begin{aligned} Fz_r = 1/l \cdot (a \cdot m_t \cdot g + m_t \cdot Ax_{SM} \cdot h_\varphi \cdot cos(\varphi) \\ + h_{\varphi_d} \cdot F_{aer} \cdot cos(\varphi)) \end{aligned} \tag{4.8}$$

$$\begin{aligned} Fy_f = -1/l \cdot (-b \cdot m_t \cdot Ay_{SM} + Fx_f \cdot l \cdot \delta \\ - Ax_{SM} \cdot h_\varphi \cdot sin(\varphi) + F_{aer} \cdot h_{\varphi_d} \cdot sin(\varphi) + Mz_f + Mz_r) \end{aligned} \tag{4.9}$$

$$\begin{aligned} Fy_r = 1/l \cdot (a \cdot m_t \cdot Ay_{SM} + Fx_f \cdot l \cdot \delta \\ - Ax_{SM} \cdot h_\varphi \cdot sin(\varphi) + F_{aer} \cdot h_{\varphi_d} \cdot sin(\varphi) + Mz_f + Mz_r) \end{aligned} \tag{4.10}$$

In the aforementioned equations, a is the longitudinal distance between the center of gravity (CoG) of the vehicle and the center of the front wheel, b is the longitudinal distance between CoG and the center of the rear wheel, l is the wheelbase ($a + b = l$). h_φ is the distance of the center of gravity from the line of intersection between the wheels with the ground (taking into account also the crown radius of the wheel [60]) and h_{φ_d} is the vertical distance between the center of pressure of the aerodynamic force F_{aer} and the line of intersection of the wheels

with the ground. Finally φ is the vehicle roll angle, Mx_f and Mx_r are the rolling resistance torques, Mz_f and Mz_r the aligning torques and M_{Gyros} the sum of the torques due to the gyroscopic moments of the wheels.

According to Savino et al. [65] the longitudinal braking force can be computed according to the analysis of the momentum equilibrium the front and rear wheels:

$$Fx_f = (My_{Bk_f} - I_{wy_f} \cdot \dot{\omega}_f)/r_{\varphi_f} \tag{4.11}$$

$$Fx_r = (My_{Bk_r} + My_{DR} - I_{wy_r} \cdot \dot{\omega}_r)/r_{\varphi_r} \tag{4.12}$$

where My_{Bk_f} is the braking torque on the front wheel, My_{Bk_f} the rear braking torque, My_{DR} is the wheel driving torque, I_{wy_f} and I_{wy_r} the angular inertias of the front and rear wheels, $\dot{\omega}_f$ and $\dot{\omega}_r$ are the wheels angular acceleration and r_{φ_f} and r_{φ_r} the rolling radius of the front and rear tires.

Focusing on the braking torques, knowing the braking pressures (P_{bkCh_1} and P_{bkCh_2}) it is possible to derive My_{Bk_f} and My_{Bk_r} as follows:

$$My_{Bk_f} = -P_{bkCh_1} \cdot k_f \tag{4.13}$$

$$My_{Bk_r} = -P_{bkCh_2} \cdot k_r \tag{4.14}$$

where k_f and k_r can be computed from the characteristics the braking circuits. More in detail, they are function of the friction coefficients of the brake pads, the radius of the brake discs and the total area of the pistons inside the brake calipers. For more details, refer to Savino, Giovannini, et al. [65]. It is important to say that the aforementioned linear relation between the braking toques, the pressure and characteristics of the brakes is not completely true due to the non-linearity of the friction of the pads and the non-linearity of the fluid transmission inside the brake circuit. In any case the experimental data proved the good accuracy of Eq.4.13 and Eq.4.14, even considering the aforementioned simplifications.

Once the longitudinal and lateral forces are computed the tire-road friction coefficient (μ) can be derived by the following equations:

$$\mu_{x_f} = Fx_f/Fz_f \tag{4.15}$$

$$\mu_{x_r} = Fx_r/Fz_r \tag{4.16}$$

$$\mu_{y_f} = Fy_f/Fz_f \tag{4.17}$$

$$\mu_{y_r} = Fy_r/Fz_r \tag{4.18}$$

The curve radius

The curvature radius R and the path curvature Cu can be computed according to Giovannini et al. [15]:

$$R = (Vx^2)/((Ay_{sens} - sin(\varphi) \cdot g)/cos(\varphi)) \qquad Cu = 1/R \tag{4.19}$$

The experimental tests proved that the description of the curve radius by this formula gives a satisfactory characterization of the vehicle steering and handling behaviors. This simple model assumes that the curvature radius is directly computed neglecting the effect of the tires slip. However, concerning the activity carried out in this work, this simplification does not significantly influences the results.

Tire kinematics

Increasing the complexity of the model described above, a much more detail analysis of the tire behavior should be addressed. According to the investigation of the braking maneuvers in straight running and on turn, the analysis of the tire kinematics is fundamental. The definition of longitudinal slip follows the standard definition according to the basics of vehicle dynamics (e.g. [5, 60]), as a function of the vehicle speed Vx, the wheels angular speed ω and the tires rolling radius r_φ (function of the roll angle, [60]):

$$\kappa_f = -(Vx - r_{\varphi_f} \cdot \omega_f)/Vx \tag{4.20}$$

$$\kappa_r = -(Vx - r_{\varphi_r} \cdot \omega_r)/Vx \tag{4.21}$$

Cornering motorcycles, the sideslip has a relevant influence on the lateral dynamics, in particular for low speed and limited roll angles. Differently from cars, the sideslip angles of the motorcycles tire are limited if compared to the roll dynamics. For a standard motorcycle tire, in normal use, the range of the angle goes from $\pm 0°$to $\pm 8°$. A simplified representation of the front and rear sideslips is presented in the following equations:

$$\alpha_f = -(\delta \cdot -\frac{1}{Vx} \cdot (Vy + a \cdot \dot{\psi}_a)) \tag{4.22}$$

$$\alpha_r = -(-\frac{1}{Vx} \cdot (Vy - b \cdot \dot{\psi}_a)) \tag{4.23}$$

where Vy is the lateral vehicle speed and $\dot{\psi}_a$ is the Yaw rate of the vehicle, in the absolute system of reference. Starting from the Yaw rate signal obtained from a gyroscope sensor fixed in the CoG of the vehicle, the Yaw rate $\dot{\psi}_a$ can be derived according to Bellati et al. [66].

Vy is parameter difficult to measure directly (the best measuring performances are obtained by optical sensors), and the indirect evaluation is even much more complex. In theory it is possible to derive Vy starting from the computation of the vehicle slip rate $\dot{\beta}$, as reported in Seiniger [33], by an integration process. However,

within this activity, it was decided to skip the evaluation of α_f and α_r and to focus on the computation of the relative difference:

$$\Delta\alpha = -(\delta \cdot -l \cdot \frac{\dot{\psi}_a}{Vx}) \tag{4.24}$$

As the equation shows, $\Delta\alpha$ is easily derivable, and it does not depend on Vy. This parameter can be useful to detect the handling characteristics of the vehicle, and the observation of the evolution of its value can be an interesting index of vehicle stability while cornering. It has been adopted as one of the main variables to detect the vehicle instability in case of braking maneuvers, described in §5.2.

Acceleration of a pitching PTW

The last degree of freedom added to the vehicle model used for the investigation of the braking manoeuver is the pitch dynamics. One of the parameters affected by the pitch motion of the vehicle in case of braking or acceleration is the vehicle acceleration. The equations reported in the subsection *Forces* take into consideration the vehicle acceleration parallel to the ground.

Let us now consider the straight running condition. During standard experimental tests the acceleration of the vehicles is computed by an *Inertial Measurement Unit* (IMU) fixed on the vehicle body, thus the value is affected by the rotation of the vehicle around the y-axis. In this case, on a plain road, the value of the acceleration parallel to the ground is computed as follow:

$$Ax_{SM} = \frac{Ax_{sens} + sin(\phi) \cdot g}{cos(\phi)} \tag{4.25}$$

where ϕ is the pitch angle (sensed by the IMU), Ax_{sens} is the longitudinal acceleration measured by the sensor. However, in case of upward or downward slope, the ground slope should be taken into account for Ax_{SM} computation as well. Then the compensation turns into the following equation (Savino, Giovannini et al. [65, 67]):

$$Ax_{SM} = \frac{Ax_{sens} + sin(\phi) \cdot g}{cos(\eta)} \tag{4.26}$$

$$\eta = atan(\frac{Az_{sens} - cos(\phi) \cdot g}{Ax_{sens} + sin(\phi) \cdot g}) \tag{4.27}$$

$$\zeta = \phi - \eta \tag{4.28}$$

where Az_{sens} is the vertical acceleration sensed by the IMU, ζ is the ground slope angle and η is the component of the pitch angle due to the braking.

Finally, adding to this configuration also the roll dynamics the final compensation of the acceleration must consider also the influence of the lateral acceleration. The final layout of the vehicle is given by three rotations:

1. $Ry(\zeta)$ around the y-axis by the ground slope angle ζ;

2. $Rz'(\varphi)$ around the new z-axis, z', by the roll angle φ;
3. $Ry''(\eta)$ around the new y-axis, y", by the pitch angle due to braking η.

The result is the following transcendent system, which has no explicit solution:

$$\begin{aligned} Ax_{sens} = {} & cos(\eta) \cdot (Ax_{SM} - g \cdot sin(\zeta)) + sin(\eta) \cdot (Ay_{SM} \cdot sin(\varphi) \\ & - g \cdot cos(\varphi) \cdot cos(\zeta)) \end{aligned} \tag{4.29}$$

$$Ay_{sens} = Ay_{SM} \cdot cos(\varphi) + g \cdot cos(\zeta) \cdot sin(\varphi) \tag{4.30}$$

$$\begin{aligned} Az_{sens} = {} & sin(\eta) \cdot (Ax_{SM} - g \cdot sin(\zeta)) - cos(\eta) \cdot (Ay_{SM} \cdot sin(\varphi) \\ & - g \cdot cos(\varphi) \cdot cos(\zeta)) \end{aligned} \tag{4.31}$$

Considering η small enough that $sin(\eta) = \eta$ and $cos(\eta) = 1$, and $\zeta = \phi - \eta$ (according to the sensor measures), the final Ax_{SM} form is:

$$\begin{aligned} Ax_{SM} = {} & Ax_{sens} + g \cdot sin(\phi - \eta) - \eta((Ay_{sens} \\ & - g \cdot sin(\varphi) \cdot cos(\phi - \eta)) \cdot tan(\varphi) - g \cdot cos(\varphi) \cdot cos(\phi - \eta)) \end{aligned} \tag{4.32}$$

$$\begin{aligned} \eta^3 \cdot (-g \cdot sin(\phi)) + \eta^2 \cdot (Ay_{sens} \cdot sin(\varphi) - g \cdot cos(\phi)) \\ + \eta \cdot (Ax_{sens} \cdot cos(\varphi)) - Az_{sens} \cdot cos(\varphi) = 0 \end{aligned} \tag{4.33}$$

Therefore, substituting η in Eq.4.32 it is possible to compute Ax_{SM} taking into account the roll and pitch dynamics and the ground slope.

Verification of the motorcycle model using Bikesim

The equations reported in the paragraph above were verified using the software Bikesim®. Bikesim is a tool designed to simulate the dynamic behavior of motorcycles and scooters. The software provides a powerful and flexible virtual environment to study the vehicle behaviors in a large number of scenarios.

Bikesim®is a software developed to support the motorcycle dynamics investigations. It analyzes the response to the rider's inputs, the vehicle dynamics, including vehicle mass, geometry, tire dynamics, etc., and the environmental inputs as well (aerodynamics, road geometry and friction).

The Bikesim®math model is based on a core model developed and validated by Professors Robin Sharp [68] in AUTOSIM®. The math model is very detailed and, apart from the standard vehicle structure model, it has been extended to include a full powertrain, full nonlinear suspension kinematics, an enhanced rider positioning control, several enhanced tire model options, and other extensions needed to provide an accurate simulation of most existing motorcycle design concepts.

Due to the accuracy of the models implemented in the software, confirmed by a number of publications [52, 69, 70, 71], the simulations performed on Bikesim®were considered as a good reference to test the accuracy of the equations reported above.

In particular, the values of the forces were briefly tested in a number of running scenarios. The comparison aimed to evaluate if the description of the dynamics state of the vehicle (for the topics the concerns my activity) represented by a simple, rigid motorcycle model is satisfactory enough, in case of steady and unsteady running conditions, addressing non-linear dynamic aspects as well (as the tire model).

4.2 Real-time Friction Estimation

During emergency or critical situations, e.g. in case of an imminent collision, the rider shall try to avoid the impact by an emergency braking or a swerving maneuver or a combination of both [13, 15]. Considering more in detail the emergency braking manoeuver the rider should be able to perform the best braking manoeuver, maximizing the deceleration, thus reducing the stopping distance. The maximum deceleration the vehicle can reach during the maneuver is subjected to the flip over and to the wheel-road friction conditions. The following equation sum up the concept:

$$d_{max} = min(d_{fo}, \mu_{max} \cdot g) \tag{4.34}$$

where d_{max} is the maximum deceleration the vehicle can reach, d_{fo} is the flip over deceleration and μ_{max} is the maximum friction condition according to the road surface. It is worth noting that usually for standard motorcycles (not sports motorbikes) and scooters, in standard friction conditions (dry urban asphalt) the maximum deceleration due to the road friction coefficient is the most limiting condition, compared to the flip over. In case of high friction conditions, and in particular with super sports motorbikes, the aforementioned statement could be no more valid.

For the explanation of the algorithms described in the following paragraphs let us consider only the case of standard motorbikes and scooters.

Coming back to the description of the braking maneuver in case of critical events, the rider should be able to perform an optimal braking maneuver, reaching the maximum friction coefficient on both wheels, at the same time. Usually only very experienced rider are able to reach and keep the best friction conditions during a braking manoeuver without the assistance of any active braking systems like the ABS. For a standard rider is difficult to keep the maximum friction condition without locking the wheels. Therefore, systems like the ABS are a fundamental help for that group of users.

To assist the manoeuver in the best way the ABS needs detailed information about the wheel dynamics. The accuracy of those inputs to the active system can make the difference in the quality of the anti-lock function application. The necessity to investigate the tire dynamics stimulated a number of researches devoted to the definition of different models to characterize the tire-road friction characteristics.

Baffet et al. [72, 73] proposed the design of an observer to derive the tire forces. The observer is based on Extended Kalman Filters (EKF). The model proposed is a linear-adaptive model, and the authors validated it by virtual tests and by laboratory experiments.

Haffner et al. [74] describe a method for the friction curve identification by utilizing the evaluation of the instantaneous cornering stiffness.

Rajamani et al. [75, 76] report an interesting review on the tire-road friction estimation methods vehicle-dynamics based. The methods include slip-slope-based estimation, lateral-vehicle-dynamics-based estimation, and an EKF-based estimation method. The authors tested the methods experimentally on dry asphalts and ice-covered roads. The outcomes show a satisfactory efficiency of the methods in the friction estimation but at the same time, they point out a number of limitations to the algorithms application, such as the necessity to have sufficient tire slip to have an adequate real-time estimation.

Also Tanelli et al. [28] proposed method for the estimation of the tire-road friction condition in real time, using different techniques as recursive least squares and the maximum likelihood approach.

All the aforementioned activity were developed and tested on PFWs (powered four-wheelers). The research activity on the same topic, for PTW applications, is limited. For PFWs the estimation of tire dynamics can be simpler than PTWs where the analysis should take into account also the roll dynamics, and it is possible to use signals coming only from two wheels. The possibility to use only two wheels makes the vehicle model for the estimation more complex, in particular during combined braking, when both wheels are slipping.

The following paragraphs address the real-time tire-road friction estimation on a scooter, using vehicle-dynamics-based model, in different running conditions. The estimation methodology is based on the algorithm presented in [28], adjusted and customized for PTW application. The methodology was investigated and validated by virtual tests.

4.2.1 Algorithm for the estimation

The algorithm proposed for the investigation of the tire friction is based on the estimation of tire friction curve as a function of the longitudinal slip, $\mu = f(\kappa)$. From the point of view of the tire-road interaction the aforementioned equation is not accurate in case of lateral movements, or in general in case of cornering; also the sideslip angle (α) should be included in the computation. However, the model proposed neglects it, due to the complexity of the evaluation of its value. This simplification introduces an error in the general representation of the dynamic model. Anyhow, the results from the methodology application, both in case of braking on straight running and cornering, showed the effectiveness of the methods, even though a number of simplifications.

The main target of the friction estimation methodology is to evaluate the shape of the friction curve in real-time, as function of the inputs the estimator collects each calculation loop. Accordingly, it is possible to define the maximum value of the friction coefficient and detect the corresponding longitudinal tire slip.

The inputs to the algorithm are the longitudinal friction coefficients of the tires μ_f and μ_r and the longitudinal slips κ_f and κ_r. For the testing and validation of the methodology, within my activity, the aforementioned elements were computed

according to the formulations listed in §4.1.

The generic equation for the longitudinal friction coefficient, neglecting the lateral slip, is the following:

$$\mu_{f,r} = Fx_{f,r}(\kappa_{f,r}, K)/Fz_{f,r} \tag{4.35}$$

where K represents a set of parameters of tire and road characteristics.

As already reported in the previous paragraph, after the analysis of the state-of-the-art methods for adherence computation, Tanelli's method [28] was selected as reference method for the algorithm described in this paragraph. The linearized Burckhardt model proposed in [28] was implemented according to the following formulation (e.g. for the front braking):

$$Fx_f = a_1 e^{-b_1\kappa} + a_2 e^{-b_2\kappa} + a_3 e^{-b_3\kappa} + a_4 e^{-b_4\kappa} + a_5\kappa + a_6 \tag{4.36}$$

The coefficients b_j were computed with a trial-and-error methodology, by number of simulations of emergency braking maneuvers, in different road conditions (dry and wet asphalt) leading the wheel to lock. The values of the coefficients were selected aiming to get the best estimation performances for different scenarios. The values selected were 5, 20, 80, and 240.

Once the estimator receives, in real-time, the inputs for the estimation, the longitudinal slip and the tire-road adherence coefficient, it can derive the coefficients a_i via best-fit method. As soon as those coefficients are computed it is possible to evaluate the shape of the friction curve, thus the maximum friction coefficient and the corresponding longitudinal slip.

Due to the Eq.4.36 the best-fit method adopted for the computation is a nonlinear regression, based on the Lavenberg-Marquardt algorithm [77].

In statistics, the non-linear regression is generally expressed by the following equation:

$$y = f(x, \theta) + \epsilon \tag{4.37}$$

where y and x are the variables of the system, θ represents the coefficients characterizing the curve shape and ϵ is the error coming from the computation.

The method was developed in MATLAB®by the regression function *nlinfit*. This function computes the fits via non-linear least squares, that iteratively refits the regression and adjusts the coefficients.

Braking on a straight path

The aforementioned algorithm for friction curve estimation was tested in virtual environment, by a virtual model of a scooter, a Piaggio Beverly300. In order to obtain realistic results from the simulations, the virtual PTW model was previously validated by a number of comparisons between experimental data (2BeSafe database) collected during on-road braking maneuvers along a straight path, with the same vehicle and the multibody simulations. The values of the friction coefficients and the longitudinal speed were extracted from the experimental data using the braking pressures, the vehicle acceleration, and the wheels dynamics.

Table 4.1: Events selected for the normal braking analysis

Case	A	B	C
Braking Manoeuver	Combined	Front	Rear
Duration (s)	3.2	6.5	2.7
Mean Deceleration (m/s^2)	2.2	2.0	3.1
Friction conditions	High, dry	High, dry	High, dry

First of all the relation between the braking pressures and the braking torques was derived. The experimental tests used for the calibration comes from a set of braking maneuvers preformed separately from the runs collected in a *naturalistic* riding database.

During the calibration runs, the riders were asked to perform a number of braking maneuvers, operating on one single braking channel at a time, keep the braking force constant. More in detail the rider had to brake with three different level of deceleration (low, medium, high), starting from a running speed of 50 km/h, 5 times for each configuration.

The pressure values in the braking system were sensed with standard pressure sensors for automotive applications, and the acceleration was measured with an Inertial Measurement Unit (IMU), compensating the Ax_{SM} function of the pitch angle according to the Eq.4.32.

The experimental data were extracted from the acquisitions collected in the EC funded 2BeSafe project, carried out by the team of the University of Florence [78]. The objective of the 2BeSafe project was to target behavioral and ergonomics research to develop countermeasures for enhancing Powered Two Wheeler (PTW), rider's safety, including research on crash causes and human errors. The PTW used in the test was a fully instrumented Piaggio Beverly300. The scooter was equipped with wheel speed sensors, accelerometers, gyroscopes, pressure sensors and a steering sensor. The system recorded the riding behavior of six riders in their usual routes.

The data extracted, to be used within the friction estimator validation, were selected according to strict criteria: the braking manoeuver should have had a minimum duration of 2 seconds, the vehicle should have been in upright position and the braking pressure should have exceeded 0.8 bar. According to this limitation, 1078 cases were found. Among this number three subcases, representing a front braking a rear braking and a combined braking (Table 4.1), were investigated in detail. A posteriori, the selected cases well represent the typical results.

All the data needed for the investigation of the braking maneuver and the friction estimation were extracted from the recorded data of the aforementioned three cases.

The braking maneuvers were firstly reproduced virtually in Simulink environment, using a costumed motorcycle based on the Sharp multibody model [70] (Figure 4.2). The base software used for the organization and design of the

Figure 4.2: Multibody model of the Piaggio Beverly300. The vehicle shape depicted in the picture is used only for the animation and it does not affect the simulation results

Table 4.2: Beverly300 overall mass distribution, with and without rider

Parameters	w/o Rider	w Rider
a	0.924	0.911
b	0.546	0.559
h	0.501	0.642

simulations was Bikesim®[2].

The Piaggio Beverly300 model has been characterized with the mass distribution of the real vehicle (Figure 4.3 and Table 4.2), measured experimentally.

The geometrical and inertial parameters (e.g. braking torques) of the PTW used in experimental tests were implemented in the virtual model. E.g. the position (height and longitudinal displacement) of the center of gravity the real Beverly300 was derived according to the method explained by Cossalter in [5].

The braking maneuvers simulated in Bikesim®and the corresponding real maneuvers were compared in terms of the vehicle speed and friction coefficients estimation. Figure 4.4 depicts this comparison. The curves, both referring to PTW speed and the front and rear adherence coefficients, figures out a good accordance between the experimental data and the corresponding simulation. The same conclusion is valid for all the braking configurations, thus validating the motorcycle virtual model for the braking test along a straight path.

Once the validation of the vehicle model was completed, the friction curve estimator was tested via virtual simulations, performing hard braking maneuvers

[2]For the activity described in the publication [67], by Savino et al., the virtual environment used for the simulation was SimMechanics/Matlab. The results obtained from this activity are comparable to the results obtained reproducing the same simulations in Bikesim. At the end, for the latest and future activities, Bikesim was chosen as the reference software (due to many advantages given by the software in the simulation process)

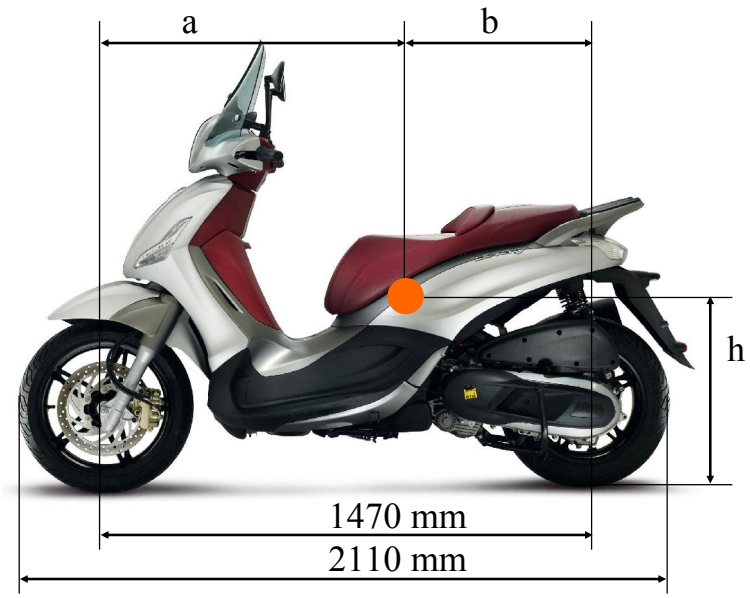

Figure 4.3: Beverly300 overall mass distribution

for different road conditions: dry asphalt and wet asphalt. For those scenarios, the maximum friction values were set respectively to 1.15 and 0.6. Moreover, the braking maneuvers were performed only with the front brake.

The inputs needed by the algorithms are derived from the signal given by the simulation software. It is worth noting that the virtual signals are not affected by the same noise that characterizes the standard sensors. Therefore, in order to have a better evaluation of the method effectiveness and potentialities, in terms of implementation on a real vehicle, some typical noise characterizing the motorcycle sensors was added to the signals used in the multibody model.

First, the analysis of the signals from the experimental data was carried out, and the Signal-to-Noise Ratios (SNR) of all the signals involved in the computation of friction estimator inputs were found (braking pressure, wheels speed, longitudinal acceleration, pitch angle and vehicle speed). 10 real front braking maneuvers were selected and investigated for the aforementioned purpose.

According to the theory of Signal Processing, the SNR in decibel (SNR_{dB}) was computed with the following equation:

$$SNR_{dB} = 20log_{10}(\frac{A_s}{A_n}) \tag{4.38}$$

where A_s is the root mean square (RMS) amplitude of the signal and A_n is the RMS amplitude of the noise.

In Figure 4.5 the results of the analysis of the 10 braking maneuvers are depicted, the SNR mean values for different signals are computed.

For each virtual signal, the noise was introduced as white Gaussian noise,

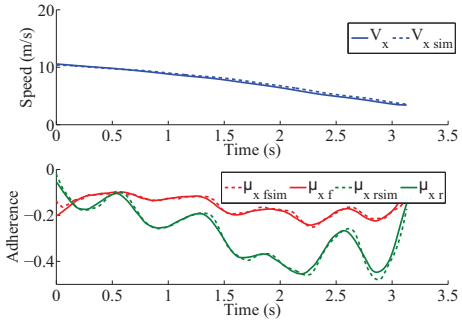

(a) Speed and adherence estimations for Case A

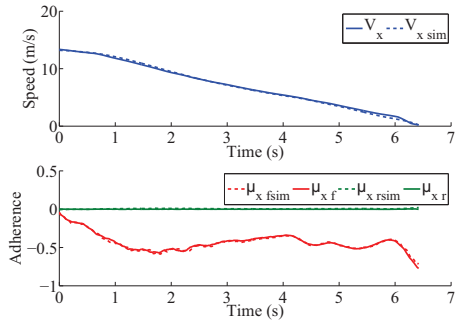

(b) Speed and adherence estimations for Case B

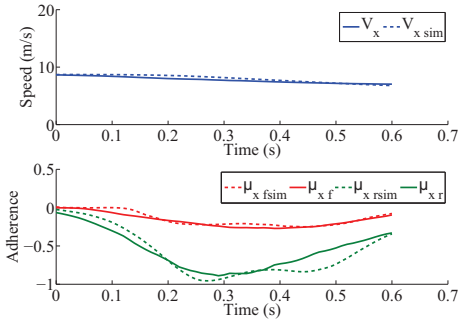

(c) Speed and adherence estimations for Case C

Figure 4.4: Speed and adherence estimation for different braking cases. Comparison between the simulated data and the experimental data

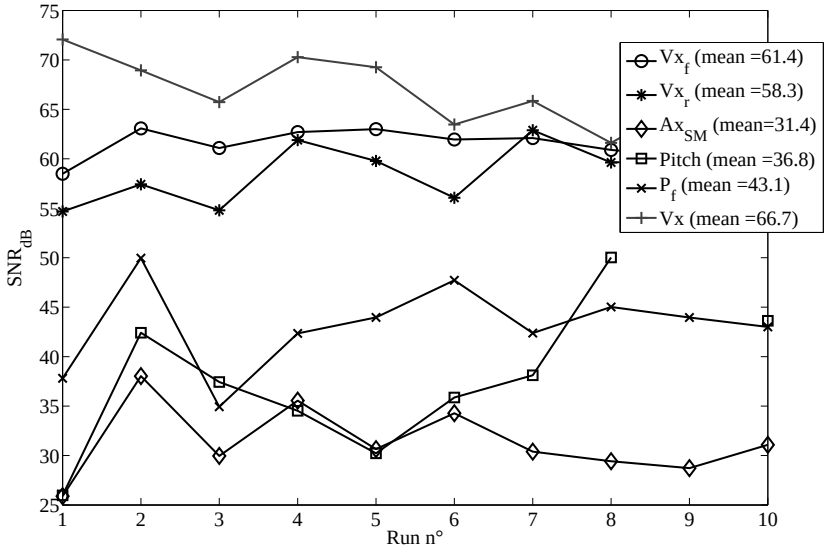

Figure 4.5: Evaluation of the SNR for different parameters

according to the investigation of the corresponding real signal, obtained for the experimental data.

The estimation algorithm uses a variable sampling window to collect the inputs needed to the system. The inputs start to be collected after the braking manoeuver exceed the braking pressure of 2 bar. The maximum value of samples collected is 70. This number was chosen after several tests on sampling windows with different sizes, aiming to find the best solution in terms of accuracy with limited sampling window. The sampling rate adopted in the simulation was 100 Hz, in accordance with the acquisition rate of the signals extracted from the 2BeSafe database.

Let us consider the time evolution of the estimation for the front wheel (for the rear wheel is the same). At each time step the estimation process check the value of μ_f and the braking pressure. When μ_f and the braking pressure exceed respectively 0.3 and 2 bar, the system starts to collect the input values (μ_f and κ_f) and computes the coefficients a_i of the Eq.4.36 by the non-linear regression fit. Once the coefficients of the equation are derived, the friction curve can be drawn and the maximum friction coefficient and the corresponding κ_f can be computed. An example of the results is given in Figure 4.6.

The time evolution of the estimation is depicted in three time steps: estimated curve and inputs when the estimation error of maximum friction coefficient is 10% (black), curve estimated when the maximum friction coefficient is reached (blue) and the real friction estimation curve (red).

The investigation of the effectiveness of the algorithm is based on the evaluation of the time step named *Sample 10%* represented in Figure 4.7 and Figure 4.8: it is

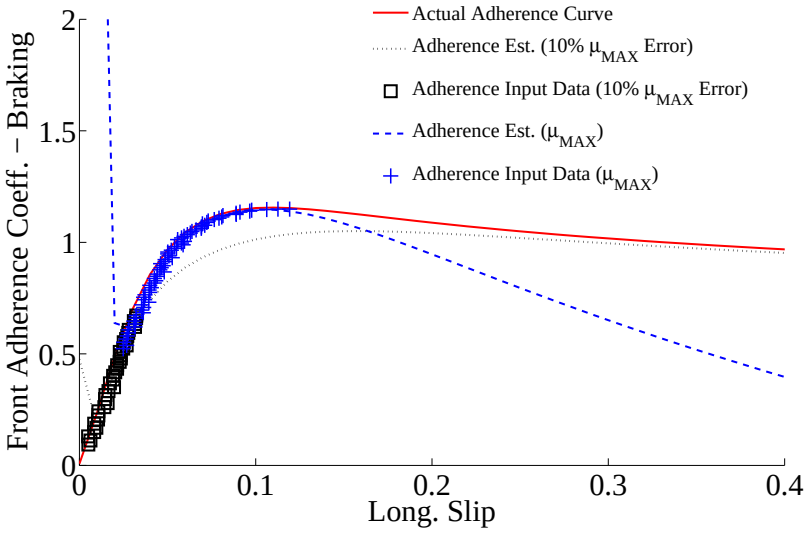

Figure 4.6: Adherence Estimation on dry asphalt. The black squared markers and the black dotted line represent the input data and the estimated friction curve when the value of the maximum estimation error of friction coefficient is 10%; the blue cross markers and the dashed blue line represent the input data and the estimated friction curve when the maximum friction coefficient is reached. The red solid line represents the actual friction curve, for the front wheel (braking)

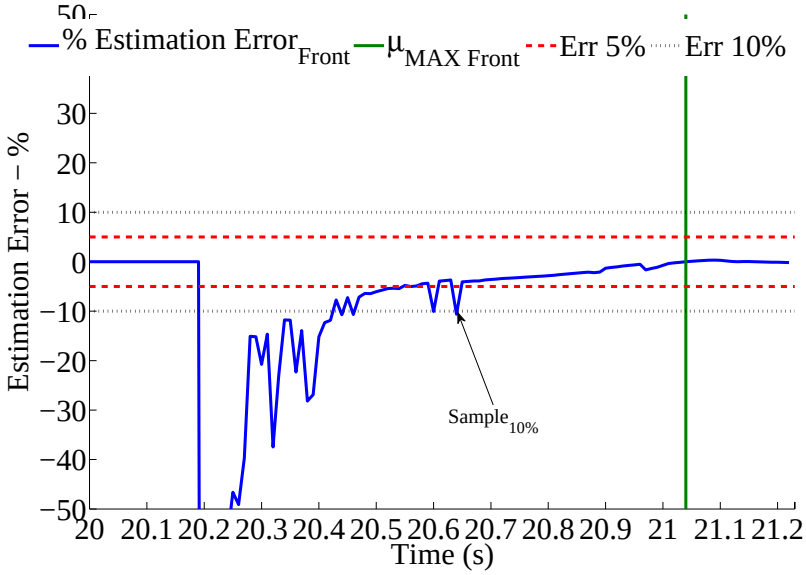

Figure 4.7: Adherence estimation error for a hard braking (wheel locking) on dry asphalt

Table 4.3: Variability of number of samples between Sample10% and the μ_{MAX} sample step

Surface	Mean	Std. Deviation
Dry	52.7	11
Wet	6.4	2.5

considered as the time step at which the estimation error stays permanently below the 10% limit.

The analysis of variability of *Sample 10%* was conducted repeating the braking manoeuver in high and low adherence 1000 times. Because of the presence of random Gaussian noise on the signals used for the equations, in every simulation different results were expected.

The outcomes of the aforementioned analysis of *Sample 10%* are summed up in Table 4.3, Figure 4.9 and Figure 4.10.

It is important to make clear that, differently from the low adherence conditions, it is not properly correct to simplify the distribution of *Sample 10%* in high friction condition as a standard Gaussian distribution, but as double distribution with two mean values, one almost 35 and the second almost 55.

The analysis of the method accuracy reveals that the algorithms adopted in data processing have good accuracy for different friction conditions. It is worth noting that the estimation performances are strongly affected by the road surface, in particular the regression methodology was more effective in the estimation of the

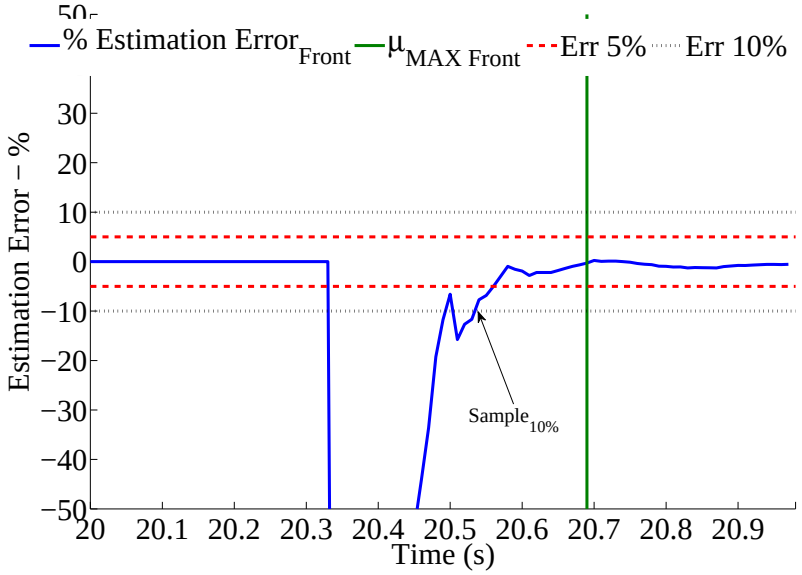

Figure 4.8: Adherence estimation error for a hard braking (wheel locking) on wet asphalt

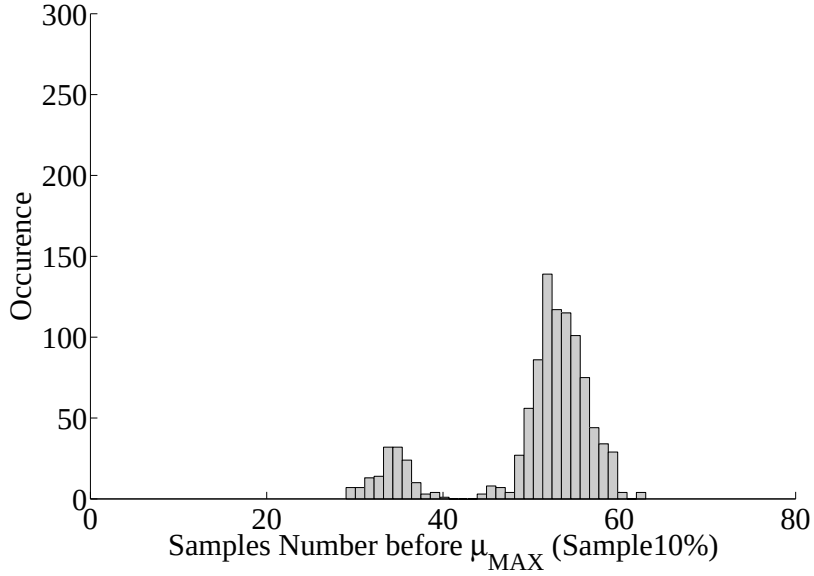

Figure 4.9: Variability of number of samples between Sample10% and the μ_{MAX} sample step. Braking on a straight path, high adherence conditions

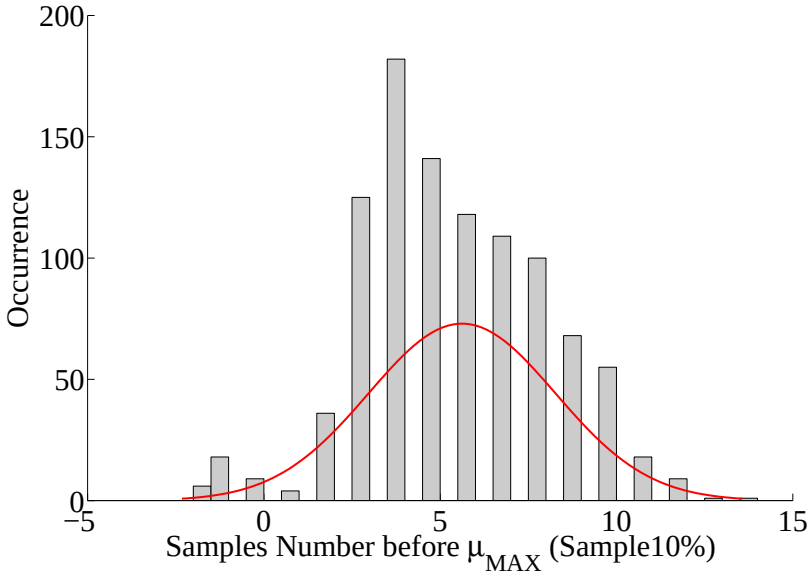

Figure 4.10: Variability of number of samples between Sample10% and the μ_{MAX} sample step. Braking on a straight path, low adherence conditions

maximum adherence in particular in case of dry conditions. Also for wet asphalt, even if in comparison with dry condition the performances are definitely lower, the estimation accuracy reached good results. Also for that running condition it is possible to predict the value of the maximum friction coefficient in advance, before reaching the time step representing the μ_{MAX}, with an absolute error below the 10%. Those are promising results for the friction estimator, thus pointing out the potentialities of such methodology in support of active braking safety systems or at least in support of system made for the continuous vehicle state detection (for safety reasons or for rider behavior investigations).

Braking on steady state cornering

Recently some preliminary studies on the friction estimation algorithm were conducted also for braking manoeuver on a curve. In particular, the analysis focused on hard braking manoeuvers on steady curves. For that purpose, the algorithm was tested directly on the virtual vehicle, neglecting the comparison with the experimental runs. This is because even if the tire model in the simulation software is enough detailed, the characteristic parameters for lateral dynamics (e.g. deformations) were not directly measured on the real tire (the setup of a standard scooter tire was chosen for the front and rear tires). For longitudinal dynamics the number of parameters involved in the tire characterization is “quite” small if compared to the characterization of the lateral tire behavior in case of combined slip. Therefore, while for straight running the standard tire model adopted can

be considered accurate to be compared with experimental runs (the comparison proved it), further investigation on lateral dynamics property of the scooter's tires should be done.

The effectiveness of the estimation method was verified in three configurations of hard braking on dry asphalt (μ_{xmax} 1.15) and wet asphalt (μ_{xmax} 0.6):

- curve radius 75m, running speed 50 km/h. Front Braking;
- curve radius 100m, running speed 50 km/h. Front Braking;
- curve radius 200m, running speed 50 km/h. Front Braking.

The maximum braking torque applied to the wheel was 600 Nm in case of dry road and 300 Nm in case of wet.

For the estimation process the same algorithm described in §4.2.1 was implemented. Again the system addresses the variation of the longitudinal friction coefficient only function of the longitudinal slip (that is implicitly affected by the roll angle, Eq.4.20), neglecting the influence of the sideslip angle. That was possible according to the characteristics of the tire implemented for the simulation. As a matter of fact the lateral deformation of the tire is limited, and also for the sharpest curve tested (curve radius 75m) the sideslip angle did not exceed 1°. Therefore, the friction curves shape (only longitudinal adherence) for the three curve radii considered is almost the same.

According to the straight braking case, the analysis of the results of this study focused on the estimation errors of the friction coefficient and the number of samples needed to achieve a satisfactory estimation (below 10% of error). An example of the outcomes is depicted in Figures 4.11 and 4.12.

The results show a good behavior of the algorithm also for the curve scenario, in particular for high adherence. No major differences can be found among the different curvature radii, in fact, the *Sample10%* time steps for different radii are comparable.

In case of high adherence, the *Sample10%* is characterized again by two distributions, each one comparable to a Gaussian distribution (Figure 4.13). The first distribution is almost between 20 and 40 samples and the second one over 40 samples. In all the running scenarios, the distribution with the majority of samples is the last one.

Instead, for the low adherence case the distribution of is very close to a single Gaussian distribution (Figure 4.14).

Looking at the examples of estimation depicted in Figures 4.11 and 4.12 it is not possible to find remarkable differences for the application of the estimator for different curvature radii. On the other side, some indications can be found in the analysis of the distribution of *Sample10%*.

In case of high adherence, Figure 4.13 shows that the mean value of the distribution is increasing for higher curve radii. As expected, as long as the curve radius increases the estimation performances increase as well. Looking at the second distribution, the one characterized by the highest number of samples, it is possible to see that the difference between the mean values is small, almost only

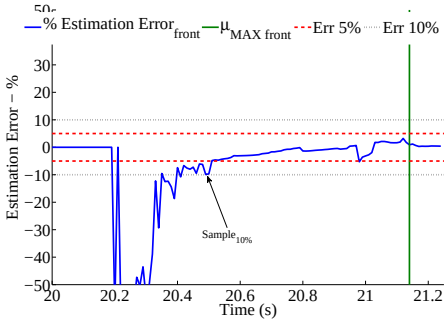

(a) Adherence estimation error for a hard braking (wheel locking) on dry asphalt. Curve radius 75m, running speed 50 km/h. Front Braking.

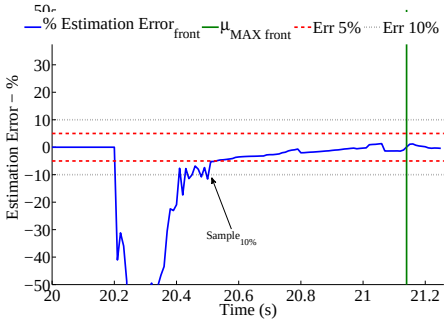

(b) Adherence estimation error for a hard braking (wheel locking) on dry asphalt. Curve radius 100m, running speed 50 km/h. Front Braking.

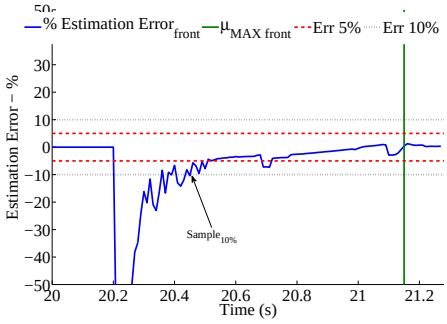

(c) Adherence estimation error for a hard braking (wheel locking) on dry asphalt. Curve radius 200m, running speed 50 km/h. Front Braking.

Figure 4.11: Adherence estimation error for a hard braking (wheel locking) on dry asphalt, addressing different curvature radii

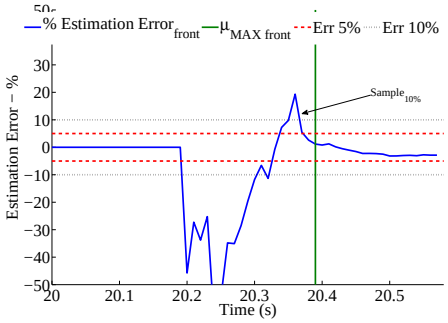

(a) Adherence estimation error for a hard braking (wheel locking) on wet asphalt. Curve radius 75m, running speed 50 km/h. Front Braking.

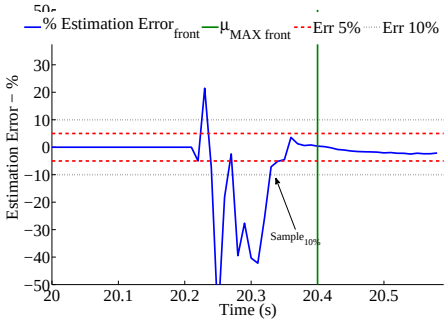

(b) Adherence estimation error for a hard braking (wheel locking) on wet asphalt. Curve radius 100m, running speed 50 km/h. Front Braking.

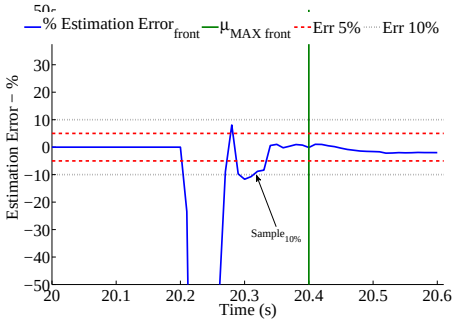

(c) Adherence estimation error for a hard braking (wheel locking) on wet asphalt. Curve radius 200m, running speed 50 km/h. Front Braking.

Figure 4.12: Adherence estimation error for a hard braking (wheel locking) on wet asphalt, addressing different curvature radii

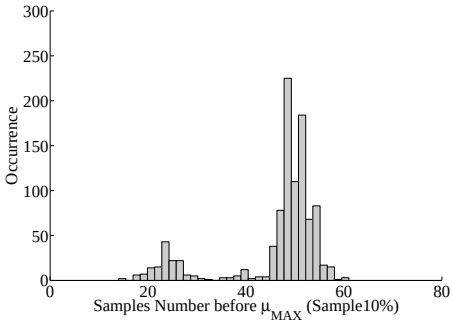

(a) Distribution of Sample10% for a front braking manoeuver, on dry asphalt, cornering with a curve radius of 75m

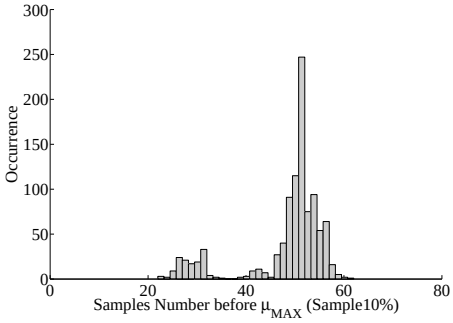

(b) Distribution of *Sample10%* for a front braking manoeuver, on dry asphalt, cornering with a curve radius of 100m

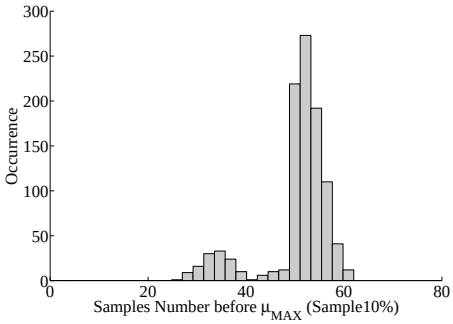

(c) Distribution of *Sample10%* for a front braking manoeuver, on dry asphalt, cornering with a curve radius of 200m

Figure 4.13: Distribution of *Sample10%* for a front braking manoeuver, for different cornering scenarios. Road condition: dry asphalt

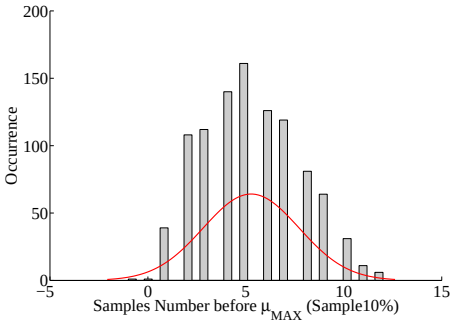

(a) Distribution of *Sample10%* for a front braking manoeuver, on wet asphalt, cornering with a curve radius of 75m

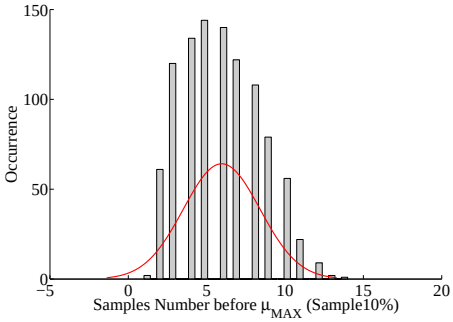

(b) Distribution of *Sample10%* for a front braking manoeuver, on wet asphalt, cornering with a curve radius of 100m

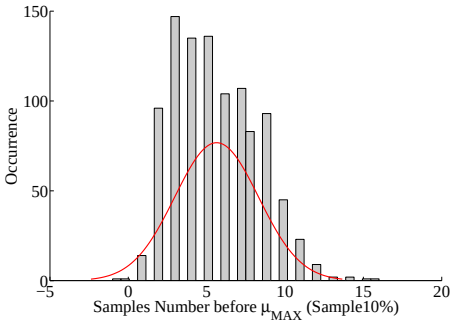

(c) Distribution of *Sample10%* for a front braking manoeuver, on wet asphalt, cornering with a curve radius of 200m

Figure 4.14: Distribution of *Sample10%* for a front braking manoeuver, for different cornering scenarios. Road condition: wet asphalt

5 samples. Instead looking at the first distribution the differences increase: the mean value moves by almost 10 samples to higher values for larger curvature radii.

Concerning low adherence case (Figure 4.14), as already said, the sample distribution is very close to a Gaussian distribution, and, in addition, for this road condition only irrelevant differences can be found among different simulations. The difference within the cases, in terms of mean value of the distributions, is almost 0.5 samples, in favor of the simulation at the largest curvature radius. This small difference is not enough to draw some other conclusion to highlight specific differences concerning the aforementioned simulation conditions.

4.3 Motorcycle speed estimation

The method presented for the tire-road friction estimation requires an accurate evaluation of the vehicle speed. The vehicle speed is a parameter that must be computed indirectly; alternatively, it can be directly measured with expensive optical sensors (e.g. laser, [57]). Excluding the possibility to use optical sensors for measuring, an algorithm for vehicle speed estimation was derived, based on the method proposed by Tanelli et al. in [28] for automotive application. In the literature, there are a number of vehicle speed estimation algorithms, involving mainly static and dynamics observers, and Kalman filters. In [79] the authors present a vehicle speed estimation method based on Dugoff's tire model and vehicle dynamics. The algorithm computes the vehicle speed by a non-linear observer that uses the difference between measured and estimated accelerations as feedback terms to lead the estimation to converge. In [80], Gao et al. derived the vehicle speed of an electric vehicle by an adaptive Kalman filter, in case of unknown road conditions, considering as inputs the wheels speed and the vehicle acceleration.

In the works taken as example, the algorithms implemented were designed for car application. No relevant work addressing the same task for PTW application was found. Therefore, it was decided to derive a dedicated algorithm for PTW speed estimation from one of the methods adopted for four wheeled vehicles. Aiming to define an estimation strategy with a low computational effort and easy to implement, the method proposed by Tanelli et al. [28] was adopted as reference.

The algorithm redesigned from Tanelli's takes into account, as input, the wheels speed, the axial accelerations of the accelerometers fixed to the vehicle main frame, the braking pressures and the pitch and the roll angles.

The general layout of the estimation logic flow is depicted in the flow chart in Figure 4.15.

The starting point of the process is the generation of the input array needed for the estimation. The signals acquired from the sensors are filtered by running average considering a specific dimension of the filtering window. More in detail, for the application of the method on the experimental data available a sampling window of 30 samples (in case of 100 Hz sampling frequency) was chosen, as the results from the tuning process of the algorithm. Considering the aforementioned condition, it worth noting that a delay of 0.3 s is introduced in the estimation loop. It is possible to reduce the number of samples, thus improving the speed

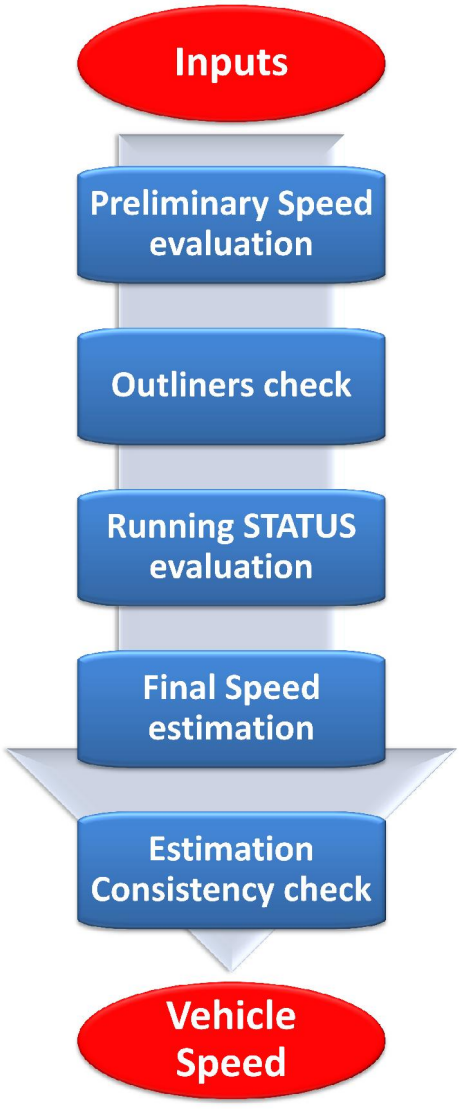

Figure 4.15: Representation of the logic flow chart of the speed estimation methodology

Table 4.4: Additional variables and thresholds needed for the estimation process

Par.	Value	Description
B	0.8	Decel. threshold to identity for braking status
D	0.1	Accel. threshold to identify for acceleration status
h	0.1	Threshold (relative) used for computing V_m
h_a	0.1	Hysteresis threshold for accel./decel. status
h_v	0.2	Hysteresis threshold for low speed status
M	30	N. of back-propagation samples (initialization)
v	0.01	Threshold for checking speed consistency while braking (m/s)
v_1	0.6	Threshold used to detect outliers(m/s)
v_{min}	1	Vel. threshold to identify low speed status (m/s)

of computation of the estimator; however, that reduces the attenuation of the sensors noise and increases the possibilities to have not negligible mistakes on the estimation process.

In addition, a number of constant parameters (Table 4.4) have been introduced to be used as thresholds in the equations of the algorithm.

The second step consists on the preliminary definition of the front and rear peripheral wheels speed, Vx_f and Vx_r, function of the corresponding angular wheels speed, ω_f and ω_r and rolling radii.

Moreover, additional reference speeds are introduced: $V_{m_{base}} = (Vx_f + Vx_r)/2$, $V_{est} = V_{m_{base}}$, $V_{ref} = V_{m_{base}}$ and $V_m = V_{m_{base}}$. These parameters are used in the following part of the algorithm.

Then, in the third phase the outliers of the speed value are detected and removed. Since we have only two wheels, when their speeds have a relevant difference, the outliers are identified based on the expected speed $V_{ref} = V_{m_{t-1}} + Ax_{SM} * ts$, where ts is the sampling time step.

The outliers are excluded following the according the following criteria:

- in 1 time step the maximum peripheral acceleration the wheels can have is 1g;
- if $(Vx_f - Vx_r) < v_1$ OR $(V_m > v_{min}\ AND\ |V_{f/r} - V_{ref}|/|V_{ref}| > h) \rightarrow V_m = (Vx_f + Vx_r)/2$;
- if $(Vx_f - Vx_r) \geq v_1$ OR $(V_m \leq v_{min}\ AND\ |V_{f/r} - V_{ref}|/|V_{ref}| \geq h) \rightarrow Vx_f = V_{ref}$, $Vx_r = V_{ref}$ and $V_m = (Vx_f + Vx_r)/2$.

Once the outliers are excluded, it is possible to define the running status of the motorcycle. The status S has the following values:

The definition of S depends on the logic below, reported in MATLAB language:

```
if (S(i-1)==-2 && v_m(i)<=v_min+h_v) ...
|| (S(i-1)~=-2 && v_m(i)<=v_min)
```

Table 4.5: Different values of the running *Status*

Status	Meaning
-2	Speed vehicle very low
-1	Vehicle is accelerating
0	Constant speed or mild deceleration
1	Vehicle is braking

```
S(i)=-2;

if (S(i-1)==-2 && v_m(i)>v_min+h_v && ax_corr(i)>=D) ...
|| (S(i-1) ~= -2 && S(i-1) ~= 0 && v_m(i)>v_min ...
    && ax_corr(i)>=D)...
|| (S(i-1) ==0 &&  v_m(i)>v_min && ax_corr(i)>=D+h_a)

S(i)=-1;

if (S(i-1)==-2 && v_m(i)>v_min+h_v ...
    && ax_corr(i)>=-B && ax_corr(i)<D) ...
|| (S(i-1) == 1 && ax_corr(i)>=(-B+h_a) ...
    && ax_corr(i)<D &&v_m(i)>v_min) ...
|| (S(i-1)==-1 && ax_corr(i)>=-B ...
    && ax_corr(i)<D &&v_m(i)>v_min) ...
|| (S(i-1)== 0 && ax_corr(i)>=-B ...
    && ax_corr(i)<D + h_a && v_m(i)>v_min)

S(i)=0;

else
S(i)=1;
end
```

where i represents the sample step and ax_{corr} is Ax_{SM}.

The last step computes the final value of the speed. In case the Status assumes the values of -2, 0 or -1 (constant speed, low speed or accelerating) the estimated vehicle speed is $V_{est} = Vx_f$.

It has been assumed that in all these conditions the front wheel had a longitudinal slip different from zero, or, at least, smaller than the rear wheel slip.

The most crucial phase is the braking phase ($S = 1$), in particular in case both wheels are decelerating. The different braking scenarios are addressed according to the braking pressure values as follows:

1. in case of rear braking or combined braking with soft front braking ($P_f < 2\ bar$) $\rightarrow V_{est} = Vx_f$;
2. in case of medium-hard front braking ($P_f > 2\ bar$), combined braking with

medium-hard front braking or combined medium-hard braking, the V_{est} is computed via back propagation of V_{est} by Ax_{SM} for M samples, as reported in [28].

Finally, the consistency of V_{est} is checked whether $V_{est} - V_{est_{t-1}} > v$ (that guarantees the monotonic decrease) and the deceleration estimated within two time steps is below 2 g.

4.3.1 Virtual validation

The effectiveness was tested mainly in a virtual environment, to understand the quality of the estimation loop. The signals acquired from the sensors installed on the virtual motorcycle were disturbed with the same noise described in §4.2.

The simulations made consisted on the following scenarios:

1. braking on straight line, with different initial speeds (50, 100, 150 km/h), different braking torques (from 160 Nm to 700 Nm) and different braking distributions (Front, Rear, Front and Rear);

2. a racetrack (length 2273m), characterized by a number of curves, slopes, braking maneuvers and accelerations.

All simulations were carried out in Bikesim®using a sports motorcycle, (for the geometrical values, the braking circuit features and inertial characteristics, the default values given by the software were considered satisfactory for the simulation) with a standard tires (implementing the full *Magic Formula* formulation for the tire forces computation). The road conditions adopted for the simulation were dry asphalt with a maximum friction coefficient equal to 1.15.

For the first group of simulations, the braking input was given as a force input on the front brake lever and the rear brake pedal. However, due to different characteristics of the front and rear braking circuits, the same input (in terms of absolute value) corresponds to different braking torques. To make clear the braking conditions of the simulations, the examples reported in this paragraph will be described addressing the braking torques.

Figure 4.16 represents the simulation of a combined braking on a straight path, with 425 Nm on the front wheel and 163 Nm on the rear wheel, starting from a longitudinal speed of 50 km/h (13.6 m/s). The max speed error detected is 2.4% with a mean value of 0.41% (also including the interval at constant speed, before braking). Concerning the difference between the estimated and real κ, the maximum difference is on the rear wheel, with a value of 0.028.

The aforementioned values shows good applicability of the estimation algorithm and the errors remain below the 5% (that can be considered as the efficiency threshold for the potential implementation of the system on active braking systems, like the ABS).

Also in Figure 4.17 and Figure 4.18 it is possible to observe the same results. Those figures represent respectively a front braking manoeuver on a straight path, with 425 Nm on the front wheel, starting from a longitudinal speed of 50 km/h (13.6 m/s) and a rear braking manoeuver on a straight path (starting with the same

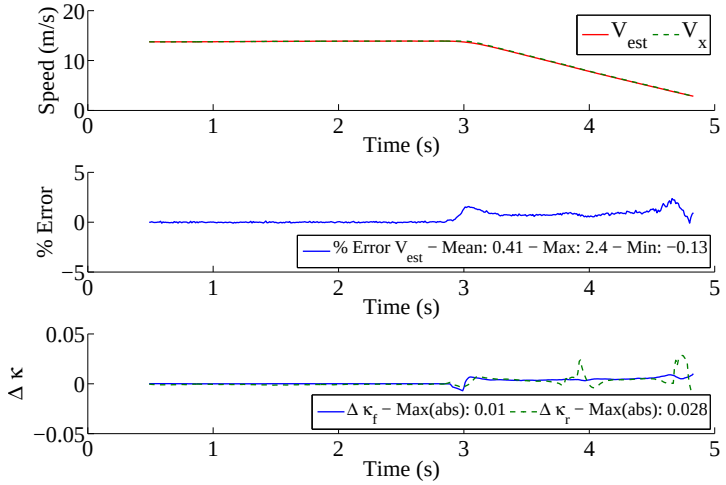

Figure 4.16: Evaluation of the algorithm for the speed estimation, during braking maneuvers: combined braking on a straight path, with 425 Nm on the front wheel and 163 Nm on the rear wheel, starting from a longitudinal speed of 50 km/h

speed). The rear braking shows better results mainly because the evaluation of the speed is based directly on the fastest wheel (front) instead of the back-propagation process.

Figure 4.19 represents combined braking maneuvers on a straight path, with 700 Nm on the front wheel and 270 Nm on the rear, starting from different longitudinal speeds: respectively 50 km/h, 100 km/h and 150 km/h. In those conditions the rear wheel locks, due to the load transfer and the high braking torque. Those scenarios were considered interesting to evaluate the effectiveness of the algorithm during emergency events.

Looking at Figure 4.19 it is possible to see that the speed error still remains below 5% for each running speed tested. However the $\Delta\kappa$ has lots of oscillations, and in particular κ_r reaches 0.32 in case of the low initial speed. As the speed increases the error decreases until 0.1. It is hypothesized that such error is mainly function of the acceleration calculation that, in this braking scenario, strongly affects the back-propagation process.

From the picture and the other simulations of braking on straight paths, in different configuration, it is possible to find out the good applicability of the algorithm in case of front braking and combined braking for low-medium decelerations. For high decelerations (hard braking), the algorithm shows a lack of accuracy on the rear wheel. This is a relevant limitation for the algorithm, looking at the possible application of such methods in the ABS. However it worth noting that the most relevant oscillations appear when the rear wheel is almost locked and κ_r is almost 1. This condition in terms of κ_r does not represent the working range of the ABS

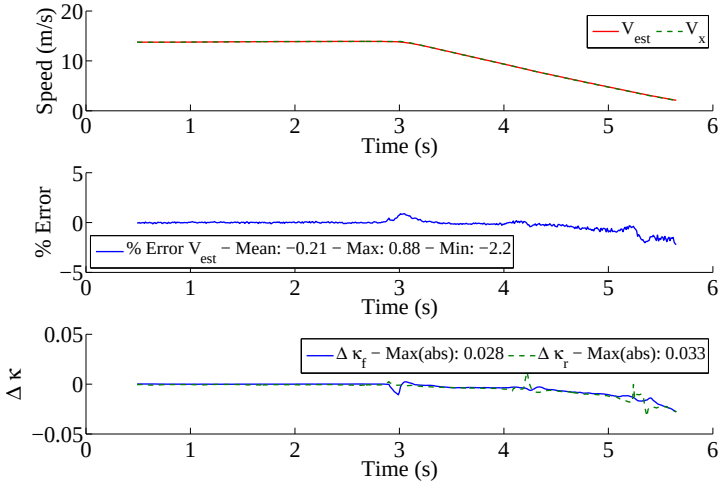

Figure 4.17: Evaluation of the algorithm for the speed estimation, during braking maneuvers: front braking on a straight path, with 425 Nm on the front wheel, starting from a longitudinal speed of 50 km/h

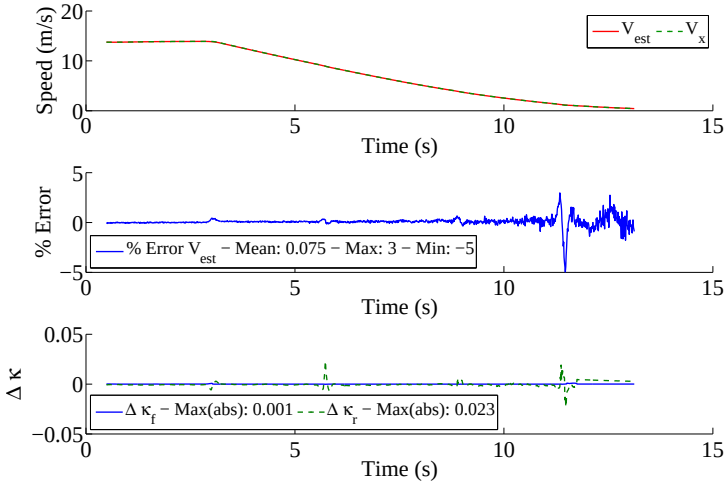

Figure 4.18: Evaluation of the algorithm for the speed estimation, during braking maneuvers: rear braking on a straight path, with 163 Nm on the rear wheel, starting from a longitudinal speed of 50 km/h

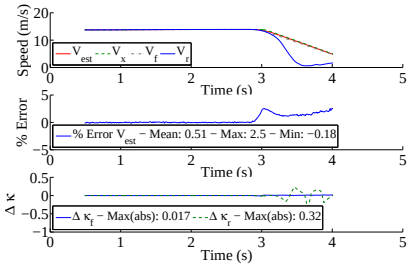

(a) Evaluation of the algorithm for the speed estimation, during a hard braking maneuver: longitudinal speed of 50 km/h.

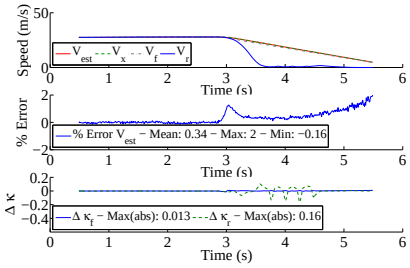

(b) Evaluation of the algorithm for the speed estimation, during a hard braking maneuver: longitudinal speed of 100 km/h.

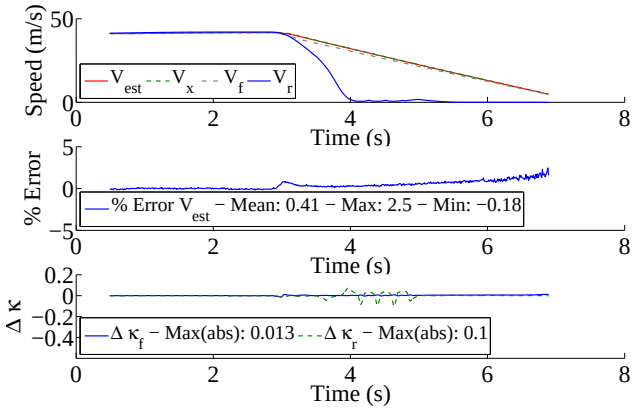

(c) Evaluation of the algorithm for the speed estimation, during a hard braking maneuver: longitudinal speed of 150 km/h.

Figure 4.19: Evaluation of the algorithm for the speed estimation, during hard braking maneuvers (with wheel locking): combined braking on a straight path, with 700 Nm on the front wheel and 270 Nm on the rear wheel, starting from a longitudinal speed of 50 km/h, 100 km/h and 150 km/h

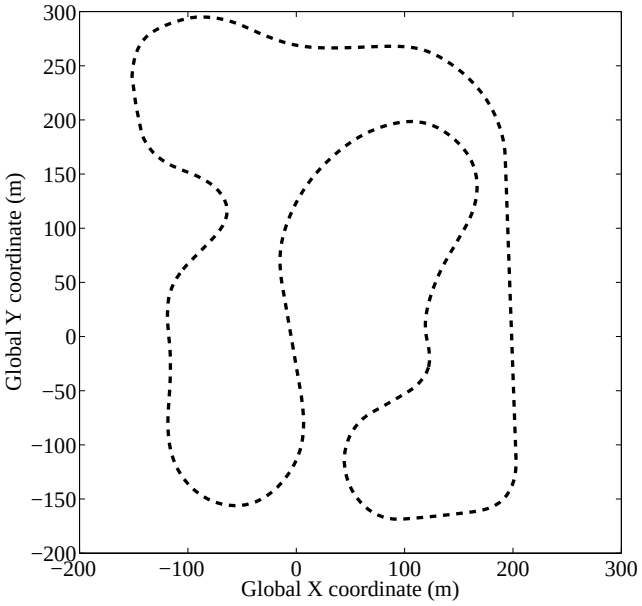

Figure 4.20: Racetrack used for the speed estimator evaluation

(0.1-0.2). In any case, a number of modifications for the hard braking maneuvers should be addressed in the next version of the algorithm, aiming to provide a good accuracy of the vehicle speed for ABS and other active braking system application.

The speed estimation described was also tested in a virtual racing track, with several curves and slopes. The general layout of the track is reported in Figure 4.20. The maximum friction coefficient is 1.15.

The results show again a good speed estimation (max error below 2.8%) and a good estimation of the longitudinal slips. The major errors detected from the analysis of $\Delta\kappa$ can be found for constant speed running or at the end of the braking maneuvers.

Then a preliminary analysis of the methods on real vehicle was carried out as well. Due to the impossibility to compare the estimated speed with the actual vehicle speed (e.g. measured by an optical device, as in [28]) the method was verified only addressing evident estimation errors.

In Figure 4.22 it is possible to see an example of application of the algorithm to an experimental run extracted from the naturalistic riding database 2BeSafe. The friction estimation algorithm was applied to 12 similar runs, each one performed in the urban area of Florence.

The preliminary analysis of the friction estimation applied on real data focused on the qualitative investigation on the good results and weakness points of the algorithm. The main relevant aspects are depicted in the next pictures.

In general, the algorithm does not show particular estimation errors: looking at the longitudinal slip during the run it is possible to see that the slip value (both

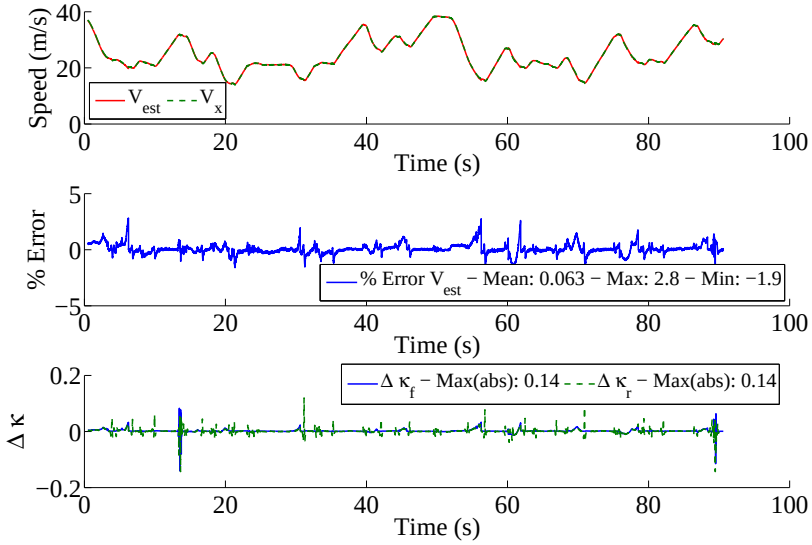

Figure 4.21: Evaluation of the speed estimation effectiveness, tested on a race circuit

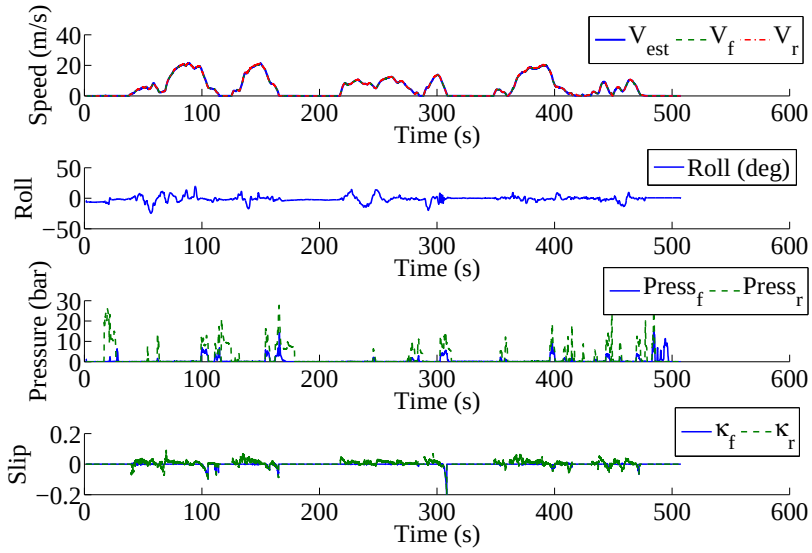

Figure 4.22: Evaluation of the speed estimation effectiveness, tested on real data representing a riding in urban scenario. The evaluation is qualitative (comparison of V_{est} with Vx_f and Vx_r), due to the absence of a reference speed signal

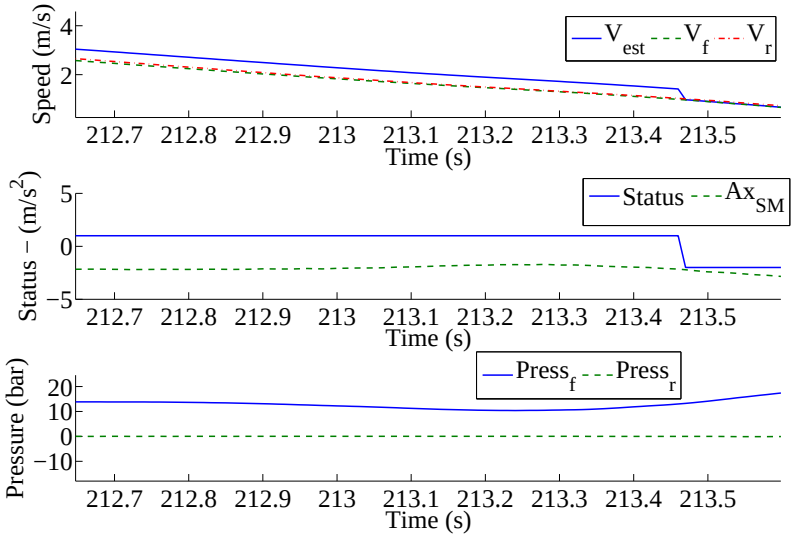

Figure 4.23: Application of the speed estimation on naturalistic riding data. Example of error caused by the misinterpretation of the correct deceleration via back-propagation method

for front and rear wheels) remains within $0.1/-0.1$, and only in few cases the absolute slip value exceeds 0.2.

These behaviors characterize mainly the braking maneuvers with the front brake. In this condition the speed estimation is based on the back-propagation of V_{est} and Ax_{SM}. Then, the accuracy of the estimation is mainly determined by the accuracy of the acceleration, and in case of a wrong evaluation of the correct value of the acceleration signal in the initial phase of the braking manoeuver the error generated propagates over the whole estimation period. An example of the error cited above is depicted in Figure 4.23. This figure was chosen as example of the back-propagation error due to the value of the longitudinal slip during the manoeuver. As example, if computed at the time step 212.7, the front slip is 0.15. Such value for the observed braking pressures (max below 15 bar), road conditions (dry asphalt, extracted from the data reports) and, most important, the acceleration, is reasonably not correct. A value of 0.15 in dry asphalt characterizes the best braking conditions (max friction coefficient) and it was not the case for this manoeuver.

In addition, the figure shows the limitations of the algorithm based on four static values of the running status S. At the end of the braking manoeuver, as soon as the status changes, the equation for the friction estimation changes as well, thus leading a discontinuity in the speed estimation curve.

Then, addressing the good results, the algorithm seems effective in case of rear

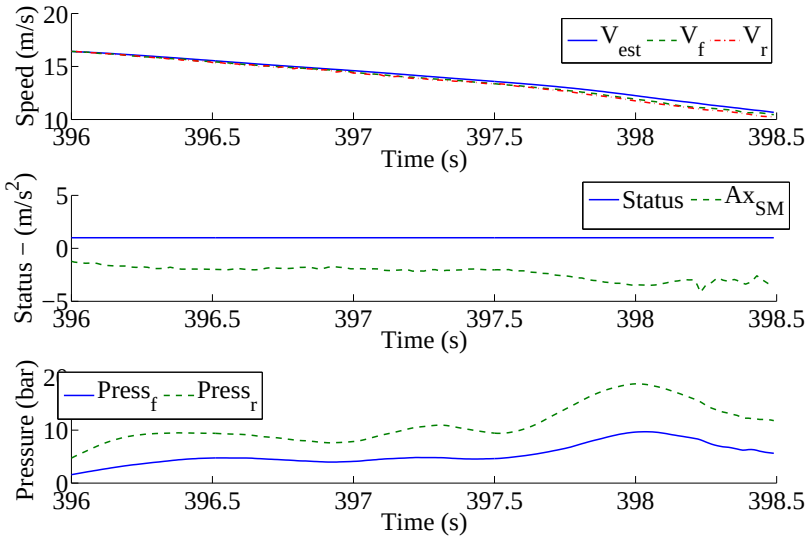

Figure 4.24: Application of the speed estimation on naturalistic riding data. Example of speed computation via accurate back-propagation method, in case of rear braking

braking (or combined braking with $P_r > P_f$). Figure 4.24 shows that in this case the back-propagation shows a good estimation of V_{est} considering the longitudinal slip value, that reaches the maximum values of 0.05 at the end of the braking, that is qualitative correct.

In case of hard rear braking the algorithm works properly as well. Figure 4.25 shows that the estimation during the emergency manoeuver is composed by a first part of back propagation and a second one of estimation based on the front wheel speed. It is clear that in that event the use of the fastest wheel as the main reference for the estimation is the correct solution; in particular whether the front wheel is almost not braked (this is the case).

A more detailed investigation of the algorithm effectiveness in real application will be carried out on future research activities, where an intensive experimental campaign will address the validation of the algorithm described in this thesis.

4.4 Discussion

The present chapter described the model and the equations used to the find out the dynamic state of a powered two-wheeler, referring in particular to the braking maneuver. More precisely, the first part addressed the model adopted to derive the main parameters necessary to have a clear understanding of the braking manoeuver. The model, even simple, provides all the parameter necessary for potential active braking systems, to be installed on a PTW.

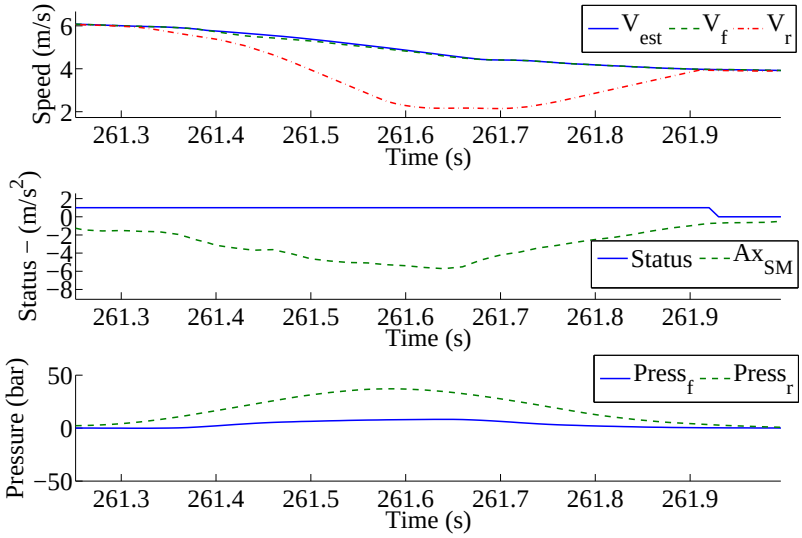

Figure 4.25: Application of the speed estimation on naturalistic riding data. Example of speed computation via accurate back-propagation method, in case of hard rear braking, leading to rear wheel locking

It has been supposed that the dynamic state could be detected using standard motorcycle sensors, like IMU, pressure sensors, wheel speed sensors, etc. In case some parameters could not be directly measured, like the vehicle speed or the actual friction condition, they have been estimated, starting from the data and parameters available from the sensors.

For active braking systems application the computation of the vehicle speed and the current friction coefficient are strategic parameters to detect and evaluate with a good accuracy. Using such variables, it is possible to design effective safety systems, with remarkable potentialities.

The algorithm proposed for the friction estimation in real-time showed promising results, even if only validated in virtual scenarios, partially supported by experimental data. The application of the methodology turn out to be effective for different road conditions: it has been able to detect the tire-road friction curve with a good accuracy, with some time step in advance before reaching the maximum friction condition (in case of hard braking leading to wheel locking). Similar results were found for different road surfaces, e.g. dry and wet asphalt. The validation process, in addition demonstrated, the effectiveness of the method also in case of sensors noise (introduced in the simulations as white Gaussian noise).

It is worth noting that the quality of the results strictly depends on the quality of the inputs. For the friction estimation methodology the most critical parameter to provide to the estimator is the tire longitudinal slip. That is because it is directly

related to the evaluation of the vehicle speed, that cannot be directly measured with the sensors available, but need to be estimated. The method proposed for the vehicle speed evaluation turned out to be promising. Again, the preliminary tests on this algorithm have been conducted in a virtual environment. The validation process of that algorithm is at a starting phase, thus not giving a full evaluation of the applicability of the system on real vehicles. In any case the simulations gave the possibility to test the effectiveness of the algorithm concept and the results showed that, in theory (if smooth signals similar to those ones obtained by the simulation software would be available), the speed estimation process can estimate the vehicle speed with an error below the 5%. That would give the possibility to apply the methodology directly on real vehicle and develop reliable active safety devices.

Chapter 5

Analysis of motorcycle fall dynamics

5.1 Motorcycle fall dynamics

The Powered Two-Wheelers dynamics is generally more complex to address than car dynamics, due to the implicit vehicle instability. In every running condition, the rider must control at the same time the steering movements and the roll movements in order to handle properly the vehicle and balance the overall dynamics. Without an adequate control the vehicle can fall, also during simple straight running. It is clear that maneuvers such as braking or swerving, require additional abilities of control to avoid the motorcycle fall, in particular during emergency events as a panic braking or a last second swerving.

Addressing the emergency braking maneuvers, in those situations the vehicle control is very demanding due to the necessity to adjust the braking intensity in the proper way. In standard vehicles, not equipped with ABS system, a common cause of accident is the wheel locking and the consequent loss of adherence. Concerning PTWs, the loss of adherence determines a high probability of motorcycle fall, especially in case of cornering.

The motorcycle fall while cornering can be divided in three groups: low-side fall due front braking, low-side fall due rear braking and high-side fall (Figure 5.1).

Cossalter and al. [81] investigated in detail the dynamics of the aforementioned three categories of motorcycle fall by a number of simulations of motorcycle crash. The authors analyzed the different phases of the fall dynamics, addressing the behaviors of the rider and the motorcycle during the events evolution. The scenario addressed for low-side and high side falls is the hard braking maneuver in steady

Figure 5.1: Real cases of low-side fall due to front braking, low-side fall due to rear braking and high-side fall

turning.

Concerning the low-side fall due to the front braking it happens mainly in case of panic braking, to avoid a collision, or in case of hard braking on slippery surfaces.

If the front braking maneuver is performed in a curve, the fall dynamics is really fast and difficult to control. The hard braking force on the front wheel introduces a rapid change on the sideslip angle of the tire. As soon as the braking force increases, in order to keep the curve trajectory the tire increases its sideslip angle. At the same time, the rider, in order to follow the trajectory, increases the steering angle as well. Let us consider constant the roll angle in the first part of the maneuver that means the curvature radius decreases with the speed, then the steering angle must increases as well, until its rotational limit. When the lateral force required keeping the trajectory exceeds the maximum value of lateral adherence the vehicle starts to slip laterally.

That it is the instant when the roll rate starts to increases quickly, and the rider has no more possibility to recover the vehicle stability, if the braking action continues.

From that point, the roll rate and the yaw rate increase until the motorcycle falls down. Due to the front wheel sliding out of the curve, the yaw rate, for a left turning and the system of reference with z-axis upwards, decreases and the rider is projected frontward.

Concerning the rear braking maneuver and the corresponding low-side fall, the motorcycle and rider behaviors are similar to the front braking case. Differently from the front braking case, the motorcycle rotation during the lateral slippage is inside the curve, then the rider is projected backward and the yaw rate, again in case of left turning and the same system of reference as before, increases. It is possible to observe this kind of falls quite frequently in racing competitions, and almost every time the rider falls behind the vehicle due to the direction of rotation described above.

Both in low-side due to front braking and low-side due to rear braking the braking action is kept until the motorcycle falls down. In case the rider, during the slippage phase, releases the brake, the vehicle will be subjected to a high-side movement. Due to brake release, the lateral force increases drastically because of the large sideslip angle reached during the maneuver. The new lateral force is too high for the actual trajectory and it is not balanced, thus generating a violent rotation of the vehicle in upward position, pushing the rider upward as well. In case of violent movements, the rider can lose the contact with motorcycle and be projected in the air, over the motorcycle.

The detailed investigation of the fall dynamics and good knowledge about motorcycle and rider's behaviors in crash events helps the development of active and passive safety systems. As example, Dainese s.p.a. and the University of Padova studied the fall dynamics to define a "fall predictive" algorithm for the activation of an airbag jacket for PTWs application. The fall behaviors of the rider and the motorcycle analyzed with virtual simulations [81, 82] and experimental data [83] gave the basis for the development of the control logic for the activation of the airbag jacket.

In [66] and [84] Cossalter et al. showed the equations for the detection of the rider fall, investigating different kind of riding scenarios.

The algorithm presented and patented by the authors, is function of the roll, pitch and yaw rates, and the longitudinal, lateral and vertical accelerations of the rider and the motorcycle. The fall detection algorithm is expressed by the following risk function:

$$RISK = f(\dot{\varphi}_{sens}, \dot{\phi}_{sens}, \dot{\psi}_{sens}, Ax_{sens}, Ay_{sens}, Az_{sens}) \tag{5.1}$$

where $\dot{\varphi}_{sens}$, $\dot{\phi}_{sens}$ and $\dot{\psi}_{sens}$ are roll, pitch and yaw rates sensed by the sensors (body fixed reference) and Ax_{sens}, Ay_{sens} and Az_{sens} longitudinal, lateral and vertical accelerations sensed by the sensor (body fixed reference). From the analysis of experimental data and virtual simulations, the authors fixed the thresholds to the risk function. The preliminary analysis of the application of Eq.5.1 on virtual simulations confirmed the applicability of an airbag jacket with such activation algorithm and showed the befits of this technology.

Also Boubezoul et al. [85] proposed an algorithm for the activation of an airbag jacket. In general, terms the algorithm considers the same parameters of Cossalter et al. and it was tested on real vehicles, under different riding situations, such as extreme braking, acceleration, fall-like maneuvers, etc. (carried out by professional riders).

An algorithm similar to those ones described above has been studied and designed to be adopted as parameters for potential falls detection. During the activity, a set of parameters to predict potential critical events related to hard braking and vehicle stability has been derived and verified, by virtual simulations and experimental data. The design process of this set of parameters, named $RISK_i$ parameters will be described in the following paragraphs.

5.2 Identification of the risk of fall

The definition of parameters able to detect the motorcycle fall is strictly related to the conditions addressed as critical condition for the motorcycle and the rider. In Ambrogi et al.[84] the target adopted for the definition of the RISK parameters was the rider safety in case of unavoidable fall at high accelerations. Then the critical event in the aforementioned conditions is the impact of the rider with the ground. In that situation, the functionality of the fall detection parameters is projected on the time interval between the destabilization of the motorcycle/rider and the imminent impact of the rider with the ground. Therefore the main goal of RISK in [84] and [66] was to guarantee the rider a soft impact with the road surface, by the activation on time of the airbag jacket.

For my activity purpose the general target to address remains the same, the rider safety, but with some differences in terms of time, initial and final conditions. Concerning the time interval, the parameters derived by Ambrogi et al. were related to a running condition in which it was not possible anymore to recover the vehicle stability and the rider fall was unavoidable. On the other side, the

parameters that will be introduced in this chapter are used to detect the instability condition of the motorcycle before the vehicle could lose the stability irreversibly. It is possible to assess that the parameters developed aimed to predict the fall, in order to give the possibility to an active safety system to modify properly the vehicle dynamics, to increase the stability of the vehicle during the maneuver.

Then, the initial condition is different. Ambrogi et al. do not pose any limitation in the activation of the safety system due to the alert given by the RISK parameters. The system works in every running condition, including braking, acceleration and steady running (straight or cornering). Differently, the algorithms here proposed are limited to the braking maneuvers, in straight running or while cornering. The other running conditions are not addressed.

Also regarding the final conditions the approach adopted for the definition the fall detection parameters is different. In my case the final target condition is the *Safe Braking*. It is considered as *Safe Braking* a braking maneuver, starting from any dynamic condition (straight running, steady cornering, curve entry, etc.), that allows the vehicle to stop in upright position, safely, with a limited number of oscillations, and a limited effort for the rider to control the steering bar.

Finally, the rider dynamics is not addressed. The rider was considered in a stable position on the saddle. That consideration is in accordance with the general target of the method: to predict a potential destabilization. In the time interval before the condition of unavoidable motorcycle fall, the dynamic state of the rider can be considered almost stationary, referred to the motorcycle, according to the observations of the simulation reported in [84, 81, 83].

Summing up, the parameters proposed aim to detect any critical braking condition before the fall become unavoidable.

In these paragraphs, the parameters will be introduced and described, then the verification and validation processes will be presented.

$RISK_2$ and $RISK_{2T}$

The first parameter adopted for monitoring the vehicle state is $RISK_2$. The target imposed is the stability of the steering movements. The definition of this parameter follows the hypotheses that in steady condition (e.g. steady cornering) or in unsteady conditions (e.g. curve entry, limited *Wobble*) under the full control of the rider the steering rate $\dot{\delta}$ is limited. On the other side, in case of unsteadiness difficult to control (e.g. a sudden sideslip angle increase or a hard *Wobble*), the value of the steering rate should change faster than the path curvature rate $\dot{Cu}$ (qualitative comparison, taking into account the really first phase of the maneuver and considering the case of front low-side fall and high-side fall which started from a front low-side). The aforementioned consideration cannon be considered completely satisfied in case of rear low-side, where the unsteadiness of steer dynamics is faster than the roll dynamics only in the first past of the braking maneuver, when the rider try to correct the lack of rear friction with the steer [81]. In the second part of the braking (and fall), the roll dynamics is faster than the steer dynamics.

According to Cossalter [5], the curvature of a path, in steady conditions depends on the front tire contact point and the kinematic steering angle δ. It can be simplified

with the equation $Cu \cong tan(\delta)/l$, where l is the vehicle wheelbase. Deriving the previous equation and substituting l, it is possible to obtain as follows:

$$Cu \cdot \dot{tan}(\delta) \cong \dot{Cu} \cdot tan(\delta) \tag{5.2}$$

In case of perturbation of the steady conditions Eq.5.2 is not true anymore.

To consider all the aforementioned hypotheses the fall detection parameters were defined taking into account following main variables:

- $tan(\delta)$
- $\dot{tan}(\delta)$
- Cu
- $\dot{Cu}$

In addition, to take into account the hard braking condition, with the reference mainly to the wheel locking, also $1/(Vx_f + Vx_r)$ was considered.

According to the detail reported above $RISK_2$ and the corresponding threshold was computed as follows:

$$RISK_2 = \frac{|\dot{tan}(\delta) \cdot Cu|}{Vx_f + Vx_r} \tag{5.3}$$

$$RISK_{2T} = \frac{K_2 + |\dot{Cu} \cdot tan(\delta)|}{2 \cdot max(Vx_f, Vx_r)} \tag{5.4}$$

$$K_2 = 2 \cdot |Cu| \tag{5.5}$$

Differently from $RISK_2$, $RISK_{2T}$ is divided by $2 \cdot max(Vx_f, Vx_r)$. Accordingly to this formulation the value of $RISK_{2T}$ will be less influenced by the deceleration of the wheels in case of locking of only one wheel. This leads $RISK_{2T}$ to change slower than $RISK_2$.

The additional offset value reported in Eq.5.5 was introduced to take into account the unsteadiness of a motorcycle running in normal conditions (accelerations, curve entry, slalom, etc.). Then, the threshold considered was fixed according to the observation of the simulation of front low-side fall and rear low-side fall in [81]. The value of $\dot{tan}(\delta)$, in the falling phase, was within the range of (approximately) $2\ rad/s \div 4\ rad/s$. It was chosen the lowest one, $2\ rad/s$, to address also the "slow" variations of the steering angle.

$RISK_3$ and $RISK_{3T}$

The second parameter $RISK_3$ addressed the unsteadiness of the main frame by the difference of the sideslip angles, computed with Eq.4.24. The simulations

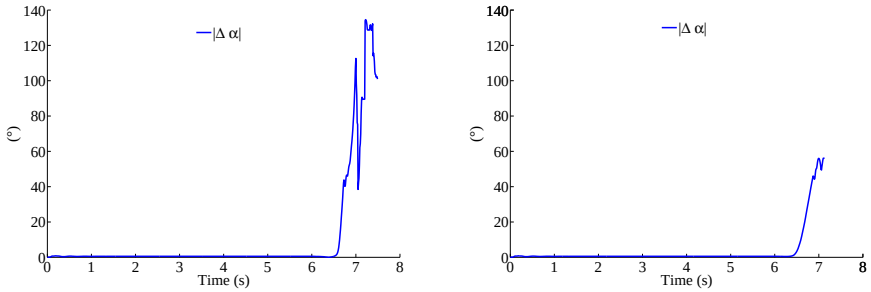

(a) $\Delta\alpha$ in case of low side due to front wheel locking

(b) $\Delta\alpha$ in case of low side due to rear wheel locking

Figure 5.2: Time evolution of $\Delta\alpha$ in case of low side due to front wheel locking and rear wheel locking

showed that in case of hard front or hard rear braking with consequent lack of friction, the difference between the sideslip angles quickly diverges (Figure 5.2).

$$RISK_3 = \frac{|\Delta\alpha|}{Vx_f + Vx_r} \tag{5.6}$$

Then only $\Delta\alpha$ was addressed as risk parameter, without any other components, apart from the wheels speed difference, again to increase parameters sensibility to the lack of adherence conditions.

$$RISK_{3T} = \frac{K_3}{2 \cdot max(Vx_f, Vx_r)} \tag{5.7}$$

$$K_3 = 0.07\ rad \tag{5.8}$$

The threshold K_3 introduced in $RISK_{3T}$ was decided according to the simulations made to calibrate the parameters (§5.3). In the simulations, excluding those ones that led the vehicle to fall down due to lack of longitudinal or lateral adherence, according to the tire model used for the virtual model,$|\Delta\alpha|$ stays below $4°(0.07\ rad)$. That value was chosen as K_3.

The value of 0.07 rad was chosen for the particular tire model adopted on the vehicles. Then, it is worth noting that this parameter needs to be modified if different tire properties are addressed in the model.

$RISK_{4.i}$ and $RISK_{4.iT}$

The last set of parameters named $RISK_{4.i}$ addresses the longitudinal dynamics of the braking maneuvers. Differently from the previous parameters they do consider only the in-plane motion of the vehicle, neglecting the roll or steer dynamics. Parameters $RISK_{4.i}$ aim to detect the threshold that separates a complete *Safe Braking* maneuver (even hard braking, but completely safe, considering the wheels

always below the friction limit) from a dangerous braking or at least potentially dangerous.

For my purpose it has been considered "dangerous" a maneuver in which the tires start to slip, during a hard braking. Of course, due to the events evolution in the scenario, the dangerous maneuver can turn into a safe maneuver. It is clear how much the detection of the dangerous condition depends not only on vehicle dynamics but also on the road scenario. In the next paragraph it will be explained how this problem has been addressed in order to define properly the threshold of the parameters.

Considering the rider fixed on the motorcycle main frame, the main parameters used for $RISK_{4.i}$ were:

- $\dot{\phi}$, the pitch angle rate;
- Ax_{SM}, the longitudinal acceleration of the vehicle, parallel to the ground;
- $Vx_f - Vx_r$, the difference between the peripheral speeds of front and rear wheels.

More in detail, considering the vehicle longitudinal dynamics, in case of braking the pitch rate and the longitudinal acceleration address the load transfer, the intensity of braking and the mass distribution modification, then wheels speed difference takes into account the tire-road friction condition.

Parameter $RISK_{4.0}$ considers the three variables all together, with a simple multiplication. That was made to match the contributions coming from $\dot{\phi}$ and Ax_{SM}, contributions that can have similar or different phases (it depends on the suspensions reaction).

$$RISK_{4.0} = |\dot{\phi} \cdot Ax_{SM} \cdot (Vx_f - Vx_r)| \tag{5.9}$$

Parameters $RISK_{4.1}$ and $RISK_{4.2}$ were set up to consider separately the contribution of the acceleration and the pitch rate. In addition $\dot{\phi}$ has been multiplied by $(Vx_f - Vx_r)$ to "extend" the effect of the pitch rate in case the tire starts to slip. In order to emphasize the individual contribution of $\dot{\phi}$ and Ax_{SM}, the quadratic values of each one were considered in $RISK_{4.2}$.

F was introduced to make comparable the value of $\dot{\phi} \cdot (Vx_f - Vx_r)$ and Ax_{SM}. Its value was found via virtual calibration.

$$RISK_{4.1} = (|F \cdot \dot{\phi} \cdot (Vx_f - Vx_r)| + |Ax_{SM}|) \cdot |Vx_f - Vx_r| \tag{5.10}$$

$$RISK_{4.2} = (F^2 \cdot (\dot{\phi} \cdot (Vx_f - Vx_r))^2 + Ax_{SM}^2) \cdot (Vx_f - Vx_r)^2 \tag{5.11}$$

The corresponding thresholds of parameters $RISK_{4.i}$ were found experimentally with a calibration process on virtual data and on experimental data. They are function of the speed and the braking pressures distribution. All the constants K_{4ii} and TRH_{4i} were set up by a further calibration process.

$$RISK_{4.0T} = TRH_{40} + K_{400} \cdot \frac{|K_{401} + K_{402} \cdot Vx + K_{403} \cdot Vx^2|}{1 + K_{404} \cdot \frac{P_r}{P_f + P_r}} \tag{5.12}$$

$$RISK_{4.1T} = TRH_{41} + K_{410} \cdot \frac{|K_{411} + K_{412} \cdot Vx + K_{413} \cdot Vx^2|}{1 + K_{414} \cdot \frac{P_r}{P_f + P_r}} \tag{5.13}$$

$$RISK_{4.2T} = TRH_{42} + K_{420} \cdot \frac{(K_{421} + K_{422} \cdot Vx + K_{423} \cdot Vx^2)^2}{1 + K_{424} \cdot \frac{P_r}{P_f + P_r}} \tag{5.14}$$

$RISK_{4.i}$ do not work separately and they are taken into account at the same time. Due to the variability of road scenarios and the possibility to calibrate the parameters only on a very small part of these scenarios it was imposed that the warning signal given by parameters $RISK_{4.i}$ is reliable only in case the three parameters exceed the corresponding thresholds at the same time. This condition can be considered also for conservative reasons, thus limiting the number of false-positive warnings.

5.3 Calibration of $RISK_i$ parameters

5.3.1 Verification of $RISK_2$ and $RISK_3$ on virtual data

The reliability of parameters $RISK_2$ and $RISK_3$ was evaluated on a number of simulations including swerving and braking maneuvers. More in detail, the full protocol of simulations is summed up in the following lists.

- Front braking: high decelerations leading to wheel locking (max braking torque 660 Nm, dry asphalt, max μ_x 1.15). Target conditions (to perform a deeper investigation, in addition, also some rear braking maneuvers were considered)

- Initial speed, 50 km/h, 100 km/h, 150 km/h;
- Target roll angle, 0°, 10°, 20°, 30°.

- Swerving maneuver: fast cornering, e.g. fast lane change, with a roll rate below 60°/s.

- Initial speed, 50 km/h, 100 km/h, 150 km/h;
- Target roll angle, 30°.

- L_{sw} maneuver [15]: fast cornering, e.g. last-second collision avoidance, with a roll rate over 60°/s and below 110°/s.

- Initial speed, 50 km/h, 100 km/h, 150 km/h;
- Target roll angle, 30°.

Concerning the braking maneuvers the vehicle ran in steady state conditions for 6 s and then applied a braking force distributed over 0.5 s (with internal fluid delays 0.7 s, [41]). A similar time evolution has been adopted for the swerving maneuvers: 6 s is the time step at which the maneuver begins.

Despite the general application of $RISK_2$ and $RISK_3$ (braking, acceleration, swerving, steady cornering, curve entry, etc.) the dangerous maneuvers addressed in the simulations were only braking maneuvers, focusing only on the main purpose of the research activity. The applicability of the parameters in other scenarios, apart from braking, will be addressed in future activities.

The simulations reported above were performed for three different vehicles: a maxi scooter Piaggio Beverly300, a super sports motorcycle[1], and a sports touring motorbike [2]. All the simulations were carried out in Bikesim®. Different vehicles were considered in order to have a preliminary evaluation of the versatility of the parameters application on different PTWs.

Due to the necessity to address mainly the instabilities related to the steering behavior and the mainframe oscillations (still connected to the steer oscillations), only the front braking and swerving maneuvers were simulated.

The swerving maneuvers (including L_{sw}) were simulated in order to address unsteady and fast maneuvers that an average rider can perform safely. It was expected that in such conditions the $RISK_2$ and $RISK_3$ would not give any alert (exceeding the thresholds). The swerving maneuvers were simulated only at the largest roll angle, because it has been considered as the most critical swerving condition (compared to the cases with lower roll angles, 10°and 20°).

The parameters $RISK_2$ and $RISK_3$ and the corresponding thresholds were defined following literature basis, and motorcycle dynamics theory. The assumptions made for the thresholds properties (values of the constants) were made according to the state of the art, therefore the evaluation the aforementioned parameters on the listed simulations aimed to verify the assumptions made and not to perform a strict calibration.

Figure 5.3 shows the application of $RISK_2$ and $RISK_3$ to the L_{sw} maneuver at different speeds (φ target 30°), for the Beverly300. At each speed the parameters never exceed the thresholds. However it worth noting that the value of the parameters in $RISK_2$ are close to the limit, especially at 50 km/h; on the other side the L_{sw} represents the upper limit of the swerving maneuver, for a standard rider. It is correct to assume this as limit condition, expecting that it is almost impossible to perform faster swerving maneuvers, especially with a big scooter.

Regarding $RISK_3$ no particular issues were detected, and the comparison, in the simulations addressed confirmed the reliability of $RISK_3$ and $RISK_{3T}$. It is interesting to notice that for increasing speeds the gap between $RISK_3$ and $RISK_{3T}$ decreases. It is hypothesized that this aspect is partially related to the steering rate $\dot{\delta}$: it was observed that at higher speeds $\dot{\delta}$ increases to achieve the target roll angle. That increases also the value of the front slip angle, thus the $\Delta\alpha$ as well.

Also for the super sports motorbike and the touring motorcycle the verification of $RISK_2$ and $RISK_3$ give good results as well. Figure 5.4 depicts the application of

[1]Default inertial, geometrical properties and mass distribution given by Bikesim®software (range of motorcycles such as the Yamaha YZF/FZ1, Honda CBR600RR, Kawasaki NINJA, and Suzuki GSX-R1000). Braking characteristics customized, similar to a Yamaha YZF/FZ1

[2]Default inertial, geometrical properties and mass distribution given by Bikesim®software (range of motorcycles such as BMW K1200 GT, Honda VFR1200, and Kawasaki 1400 GTR). Braking characteristics customized, similar to a Honda VFR1200

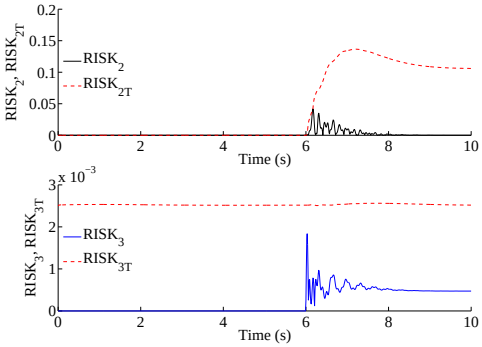

(a) $RISK_2$ and $RISK_3$ Vs. $RISK_{2T}$ and $RISK_{3T}$. Initial speed 50 km/h, Max roll angle 30°

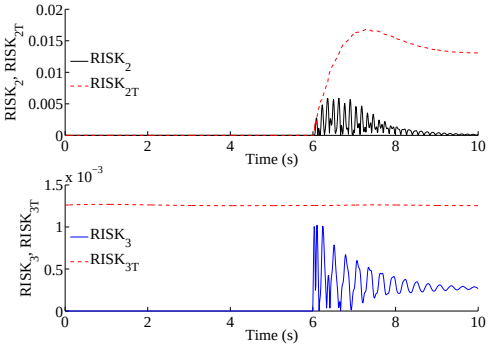

(b) $RISK_2$ and $RISK_3$ Vs. $RISK_{2T}$ and $RISK_{3T}$. Initial speed 100 km/h, Max roll angle 30°

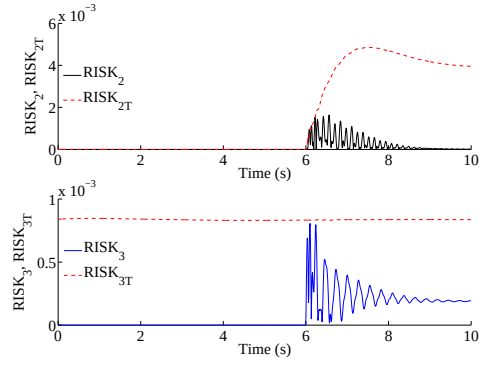

(c) $RISK_2$ and $RISK_3$ Vs. $RISK_{2T}$ and $RISK_{3T}$. Initial speed 150 km/h, Max roll angle 30°

Figure 5.3: Application of $RISK_2$ and $RISK_3$ to different L_{sw} maneuvers. Vehicle: Piaggio Beverly300

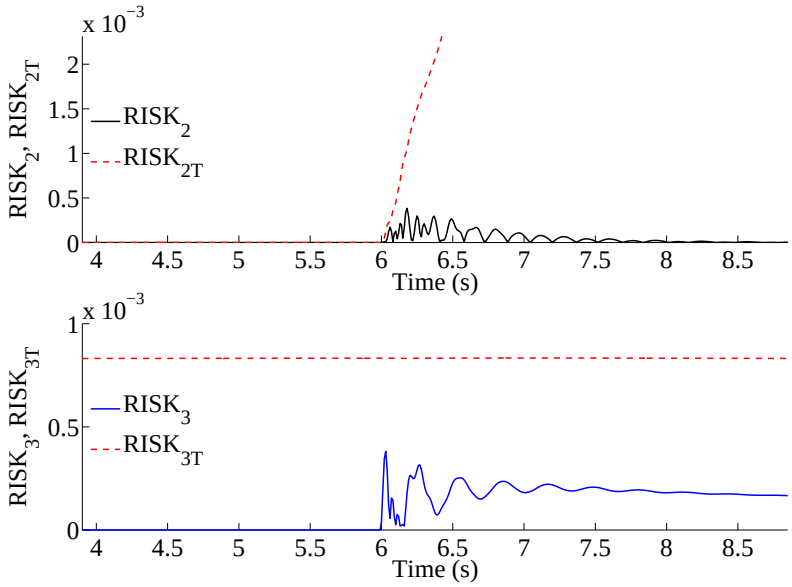

Figure 5.4: Application of $RISK_2$ and $RISK_3$ to a L_{sw} maneuver involving a super sports motorbike. Initial speed 50 km/h, Max roll angle 30°

the parameters to the super sports motorbike running at 150 km/h and performing a L_{sw} with the target roll angle of 30°.

It is possible to see, that differently from the Beverly300, the $RISK_2$ in this motorcycle is more distant from the threshold. The same is for the Touring motorbike. This small difference can be addressed focusing on the steering properties of the vehicle influenced by the mass distribution. In fact, the sports motorbikes have a distribution of masses more on the front wheel, while it is the opposite for the Beverly300, and other scooters. That can strongly influences the steering control, the vehicle maneuverability, and the risk parameters as well.

Considering the emergency braking maneuvers, at different roll angles and different initial speeds, the application of the risk parameters aims to detect the instant at which those maneuvers become unstable and not safe.

Figure 5.5 shows the results of the risk parameters application on the hard braking simulation, for different roll angles, at 50 km/h. In the cases depicted, the main parameter exceeds the threshold after 0.5-0.7 s the braking started (the time step increases for lower roll angles). At these time steps, the roll angle has not changed too much (within 2°) and the roll rate is below 10°/s (the max value is over 250°/s). That means that the potential critical event is detected in a time range sufficiently small to modify the vehicle dynamics to correct and recover the stability.

Comparing the behaviors of $RISK_2$ and $RISK_3$, it is possible to see that,

despite similar time steps in risk detection, the evolution with respect to the thresholds is different. Only $RISK_3$ stays constantly over the threshold during the maneuver, while $RISK_2$ moves across the threshold line. That shows that the use of only one parameter is not sufficient for the correct risk detection, both must be taken into consideration at the same time.

The same observations can be drawn also for the rear braking case. Figure 5.6 shows a hard rear braking, with wheel locking, at 20°and an initial speed of 50 km/h. For the rear braking case it is possible to see that $RISK_3$ anticipates the fall detection than $RISK_2$. During a hard rear braking while cornering the effect of front aligning torque on the steer, due longitudinal force on the front wheel is minimized, thus limiting the steering rate. Therefore the variation of the $\Delta\alpha$, caused by a fast change of α_r, is faster than the variations of $\dot{tan}(\delta)$, thus resulting in a faster $RISK_3$.

Also for the super sports motorcycle and the sports touring motorbike, the implementation of the risk parameters gives the same results. In Figure 5.7 the hard front braking in curve of a super sports motorcycle is depicted. Again, it is possible to notice the high number of fluctuations of $RISK_2$ compared to $RISK_3$.

Finally, the reliability of $RISK_2$ and $RISK_3$ was tested in the racetrack introduced for the validation of the tire-road friction estimation (§4.2). In Figure 5.8 the run of the Bevely300 is shown. Hereafter only the run of Beverly300 is reported because, compared to the runs of the sports motorcycles, it is the only simulation where there has been one fall detection, due to an unexpected passing on the side curb at the end of the last curve (time 96.5 s). The event caused some skids (the corresponding δ and $\dot{\delta}$ are ±6°and ±6°/s), finally controlled by the rider when the vehicle went back to the track (Figure 5.9).

Due to the low level of danger and the low potentiality of fall, the detection of risk parameters is only for few time steps.

5.3.2 Calibration of $RISK_{4.i}$ on virtual data

Differently from $RISK_2$ and $RISK_3$, parameters $RISK_{4.i}$ and the corresponding thresholds require a proper calibration. Their structure was not derived from theoretical basis, but from an arbitrary combination of variables (of course, according to specific considerations on vehicle dynamics).

The calibration of the constant variables reported in equations from 5.9 to 5.14 was made on virtual simulations and experimental data. In this section, the virtual calibration is described.

The simulations carried out were the following:

- Front braking and Rear braking: high decelerations leading to wheel locking (Max braking torque 660 Nm, dry asphalt, max μ_x 1.1). Target conditions:

  - Initial speed, 30 km/h, 50 km/h, 100 km/h, 150 km/h;

  - Target roll angle, 0°, 10°, 20°, 30°.

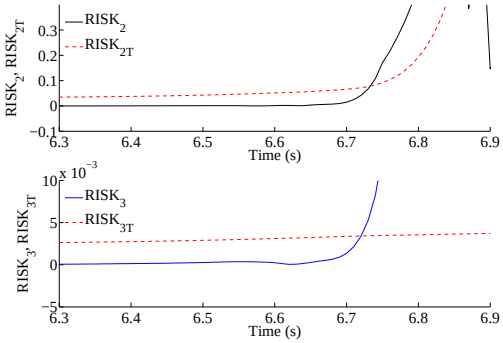

(a) $RISK_2$ and $RISK_3$ Vs. $RISK_{2T}$ and $RISK_{3T}$. Initial speed 50 km/h, Max roll angle 10°

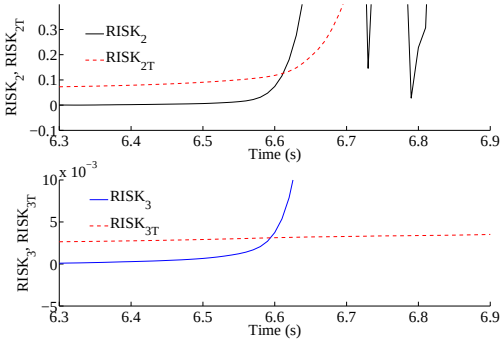

(b) $RISK_2$ and $RISK_3$ Vs. $RISK_{2T}$ and $RISK_{3T}$. Initial speed 50 km/h, Max roll angle 20°

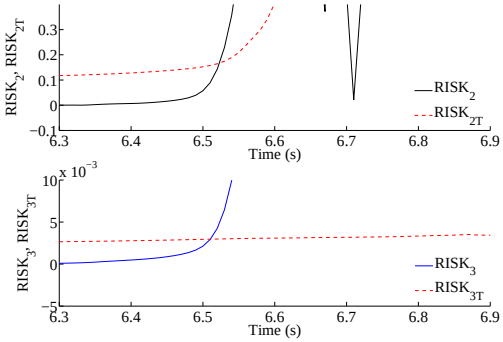

(c) $RISK_2$ and $RISK_3$ Vs. $RISK_{2T}$ and $RISK_{3T}$. Initial speed 50 km/h, Max roll angle 30°

Figure 5.5: Application of $RISK_2$ and $RISK_3$ to front hard braking maneuvers involving the Beverly300

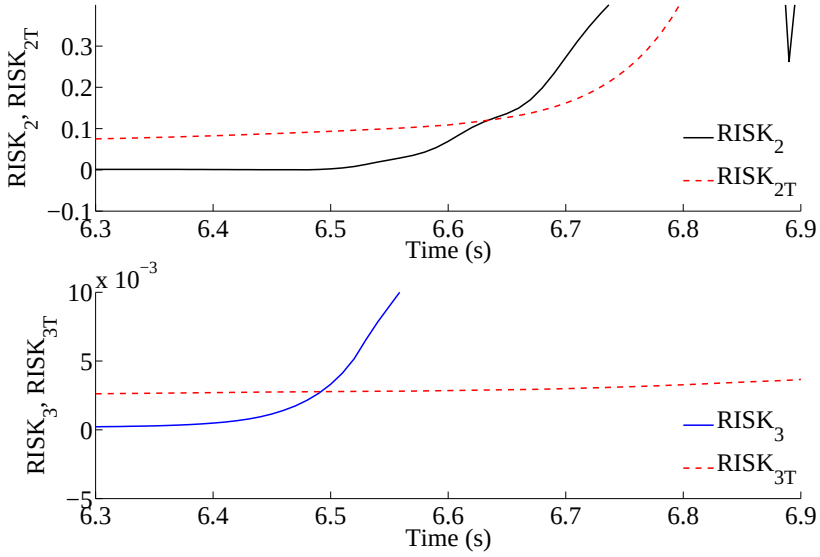

Figure 5.6: Application of $RISK_2$ and $RISK_3$ to a rear hard braking maneuver involving a Beverly300. Initial speed 50 km/h, Max roll angle 20°

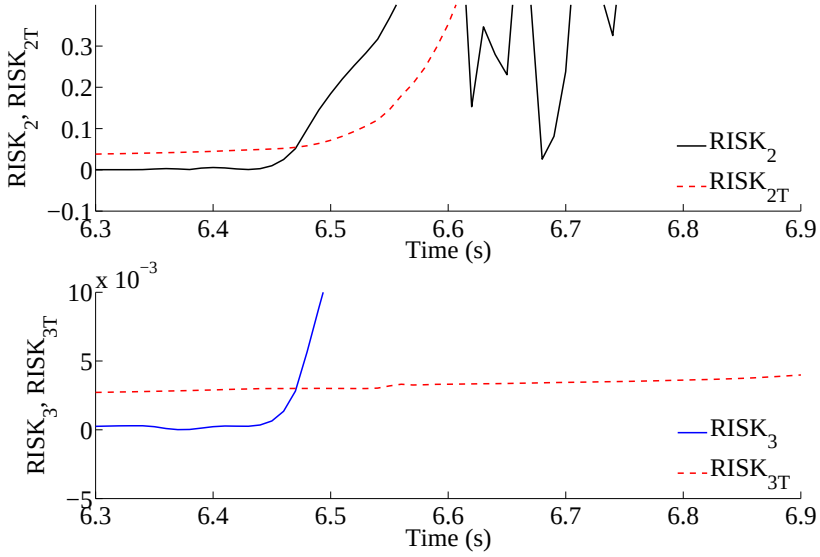

Figure 5.7: Application of $RISK_2$ and $RISK_3$ to a front hard braking maneuver involving a super sports motorbike. Initial speed 50 km/h, Max roll angle 10°

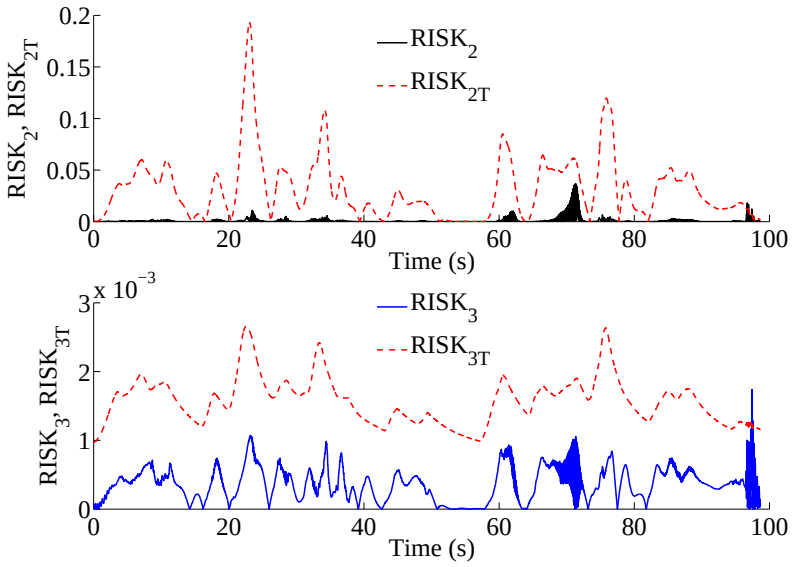

(a) $RISK_2$ and $RISK_3$ Vs. $RISK_{2T}$ and $RISK_{3T}$. Complete Run.

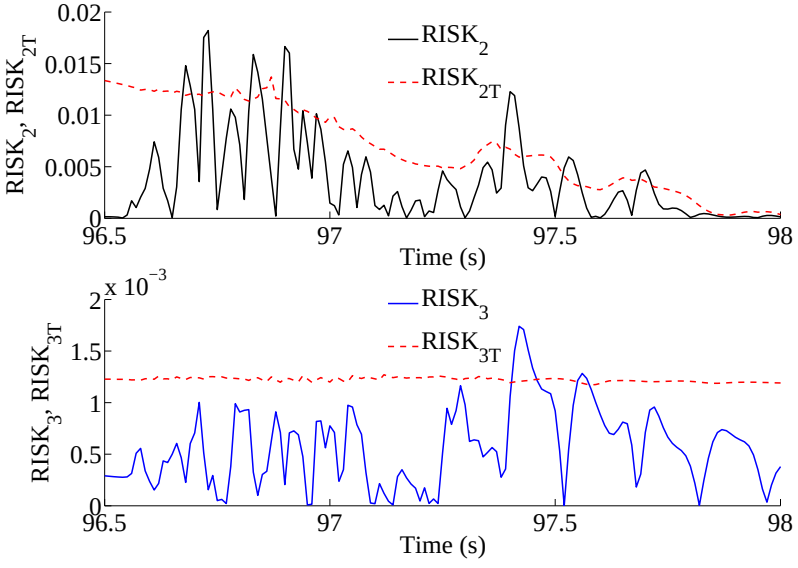

(b) $RISK_2$ and $RISK_3$ Vs. $RISK_{2T}$ and $RISK_{3T}$. Zoom on fall detection interval

Figure 5.8: Application of $RISK_2$ and $RISK_3$ to run on a race-track, involving a Beverly300

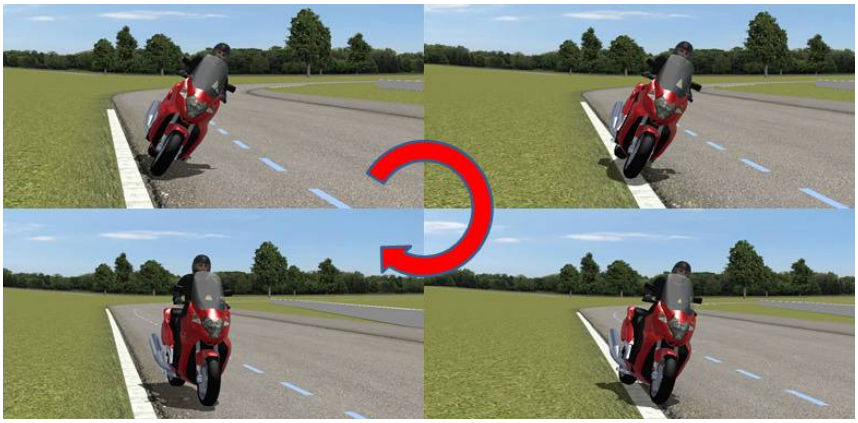

Figure 5.9: Time sequence of the critical event: track - curb - track

- Front braking and Rear braking: medium decelerations[3] without wheel locking, friction conditions always below the limit (Max braking torque 400 Nm, dry asphalt, max μ_x 1.15). Target conditions:

- Initial speed, 30 km/h, 50 km/h, 100 km/h, 150 km/h;
- Target roll angle, 0°, 10°, 20°, 30°.

For this activity only the Beverly300 was used for the calibration of $RISK_{4.i}$, due to the possibility to validate the parameters only by experimental data obtained by the scooter. In future activities, also other vehicles will be addressed, to observe the variability of the calibration equations for different PTWs.

The calibration of the constant values of parameters $RISK_{4.i}$ and the corresponding thresholds was based on the front braking maneuvers with medium decelerations.

First, the value of F was fixed by the comparison between the max values of $\dot{\phi} \cdot (Vx_f - Vx_r)$ and Ax_{SM}. The target was to take into account the same contribution to $RISK_{4.1}$ and $RISK_{4.2}$ of the aforementioned two variables. The Table 5.1 reports the ratios $max|Ax_{SM}|/max|\dot{\phi} \cdot (Vx_f - Vx_r)|$. The values reveal that this ratio has a relevant variability for different running speeds and a negligible variability for different roll angles[4].

In case of rear braking the final values follows the same variability on the roll angle (negligible), and they are 4 times bigger than front braking values, concerning the variability on the longitudinal speed.

[3]Only medium decelerations were taken into account in order to compare front and rear braking, both below the friction limits. In fact, exceeding the braking torque set for these simulations the rear braking leads to wheel locking, thus limiting the calibration only to the front wheel

[4]The value of 90.2 at 30°and 30 km/h is due to the motorcycle fall before reaching the max value of pitch rate. Then, it can be considered as an outlier

Table 5.1: Calibration of F for $RISK_{4.1}$ and $RISK_{4.2}$ for front braking with medium decelerations. Values from the ratio $max|Ax_{SM}|/max|\dot{\phi} \cdot (Vx_f - Vx_r)|$

		Speed (m/s)			
		8.33	13.89	27.78	41.67
Roll (°)	0	52.77	32.29	17.07	12.28
	10	54.33	32.49	17.17	12.32
	20	59.84	33.12	17.49	12.46
	30	90.2	35.22	18.11	13.01

Due to the low variability of the ratios as function of the roll angles, the ratios at 0°were considered to derive F. The resulting equation is the following:

$$F = \frac{1430}{1 + 3\frac{P_f}{P_f + P_r}} \cdot Vx^{-0.909} \tag{5.15}$$

A similar criterion was adopted to find out the equations of the thresholds. The maximum values of $RISK_{4.0}$, $RISK_{4.1}$ and $RISK_{4.2}$ were computed (in Tables 5.2, 5.3, 5.4), and the equations of $RISK_{4.iT}$ as functions of the longitudinal speed were derived. Again, the variability of the equations for different roll angles could be considered negligible, and then the equation at 0°was taken as reference for the thresholds. In addition, by comparing the front braking and the rear braking it was added the contribution of the braking pressure distribution in the equations of $RISK_{4.iT}$.

After the application of the computed thresholds on the simulations, with a trial-and-error methodology the values of $RISK_{4.iT}$ were tuned by a scaling factor of 1.3 for $RISK_{4.0T}$ and $RISK_{4.1T}$ and 1.2 for $RISK_{4.2T}$, in order to introduce an additional safety margin to the equation derived by the calibration process. The offsets TRH_{4i} in the Eqs.5.12, 5.13, and 5.14, were set zero for the virtual simulation, and were computed only on experimental data (see next paragraph).

Table 5.2: Calibration of $RISK_{4.0T}$ for front braking with medium decelerations. Max values of $RISK_{4.0}$

		Speed (m/s)			
		8.33	13.89	27.78	41.67
Roll (°)	0	0.137	0.230	0.495	0.844
	10	0.138	0.233	0.497	0.849
	20	0.141	0.240	0.505	0.859
	30	0.141	0.248	0.515	0.848

Table 5.3: Calibration of $RISK_{4.1T}$ for front braking with medium decelerations. Max values of $RISK_{4.1}$

		Speed (m/s)			
		8.33	13.89	27.78	41.67
Roll (°)	0	2.049	3.409	7.229	11.982
	10	2.066	3.459	7.331	12.181
	20	2.105	3.620	7.652	12.712
	30	2.095	3.885	8.238	13.453

Table 5.4: Calibration of $RISK_{4.2T}$ for front braking with medium decelerations. Max values of $RISK_{4.2}$

		Speed (m/s)			
		8.33	13.89	27.78	41.67
Roll (°)	0	2.599	7.253	34.170	100.158
	10	2.669	7.496	35.147	103.622
	20	2.863	8.291	38.792	112.837
	30	3.023	9.750	47.332	129.638

The final equations of $RISK_{4.iT}$ are the following:

$$RISK_{4.0T} = TRH_{40} + 1.3 \cdot \frac{|0.0306 + 0.0114 \cdot Vx + 0.0002 \cdot Vx^2|}{1 + 7 \cdot \frac{P_r}{P_f + P_r}} \tag{5.16}$$

$$RISK_{4.1T} = TRH_{41} + 1.3 \cdot \frac{|0.3634 + 0.1859 \cdot Vx + 0.0022 \cdot Vx^2|}{1 + 0.6 \cdot \frac{P_r}{P_f + P_r}} \tag{5.17}$$

$$RISK_{4.2T} = TRH_{42} + 1.2 \cdot \frac{(0.3634 + 0.1859 \cdot Vx + 0.0022 \cdot Vx^2)^2}{1 + 0.6 \cdot \frac{P_r}{P_f + P_r}} \tag{5.18}$$

It is worth noting that for simplicity part of the Eq.5.18 was not derived directly by the Table 5.4, but from Eq.5.17.

As example, the application of the parameters $RISK_{4.i}$ and the corresponding threshold on front braking maneuvers (medium decelerations (0.6 g) and high decelerations (0.9 g) with wheel locking) is depicted in Figure 5.10.

5.3.3 Calibration of $RISK_{4.i}$ on naturalistic riding data

The calibration of parameters $RISK_{4.i}$ and $RISK_{4.iT}$ was completed on experimental data. As already said in the previous paragraph the calibration of $RISK_{4.i}$ and $RISK_{4.iT}$ was carried out addressing only the scooter Beverly300 due to the possibility to refine the virtual calibration on experimental data only for that vehicle.

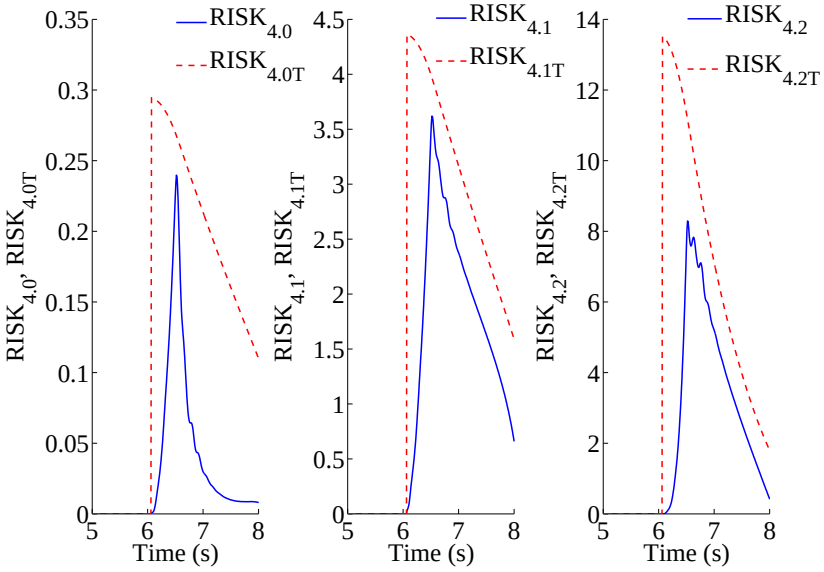

(a) $RISK_{4.i}$ vs. $RISK_{4.iT}$. Running conditions: medium deceleration (0.6 g), initial speed 50 km/h, Max roll angle 20°; Beverly300; Front braking maneuver

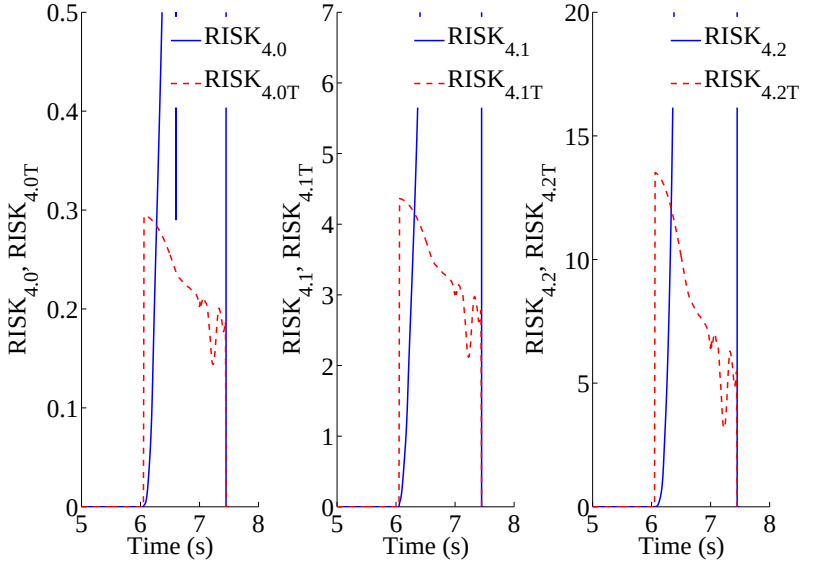

(b) $RISK_{4.i}$ vs. $RISK_{4.iT}$. Running conditions: high deceleration (0.9 g), initial speed 50 km/h, Max roll angle 20°; Beverly300; Front braking maneuver

Figure 5.10: Application of $RISK_{4.i}$ and $RISK_{4.iT}$ for different decelerations

Table 5.5: Values of the offsets TRH_{4i}

TRH_{40}	TRH_{41}	TRH_{42}
0.2	2	20

The naturalistic riding data from the 2BeSafe Database were used for the final calibration of $RISK_{4.i}$ and $RISK_{4.iT}$.

More in detail, the naturalistic riding of 6 riders was investigated. In total 250 full runs in urban and suburban scenarios were considered. Since neither accidents nor collisions happened during the acquisition period, it was expected to find a small number of potential fall detections, limited in terms of time of detection and severity as well. According to the deliverable of the project, from the analysis of all the runs, during the project 36 cases of "near missed[5]" accidents were found. Among those 36 cases, only 6 were associated to hard-medium braking maneuver performed by the riders. In the remaining cases the "near missed" accidents were related to pure swerving maneuvers or to a combination of braking and swerving.

Aiming to detect the potential critical events related only to hard braking, it was expected to find at least 6 detections, corresponding to the aforementioned 6 "near missed" accidents.

Using as reference for *potential falls* detection the aforementioned 6 cases, the offsets TRH_{4i} of $RISK_{4.iT}$ were derived. The computation of these constants is necessary to take into account the noise coming from the signal of the sensors used for the data acquisition. The offsets allow reducing the number of false detections, even if the threshold upward shift adds some delay in the detection time. In any case, it was also observed that, in real critical events, the gradient of $RISK_{4.i}$ is so high that delay can be considered not relevant.

An example of application of the $RISK_{4.i}$ and $RISK_{4.iT}$ on experimental data is depicted in Figure 5.11. It represents the detection of an emergency braking (with an initial tire slip) when a car unexpectedly crossed the road (Figure 5.12).

As expected, the detection of the critical event starts when the tire starts to slip. Then, as soon as the car is passed the brakes are immediately released and the warning by $RISK_{4.i}$ ends.

After tuning the $RISK_{4.i}$ on these 6 cases of hard braking maneuvers in naturalistic riding scenarios, the TRH_{4i} have been defined as in Table 5.5.

Finally, the calibration of the offsets briefly described above, the $RISK_{4.i}$ were applied to the whole set of experimental data.

The result of the application of the risk parameters was 31 potential fall detections. The reliability of the detections was verified by the analysis of the sensor signals and the investigation of the recorded video. The final evaluation of those cases is reported in Figure 5.13.

The 29 correct detections include critical events like wheel locking, braking to avoid imminent collisions with other vehicles, braking to avoid imminent collisions

[5]Critical events, like a panic braking or an evasive maneuver to avoid a collision. The evaluation was given based on the analysis of the video recordings of the runs

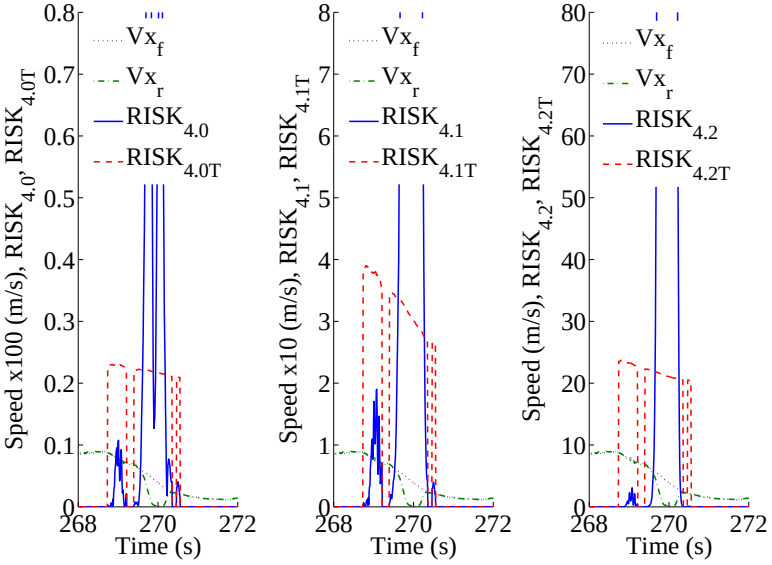

Figure 5.11: Application of $RISK_{4.i}$ and $RISK_{4.iT}$ to a naturalistic riding run

Figure 5.12: Recorded image of the critical event

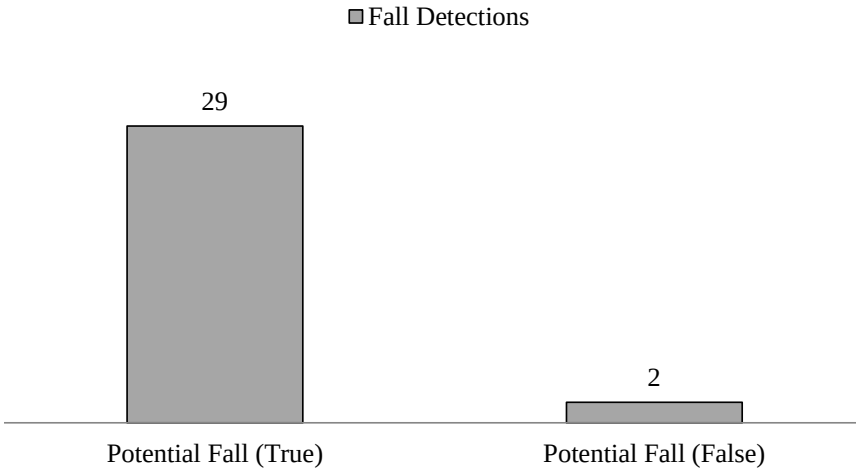

Figure 5.13: Results from the application of parameters $RISK_{4.i}$ on experimental data

with pedestrians, etc.

The 2 cases of false positive are both related to medium braking maneuvers while the motorcycle was passing over a road bump. That event introduced an acceleration on the vertical axis of the IMU, thus influencing the computation of the longitudinal accelerations (see the compensation equation in §4.1).

Despite of the presence of some false positive cases, these detections are definitely fewer than the 29 positive cases detected. It is worth noting that the sensitivity of detection is strongly influenced by the values of TRH_{4i}. Increasing the values, it is possible to exclude the events less critical, and to consider the fall detections with a higher potentiality. Furthermore, an upward shifting allows reducing the number of false positive. However, it introduces an additional delay in the potential fall detection.

Finally, also $RISK_2$ and $RISK_3$ were evaluated on the experimental data. As expected, no potential falls, related to the steering instability or vehicle oscillations, were detected. That confirmed the analyses of the results of the 2BeSafe project, in terms of critical events not related to braking.

5.4 Conclusions

In this chapter the design and development of an algorithm to detect the possibility of motorcycle fall or dangerous instability has been presented. The development of the fall detection parameters, addressing only the braking maneuvers, required the evaluation of the main aspects and parameters affecting the fall dynamics of motorcycle, in case of low-side and high-side falls.

The $RISK_i$ parameters designed for the fall detection process addressed the vehicle destabilization due to the intensity of the braking maneuvers and to the heavy oscillations of the vehicle body and the steering bar. The definition of the parameters thresholds was carried out by the analysis of the results of the application of the $RISK_i$ parameters on virtual simulations and experimental data.

The tests revealed a good prediction accuracy. Only the events potentially dangerous were detected by the system and the number of false positives turned out to be small.

The final target of the activity described above is to implement the algorithms created inside the control units used for the intervention of innovative active braking systems for stability control. The $RISK_i$ parameters aim to support the application of those systems, thus detecting the dangerous conditions for the rider and vehicle safety and providing a sudden alert to the safety system to intervene on the vehicle dynamics.

The algorithms for the computation of the $RISK_i$ parameters have been integrated on the *Active Braking Control* system described in the next chapter. The effectiveness of the system has been tested on different braking conditions, addressing the vehicle motion on a steady cornering.

Chapter 6

Modulation of the braking forces

6.1 Introduction

The stability control of the vehicles faced relevant improvements in the field of passenger's cars and heavy vehicles. The Electronic Stability Control (ESC) is available on an increasing number of cars and its effectiveness, in terms of road safety, is proved by a number of publications [86, 87, 88].

Concerning the motorcycle field, to this day only a small number of research activities addressed the motorcycle stability issue. The main reason of that aspect is the high complexity of singe track vehicles dynamics, which poses an avoidable delay on the development of new technologies for PTWs.

Due to the evident differences on in-plane and the out-of-plane dynamics, it is not possible to transfer easily the powered four-wheelers technology on PTWs; therefore, dedicated processes of technology development are needed.

Anyway, some preliminary result about the motorcycle stability control has been obtained during the recent years. As already reported in §2.2.2 the possibility to influence the vehicle dynamics via standard active systems can be found in the application of active suspensions ([4, 32, 36], etc.) or active steering systems [18, 89]. Those studies show the possibility to increase the level of stability of the vehicle, even though the complex issue of the motorcycle stability during emergency maneuvers is far to be solved.

Some preliminary results in this direction have been obtained and demonstrated by De Filippi et al., in [29] and [30]. The authors defined different active control strategies to increases the vehicle stability and support the rider maneuver (e.g. accelerating or braking), addressing steady state maneuvers and unsteady state maneuvers. It is possible to say the authors addressed fully the stability issue and posed the stability as the main target of their study.

Similarly to the aforementioned activity the study that will be presented in the next paragraphs addresses the stability issue. However, the investigation was limited only to the vehicle dynamics during a braking maneuver. Moreover, the stability has been addressed as a secondary issue respect to the deceleration. This means that main target is to define active control strategies to maximize the

deceleration and then, only in case of critical conditions for rider safety, try to increase the vehicle stability as well.

Basically, the active control strategies presented hereafter want to propose an improvement of the braking performances of the motorcycle, in terms of deceleration and stability, starting from the state of the art of standard active braking functions that is possible to find in current motorcycles. The main target is an evolution of the actual braking systems, following the same concept suggested by Seiniger [34] and recently developed by Robert Bosch GmbH (with the MSC system).

The roadmap for the development of innovative solutions requires a number of steps to follow to get the final layout of the new technology. In the next paragraph, it will be described in detail the preliminary activity carried out to develop the new concept of braking forces modulation.

The preliminary phase of the analysis focused on the definition of the vehicles to investigate and the effectiveness of the braking systems theoretically implemented on those vehicles.

Because of the main target of the activity is to propose an evolution of the standard braking functions, the investigation of the points of strength and weaknesses of the current active braking systems has been carried out, addressing different riding scenarios.

Afterwards, the findings from the phase described above guided the activity through the development of the new criteria for the longitudinal forces modulation.

It is important to highlight that the activity has been conducted in a virtual environment. The simulations gave the possibility to obtain a first evaluation of the system. Of course, for further development, the topic should be also addressed by experimental tests. However that poses a critical issue to address in terms of safe testing, and it will require an accurate definition of all the aspects correlated to the experimental campaign.

6.2 Multibody models for the analysis of the braking forces modulation

Vehicles

The motorcycles used to study the braking maneuvers have been created in Bikesim®. The vehicles investigated for the activity described in this paragraph are:

- Piaggio Beverly300
- Super Sports Motorcycle - (similar to a Yamaha YZF)

The Piaggio Beverly300 model adopted for the simulation is the same vehicle presented in §4.2.1. About the motorcycle, the same virtual vehicle described in §5.2 was used, thus no real motorcycle was taken as reference for the simulations. The geometrical and inertial features were taken similar to those one proposed by the software.

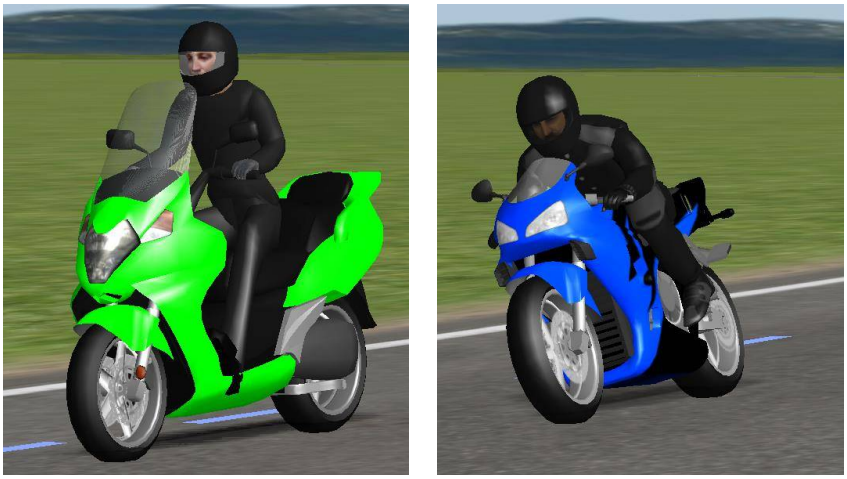

Figure 6.1: Virtual models of the Piaggio Beverly300 and the Super Sports Motorbike

For both vehicles, the brake systems were set up with the geometrical and structural properties similar to the real vehicles (taken from technical manuals). In particular, to obtain braking performances similar to real vehicles, the parameters customized were: disc effective radius, pad friction coefficient and total area of the caliper pistons (Tables 6.1 and 6.2).

Table 6.1: Sports Motorbike, brake system features

	Front wheel	Rear wheel
Wheel/Cylinder area	3215 mm^2	1607 mm^2
Disc effective radius	145 mm	100 mm
Pad friction coefficient	0.45	0.45

Table 6.2: Beverly300, brake system features

	Front wheel	Rear wheel
Wheel/Cylinder area	1962 mm^2	1962 mm^2
Disc effective radius	140 mm	110 mm
Pad friction coefficient	0.4	0.4

The vehicles addressed are very different in terms of dynamics and stability. In particular, the Beverly300 has a mass distribution that strongly influences the vehicle stability in curve. As the vehicle characteristics show, the center of gravity is located far from the front wheel, thus decreasing (generally) the stability of the *Weave* mode [5]. In the configuration used for the test, the *Weave* mode of Beverly300 becomes unstable for increasing roll angles. For example at 50 km/h the *Weave* mode becomes unstable at 15°, and for 100 km/h is always unstable.

In Figure 6.2 two examples of modal analysis are depicted to show the instability of *Weave* of Beverly300 for different roll angles and different longitudinal speeds.

Differently from Beverly300, the super sports motorbike is always stable for different roll angles, concerning the speed range investigated, from 0 to 150 km/h.

The instability of the scooter is easily balanced by the rider control. In standard running scenarios, also for fast movements, e.g. in the racetrack described in §4.2, the vehicle control is always smooth, thus showing that the scooter is stable due to the rider control.

Anyhow, the implicit instability of the vehicle can limit the vehicle control in unsteady emergency conditions, like a panic braking in curve or in case of a fast swerving maneuver. The effect the *Weave* instability, added to the instability generated by the maneuver, can reduce the possibility of control. In general terms, compared to other vehicles, for example, the super sports motorbike, during such critical events, it will be more difficult to control the Beverly300 than the other vehicles.

From the point of view of the evaluation of the effectiveness of new systems that address the vehicle stability, the possibility to test the systems (even if only virtually) on a vehicle with a low stability, gives important indications on the potentialities of the systems.

It is possible to associate the Beverly300 to the worst test conditions, thus the best way to verify the reliability of the safety systems proposed. It is expected that, the new active safety systems whose main goal is to increase the vehicle stability in case of unsteady critical events, would help more an unstable vehicle, such as the Beverly300, than a stable motorcycle such as the super sports motorbike.

Standard braking systems: ABS and C-ABS

The most common active braking systems of the motorcycle on the market, the ABS and the C-ABS, have been investigated to find out the strengths and weaknesses of those systems, in a number of hard braking scenarios, critical for the vehicle stability. It was important to understand in which conditions those systems cannot help the rider to manage the vehicle, and what were the possibilities of improvement of the performances.

More in detail, it was not investigated a specific technology, e.g. by Robert Bosch GmbH or Honda, but the safety functions themselves were addressed. Then it is possible to say that the analysis process aimed to see the effectiveness of the anti-lock function and the combination of the anti-lock + the combined braking functions in different road scenarios.

For simplicity, in the next paragraph the anti-lock function and the combination of the anti-lock + the combined braking functions will be addressed as ABS and C-ABS (CBS in case of simple combined braking).

The implementation of the anti-lock function was carried out by the modulation of the braking pressure as function of the longitudinal slip[1]. To take into account

[1]The pressure modulation is a simple on/off function based on the slip value. The maximum is fixed to 0.1 (according the road characteristics chosen for the simulations)

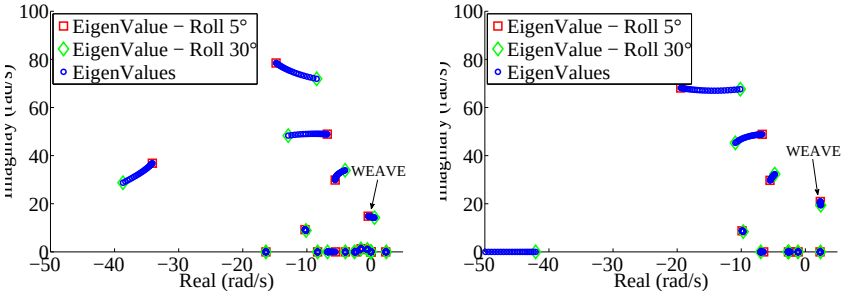

(a) Eigenvalues for 50 km/h, from 5°(red marker) to 30°(green marker)

(b) Eigenvalues for 100 km/h, from 5°(red marker) to 30°(green marker)

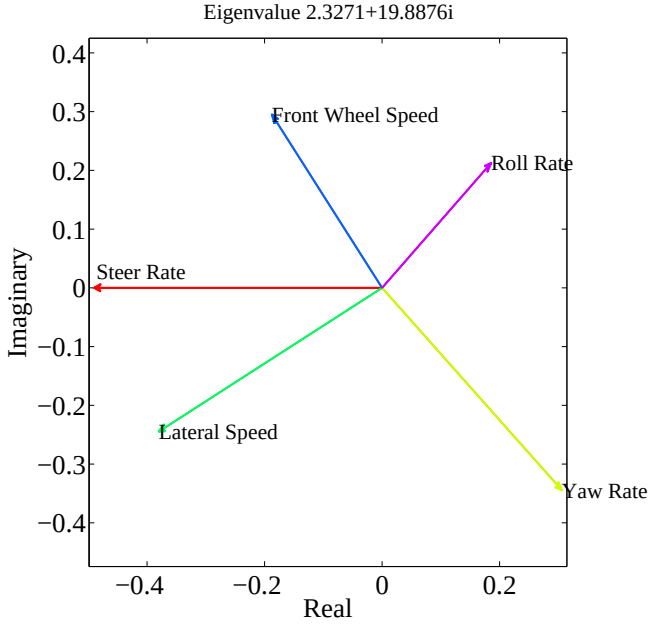

(c) Eigenvector for 100 km/h and 20°

Figure 6.2: Modal Analysis of Beverly300 running at 50 km/h and 100 km/h for different roll angles

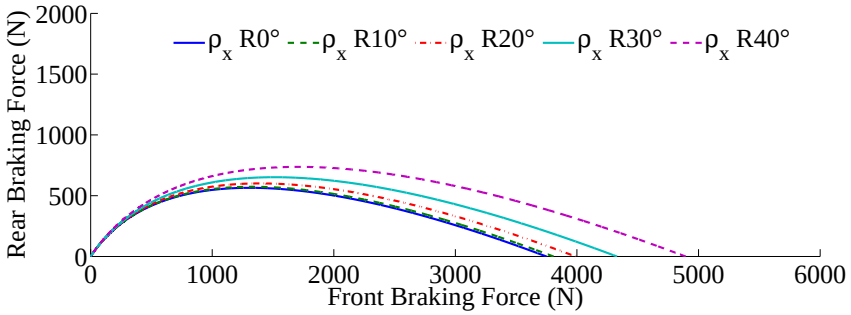

Figure 6.3: Example of optimal braking distribution for different roll angles (0°- 40°). Vehicle: Piaggio Beverly300

a physical delay of the ABS system, a delay of 7 ms was added, according to [90]. Moreover, to model the actuator dynamics, in the transmission line of braking pressure a low-pass filter with a cut-off frequency of 10 Hz was added, in accordance with [30].

The implementation of the combined braking function was made according to Cossalter [5], considering also the influence of the roll angle. The force distribution is based on the following equation (Figure 6.3):

$$\rho_x = \frac{m_t \cdot a \cdot g + h_\varphi \cdot cos(\varphi) \cdot (Fx_f + Fx_r - F_{aer})}{m_t \cdot l \cdot g} \tag{6.1}$$

The distribution operated by the CBS is carried out with a *Brake-by-Wire* approach [30]: as soon as the rider applies the braking forces on the front and rear lever (rear pedal in case of a motorcycle), the system computes the optimal braking force distribution, according to the Eq.6.1. Then the corresponding pressures are generated as outputs. Due to the combination of the combined braking function and the anti-lock function, before reaching the calipers, the pressure is modulated (if needed) by the ABS assembly. The general layout of the system is in Figure 6.4. In accordance to the simple ABS, also the ABS pressure line of the C-ABS has a delay of 7 ms and a cut-off frequency of 10 Hz.

The aforementioned value of the cut-off frequency means that the activation of the ABS can reach a maximum number of 10 loops per second. In standard Anti-lock Braking Systems, this value is lower: the standard frequency is within 3 Hz and 5 Hz that results in a rough and not precise modulation of the pressure. To provide better performances in the ABS and C-ABS activation the cut-off frequency was set to 10 Hz. Moreover, a higher value of the cut-off frequency allows providing a better modulation of the braking forces.

6.3 Effectiveness of C-ABS and ABS systems

The anti-lock braking function and the combined braking function were investigated in a number of simulations of braking manoeuvers on steady state cornering.

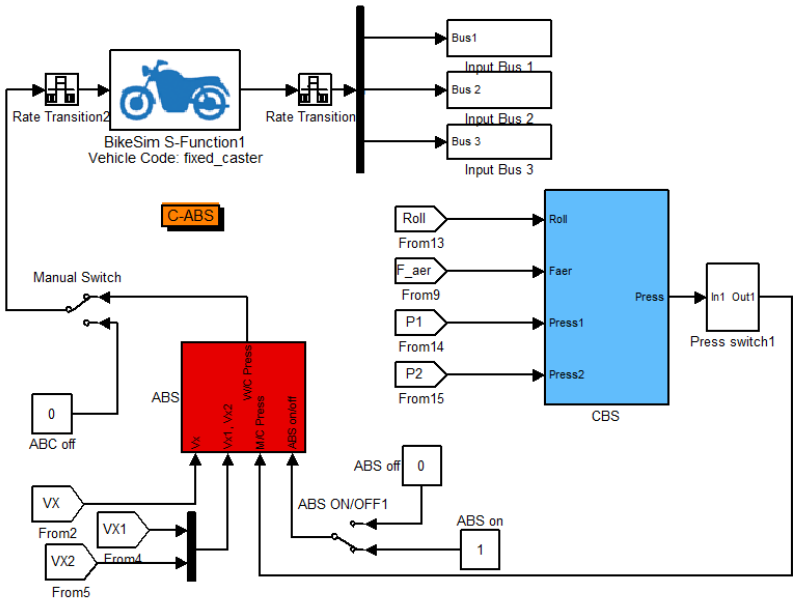

Figure 6.4: Representation of Combined Braking System matched with the Anti-lock Braking System. The model is represented in Simulink environment

In each simulation, the goal of the rider was to perform a *Safe Braking* maneuver: to stop completely the vehicle in upright position, within the street lane, following a curve with a fixed curvature radius. That was the general scenario adopted for the evaluation all the braking systems, ABS, C-ABS and ABC (*Active Braking Control*, described in the next paragraphs).

The general purpose of the investigations was to see the effect of the braking systems in case on medium-high decelerations, thus excluding the low deceleration cases. Therefore, different braking maneuvers, with different intensities, were investigated.

The braking maneuver was analyzed according to different running conditions, listed below:

- Curvature radius (m): 50, 75, 100, 125, 150, 200, 250, 300, 400;
- Longitudinal Speed (km/h): 50, 80, 100, 110, 120, 130;
- Braking Force on the lever (N): 50, 100, 120, 150;
- Braking Distribution of the lever force: Front, Rear, Front&Rear;
- Road Friction: dry asphalt(max μ_x 1.15), wet asphalt(max μ_x 0.6);
- Vehicle: Beverly300, Super Sports Motorbike.

It is worth noting that the braking forces on the lever go up to 150 N. This value can be considered over the maximum braking force that a standard rider can apply on a brake lever in critical situations (100-120 N can be considered the feasible limit). However, it can be considered applicable on the brake pedal (if the PTW has it).

To provide a uniform set of analysis the limit value of 150 N was considered both on the scooter and on the motorcycle, and theoretically it can be addressed as the worst case scenario.

In total, each braking system was tested on 2592 simulations: the results showed a different efficiency in the application of the ABS and C-ABS in general, and for specific cases.

The first analysis takes as mean of comparison the number of *Safe Braking*[2] maneuvers performed with each braking system. Considering the total number of runs (1296 per vehicle, per system) as the reference term for the comparison, the results give opposite indications for the Beverly300 and the Super Sports Motorbike. For the Beverly300 case, the vehicle with the C-ABS completed 62.9% of runs, with the ABS 58.9%. On the other side, for the Sports Motorbike application, the result was the opposite: the ABS was successful in 60.8% of the cases and the C-ABS in 55.8% of the cases.

The influence of the vehicle speed on these percentages is limited, thus the numbers reported above change insignificantly for different speeds. Instead, taking into account, separately, the two road friction coefficients investigated, the differences between the aforementioned percentages double.

In both vehicles, it is worth noting that taking into account the same braking force, the distribution of the braking forces allows reaching better braking performances in terms of stopping distances. That is mainly because, for some friction condition, to apply the total braking force only on one wheel could lead the wheel to lock up, while a proper redistribution could avoid the lock up at all. That consideration comes directly from the basics of vehicle dynamics, however it is important to point it out clearly for that investigation process.

Considering only front braking (and *Safe Braking*), in dry and wet asphalt, in terms on mean deceleration, and assuming the mean decelerations of the ABS as reference, the C-ABS turned out to be able to reach a deceleration 14.02% higher than the ABS for the Beverly and 5.25% higher than the ABS for the Sports Motorbike. The lower value of the Sports Motorbike can be related to the properties of the braking systems. The Sports Motorbike has a front brake more powerful than the Beverly's one, thus leading the single front braking of the Sports Motorbike to higher decelerations and reducing the differences between the performances of the ABS and the C-ABS.

Also for the next part of the analysis, the comparison has been carried out considering the ABS as the reference system. Then each percentage value reported hereafter expresses the effects of the application of C-ABS, based on the results provided by the application of the ABS.

To get more information on the potentialities of ABS and C-ABS on curve braking, the influence of the braking systems on the $\ddot{\psi}$ and $\ddot{\varphi}$ were considered. For

[2]Stop the vehicle in upright position

the comparison it was used the mean values of the absolute terms of the parameters (for $\ddot{\psi}$ and $\ddot{\varphi}$ the target condition was 0 rad/s^2), considering only the braking phase of the maneuvers. The average value of these accelerations, computed on the number of cases considered for the analysis, has been chosen as the final mean of comparison.

The comparison computed according to this form gives results similar to the application, on the same data, of the standard deviation.

As stated before, the percentages introduced later on have been calculated taking as reference the values of the ABS system. Therefore, once the average (on the number of runs under investigation) of mean values of $|\ddot{\psi}|$ and $|\ddot{\varphi}|$ are computed, for each braking system, the ratio between the resulting values of the C-ABS application and the ABS application have been used for the comparison.

Considering all the cases in which the vehicle did not fall down, but completed the run safely, in terms of $\ddot{\varphi}$, the C-ABS on the Beverly is less intrusive than ABS by the 33.8% and by the 36.2% for $\ddot{\psi}$. Instead, for the Sports Motorbike the results are completely the opposite: the ABS turned out to produce less fluctuation of $\ddot{\varphi}$ and $\ddot{\psi}$ by the 16.5% and the 9.8%, respectively. That gives a preliminary indication about the relevant differences between the vehicles and about their behaviors under similar running conditions.

This aspect suggests that the any modification of the braking distribution should be calibrated carefully on the vehicles separately, and it would not be possible to define a common simple method of braking modulation.

The aforementioned general considerations for Beverly and Sports Motorcycle are subjected to some variation if the analysis is brought to a deeper level. Considering only front braking or rear braking applied to the Beverly, $\ddot{\varphi}$ and $\ddot{\psi}$ show that the C-ABS guarantees a more stable braking maneuverer. Instead, it is the contrary for combined braking. In case the rider applies the same force on the front and rear braking levers the ABS turned out to be more efficient to avoid fast oscillations of the vehicle. The details of the results are reported in Table 6.3.

Table 6.3: Average values of mean $\ddot{\varphi}$ and mean $\ddot{\psi}$, in case of run completed with a *Safe Braking* maneuver. Vehicle: Beverly300. The percentages refer to the ratios between mean values generated by the C-ABS and the mean values generated by the ABS. Thus the ABS performances are the base of the comparison. A positive value means that the C-ABS generates a higher value of mean acceleration, and then, in that case, it is considered as the worst system

	$\ddot{\varphi}$	$\ddot{\psi}$
Front BK	-78.1%	-80.3%
Rear BK	-73.9%	-69.8%
Comb BK	90.5%	91.1%

The results for the Sports Motorbike show some relevant differences (Table 6.4). Concerning the motorcycle, the ABS produced better results, in particular on front braking maneuvers. The percentages again show a higher (and bad) influence of

C-ABS if the rider applies a combined braking, leading to a mean yaw acceleration larger than the yaw acceleration procured by ABS.

Table 6.4: Average values of mean $\ddot{\varphi}$ and mean $\ddot{\psi}$, in case of run completed with a *Safe Braking* maneuver. Vehicle: Super Sports Motorbike. The percentages refer to the ratios between mean values generated by the C-ABS and the mean values generated by the ABS. Thus the ABS performances are the base of the comparison. A positive value means that the C-ABS generates a higher value of mean acceleration, and then, in that case, it is considered as the worst system

	$\ddot{\varphi}$	$\ddot{\psi}$
Front BK	0.4%	-6.7%
Rear BK	-25.8%	-30.1%
Comb BK	43.1%	37.6%

A more detailed investigation revealed that the latter results of the Sports Motorbike are also influenced by the tire-friction conditions. The values show an increase of braking performances in favor of the ABS for dry road, while they turn in favor of the C-ABS for wet road conditions. This means that in the worst braking conditions, in terms of friction, it is fundamental to provide a better distribution of forces to increase the vehicle stability, while for high adherence coefficients the combined braking in some cases can reduce the vehicle control.

Concerning this riding condition the results for the scooter and the motorcycle are comparable, even if still the values of the percentages are quite far.

Isolating the hard braking maneuvers, over 100 N applied on the brake levers, the mean vales of the angular accelerations do not change so much. More in detail, the signs of the averages remain unchanged but the absolute values slightly increase for Table 6.3 and slightly decrease for Table 6.4.

In addition to the results presented, the influence of the speed and the braking forces has been verified in detail. The speed variability has not a relevant influence for the Beverly and the Sports Motorbike as well. As example, concerning the Beverly, considering all the run with a final *Safe Braking*, filtered only as function of the speed, it was found that for speed lower than the 100 km/h, in accordance with the general results, the C-ABS is the system that provides a better stability to the system in terms of mean roll acceleration and mean yaw acceleration (C-ABS, -13.7%, -13.8%). At high speed the C-ABS effectiveness increases as well (C-ABS, -73.4%, -75.5%).

All the results were used to have general indications on the potentialities of the anti-lock braking function and the combined braking function, in order to figure out the correct way to define a different braking force distribution in case of critical maneuvers. The considerations derived from those simulations will be addressed on next paragraph during the description of the Active Braking Control system, thus describing the main motivation for the new system layout.

In particular, the simulations outcomes were useful in the tuning phase to

manipulate the new braking modulation, in accordance with the interpretation of the results.

6.4 ABC (Active Braking Control) system

The investigation of the ABS and C-ABS systems showed that in many running scenarios the behaviors of those systems is different, sometimes, completely the opposite. The braking systems can affect in different ways different vehicles. Then, the challenging aspect is to define a new criteria modulation able to supply stability to the vehicle in those scenarios where the standard active braking systems have a limited margin of contribution.

The layout of the new braking modulation is based on the analysis of the vehicle motion in curve. Addressing that running condition, the correction to apply to the braking forces distribution was derived, aiming to reduce the unsteadiness of the vehicle due to the hard braking maneuver. In addition to the theoretical analysis of vehicle motion, the final layout of the modulation is based on an intensive tuning process, trial-and-error tests to find out the best system set-up.

The new braking modulation system introduced in this chapter has been named *Active Braking Control*, ABC. The name focuses on the constant monitoring of vehicle dynamics and on the prompt intervention on the braking system as soon as the riding conditions require it. In addition, the name wants to point out the application of the system only during the braking phase. It can be considered an advanced system closer to the Robert Bosch GmbH's MSC system than to the stability control proposed by De Filippi [30], that addresses the motorcycle stability issue in general terms (investigating also other running conditions, e.g. the PTW during the acceleration phase).

6.4.1 Equations of the ABC system

For the analysis of the PTW dynamics the vehicle motion has been derived considering the movement of the vehicle running in a curve (steady cornering). Considering the model reported in §4.1 (with the same limitations), the yaw motion and the roll motion in the body reference frame are explicated by the following equations (according to the forces and torque balances out-of-the plane):

Yaw motion (body-fixed system of reference):

$$\begin{aligned} &- Fx_f \cdot (a \cdot \delta) \cdot cos(\varphi) - m_t \cdot Ax_{SM} \cdot h_\varphi \cdot sin(\varphi) \cdot cos(\varphi) + Fy_f \cdot a \cdot cos(\varphi) \\ &- Fy_r \cdot b \cdot cos(\varphi) + (h_{\varphi_d} - h_\varphi) \cdot F_{aer} \cdot sin(\varphi) \cdot cos(\varphi) \\ &+ Mz'_f \cdot cos(\varphi) + Mz'_r \cdot cos(\varphi) \\ &= f(\ddot{\psi}, \ddot{\varphi}, \dot{\varphi}, \ddot{\delta}, \dot{\delta}) \end{aligned} \tag{6.2}$$

Roll motion:

$$\begin{aligned} &m_t \cdot Ay_{SM} \cdot h_\varphi \cdot cos(\varphi) - Fz_f \cdot h_\varphi \cdot sin(\varphi) - Fz_r \cdot h_\varphi \cdot sin(\varphi) \\ &+ Mx_f + Mx_r + M_{Gyros} + Fz_f \cdot t \cdot \delta \cdot cos(\varphi) \\ &= f(\ddot{\varphi}, \ddot{\psi}, \dot{\psi}, \ddot{\delta}, \dot{\delta}) \end{aligned} \tag{6.3}$$

To simplify the description of the next steps lets adopt the following formulations, to describe the unsteady terms of the equations:

$$f(\ddot{\psi}, \ddot{\varphi}, \dot{\varphi}, \ddot{\delta}, \dot{\delta}) = \Gamma(\dot{\psi}) \tag{6.4}$$

$$f(\ddot{\varphi}, \ddot{\psi}, \dot{\psi}, \ddot{\delta}, \dot{\delta}) = \Gamma(\varphi) \tag{6.5}$$

The form of these equations, with $\Gamma(\dot{\psi})$ and $\Gamma(\varphi)$, wants to underline the most relevant terms that influence Eq.6.2 and Eq.6.3

Let us focus on the Eq.6.2. Substituting the $m_t \cdot Ax_{SM}$ with the total longitudinal force Fx_T, the equation can be rewritten pointing out only the longitudinal force distribution ρ_x and grouping all the other steady terms under $\sum(Mz_i)$:

$$-\rho_x \cdot Fx_T \cdot a \cdot \delta + \sum(Mz_i) = \frac{\Gamma(\dot{\psi})}{cos(\varphi)} \tag{6.6}$$

Starting from the unsteady state conditions, the target of the method under analysis is to provide more stability to the vehicle by a modulation of the braking force distribution. Imposing to reach these equilibrium conditions (with unsteady terms null) at the time step next to the previous one characterized by the unsteadiness, by applying a correction of the braking distribution, the equation of motion (now in equilibrium) can be derived as follow:

$$-(\rho_x - \rho_c) \cdot Fx_T \cdot a \cdot \delta + \sum(Mz_i) + \epsilon_y = 0 \tag{6.7}$$

where ρ_c is the correction applied to the braking distributions and ϵ_y is a term that takes into account the time evolution of the variables involved in the equations, in order to report in Eq.6.7 the same elements of Eq.6.6. Comparing those two equations, it is possible to compute ρ_c:

$$-\rho_c \cdot Fx_T \cdot a \cdot \delta - \epsilon_y - \frac{\Gamma(\dot{\psi})}{cos(\varphi)} = 0 \tag{6.8}$$

$$\rho_c = \frac{-\Gamma(\dot{\psi}) - \epsilon_y}{Fx_T \cdot a \cdot \delta \cdot cos(\varphi)} \tag{6.9}$$

Following the same procedure, it is possible to derive the same correction addressing the equation of motion of the roll angle:

$$\rho_c = \frac{-\Gamma(\varphi) - \epsilon_r}{Fx_T \cdot h_\varphi \cdot \delta \cdot cos(\varphi)} \tag{6.10}$$

where ϵ_r has a meaning equivalent to ϵ_y.

According to the aforementioned equations, the main idea of the new modulation system is to define a new longitudinal forces distribution to counter balance the unsteadiness of the motion. The correction itself is a function of the unsteady terms of the equations of motion.

6.4.2 System layout

Starting from the investigation of the ABS and the C-ABS system (more precisely the investigation of the implicit safety functions), the overall evaluation of the simulation results suggests that the combined braking function guarantees the best performances both in terms of stability (vehicle oscillation) and in terms of braking performances. However it was shown how the combined braking needs improvements when the rider acts at the same time on the front and rear brakes.

Accordingly, the base of the ABC system is the general layout of the C-ABS. The combined braking function is considered the main function of the system, and the others as the anti-lock and the new force modulation can be considered as additional functions subjected to the main one. Basically, the additional functions change the braking condition imposed by the main one. The concept of the general layout described complies with the system goals: to provide the maximum acceleration and, in case the critical events, try to adjust the vehicle stability via longitudinal forces modulation.

The braking forces modulation is based on the application of the correction ρ_c to the actual braking forces combination, that means, according to the equation form, that the stability target is addressed always maximizing the deceleration. In fact the correction is function of the total longitudinal force, thus function of the maximum acceleration/deceleration that the rider tents to achieve.

Figure 6.5 depicts the general layout of the braking system. The graphics shows the integrations of the Combined Braking function (CB, yellow), the Anti-Lock function (AL, light blue), the RISK function (green) and the Active Braking, or braking modulation, function (AB, white). The hierarchy of the functions is the following (Figure 6.6):

1. First, in every braking maneuver the combined braking is applied. It maximizes the vehicle deceleration in every braking scenario;
2. In case of wheel slip over the threshold the anti-lock (AL) unit is activated;
3. During the maneuver the vehicle state is constantly under control. If a critical event is detected, the RISK unit sends a warning signal to the AB unit;
4. The active braking (AB) unit is activated as soon as the RISK unit sends an alert. The AB function acts directly on the CB function.

As Figure 6.6 shows, the combined braking is the main and the starting function. The intervention of the braking modulation control unit is made directly on the braking forces rate ρ_x. According to the final equation in §6.4.1 the correction

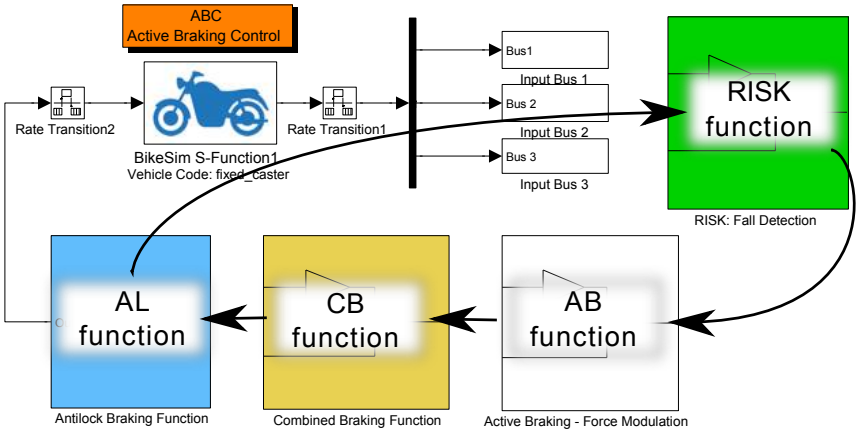

Figure 6.5: General layout of the advanced braking system. It composed of the Combined Braking function (CB, yellow), the Anti-Lock function (AL, light blue), RISK function (green) and the Active Braking, or braking modulation, function (AB, white)

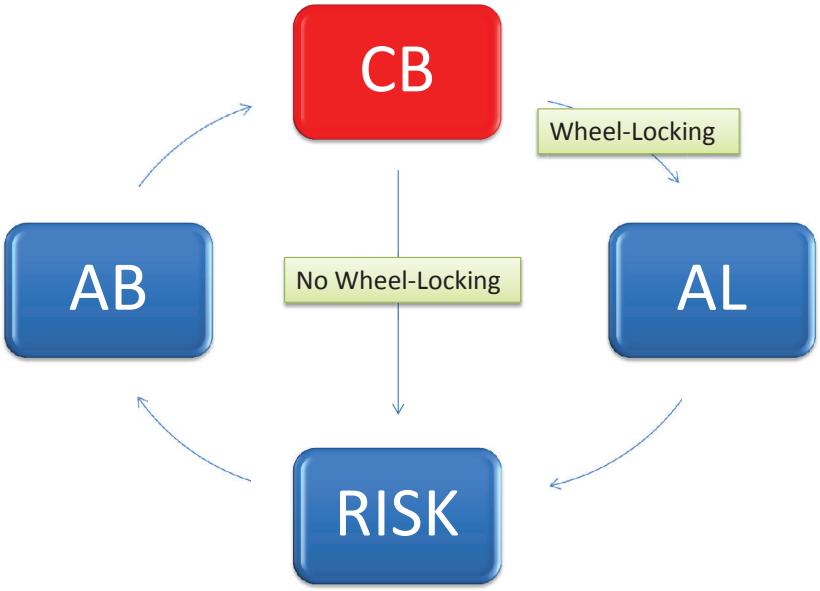

Figure 6.6: Logical sequence of the activation of the different safety functions of the braking system

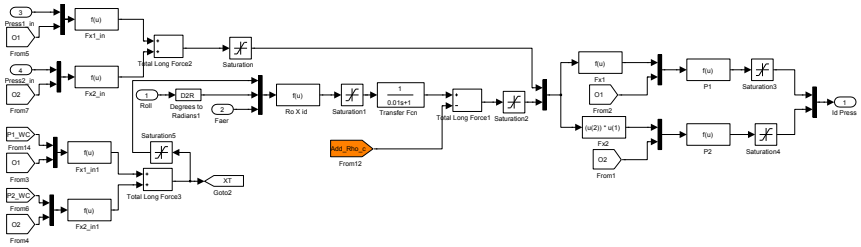

Figure 6.7: Simulink representation of the Combined Braking function and the correction applied by the Active Braking unit

ρ_c is subtracted from the original force distribution. Therefore, once the active braking unit is activated, and the correction is computed, the force combination is modulated in order to produce the new braking balance. Figure 6.7 depicts the general layout of the combined braking unit, including the correction from the active braking unit.

The theoretical application of ρ_c has been subjected to number of modifications in order to simplify the practical application. Considering the Eqs.6.9 and 6.10 the first one has been selected for the correction. As the equations form shows the Eqs.6.9 and 6.10 have the same number of variables at numerator, three variable for Eq.6.9 at denominator and four variables (also h_φ is variable, [60]) for Eq.6.10 at denominator. Therefore, Eq.6.9 was selected according to the lower number of variable to address. This is a relevant simplification, and in the future the selection should be addressed again, considering also possible additional analyses, like the transmission zeroes of the controller function of the selected inputs [30]. However it is important to say that the correction based on Eq.6.10 was partially tested, and turned out to be less effective than the other solution, thus giving an additional support to the decision about the control strategies.

A further and more relevant simplification was considered for $\Gamma(\dot{\psi})$. Again, aiming to simplify the control, only the most influential term of the equation was selected. For the specific case, considering the yaw rate motion, $f(\ddot{\psi})$ was selected. The final form of $\Gamma(\dot{\psi})$ can be derived as follow:

$$\Gamma(\dot{\psi}) = Izz \cdot \ddot{\psi} \tag{6.11}$$

where Izz represents the yaw inertia of the PTW in the body-fixed system of reference.

The final ρ_c chosen for the braking modulation is:

$$\rho_c = \frac{-Izz \cdot \ddot{\psi} - \epsilon_y}{Fx_T \cdot a \cdot \delta \cdot cos(\varphi)} \tag{6.12}$$

The unknown variable ϵ_y has been defined as a term proportional to the integral

of $\ddot{\psi}$[3], thus turning the simple modulation into a PI controller.

$$\epsilon_y = k_i \cdot \int \ddot{\psi} dt \tag{6.13}$$

Summing up the final equation of control:

$$\rho_c = k_p \cdot \ddot{\psi} + k_i \cdot \int \ddot{\psi} dt \tag{6.14}$$

where k_p is $Izz/(Fx_T \cdot a \cdot \delta \cdot cos(\varphi))$ and k_i is $Izz \cdot C_i/(Fx_T \cdot a \cdot \delta \cdot cos(\varphi))$. By a trial-and-error meteorology the value of C_i has been fixed equal to 35 for speeds $\leq 100\ km/h$ and 20 for speeds $\geq 100\ km/h$, both for the Beverly300 and the Super Sports Motorbike.

In addition, only for the Beverly300, an additional term proportional to derivative of $\ddot{\psi}$ was included (k_d is $Izz \cdot C_d/(Fx_T \cdot a \cdot \delta \cdot cos(\varphi))$. Again, by a trial-and-error meteorology the value of C_d has been fixed 0.01 for speeds $\leq 100\ km/h$ and 0.001 for speeds $\geq 100\ km/h$, only for single braking maneuvers (not combined braking)

The general layout of the PI (PID) controller for the braking force modulation is depicted in Figure 6.8.

It worth noting that the activation of the new modulation is subjected to the braking maneuvers. Therefore, the correction has not any influence on the acceleration phase.

The $RISK$ function integrated in the general layout is the virtual representation of the equations described in paragraph §5.2. It includes $RISK_2$, $RISK_3$, $RISK_{4.i}$ and the corresponding thresholds. In the previous chapter it was already reported that the equations for $RISK_{4.i}$ were calibrated only for the scooter Beverly300. Therefore, for the application of the $RISK$ unit functionalities on the sports motorcycle model, the equations derived for Beverly300 were adopted.

The alert sent to the active braking (AB) unit is given from a combination of the $RISK_i$ parameters. The AB activation due to the fall detection is also function of the speed. Several tests showed that the fall detection parameters can be fully implemented without restriction for speed lower than 100 km/h, but for higher speed the $RISK$ function layout should be revised.

For speeds lower than 100 km/h once one of $RISK_i$ parameters exceeds the corresponding threshold, the AB is activated. The activation follows strictly the thresholds defined in §5.2.

On the other side, for high speeds the AB activation is limited and subjected mainly to $RISK_2$ and $RISK_3$; the $RISK$ function, in case of braking, influences only the activation of the contribution of the derivative and integral terms of the PID controller of the AB unit, leaving the general AB modulation always active.

That configuration has been introduced for conservative reasons. In fact at high speeds the tests made on the system, revealed that, under these conditions, the fall detector is too late to permit a prompt and efficient action (by the AB unit) on the

[3]It would be more correct to consider $\Delta\ddot{\psi}$, however the target yaw acceleration is 0, thus allowing the equation form reported

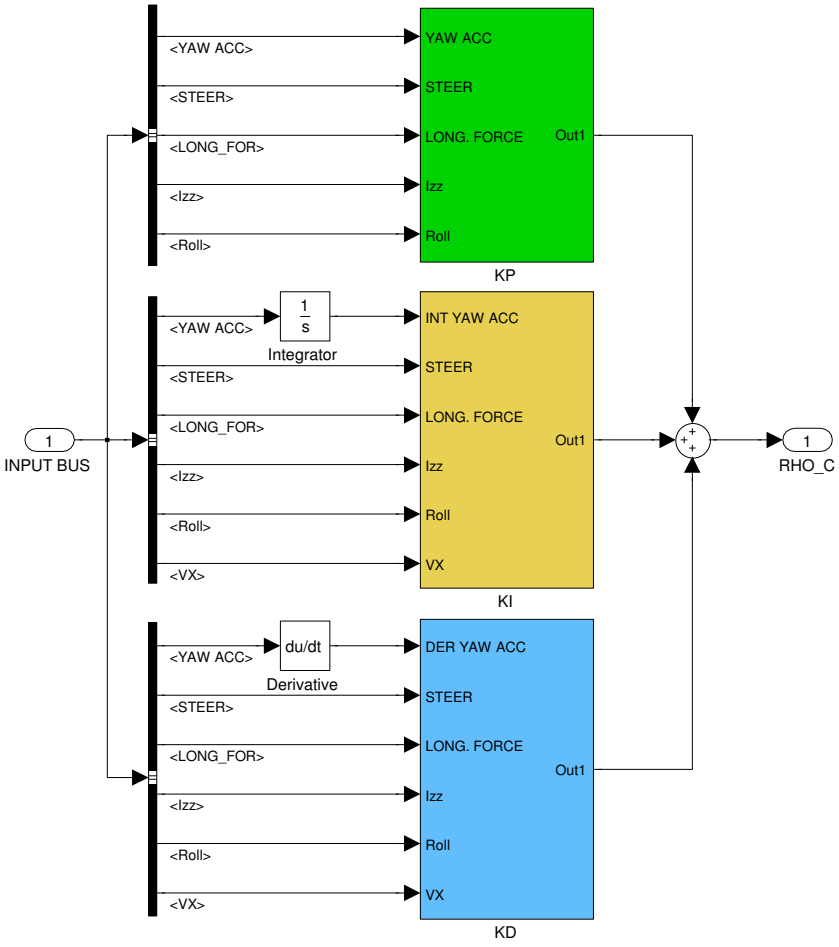

Figure 6.8: The general layout of the PID controller for the braking force modulation. Vehicle: Beverly300

vehicle dynamics. Therefore, a constant application of the modulation is needed over a certain running speed. On the other side the continuous application of the braking modulation reduces the braking performances in case of normal braking, thus limiting the benefits of the combined braking action.

Moreover, the influence of $RISK$ unit of the PID controller of the AB, is subjected mainly to $RISK_2$ and $RISK_3$. This means that, in case the $RISK_{4.i}$ exceed the thresholds[4], the AB modulation is not activated until $RISK_2$ or $RISK_3$ exceeds the corresponding threshold.

The aforementioned criteria aimed to postpone the activation of the derivative and integral contributions of PID controller until the $RISK$ function detects the necessity to activate the stability control.

Additional tuning of the ABC system

The optimization process of the braking force modulation required a further tuning process on the value of ρ_c. Considering the raw value of ρ_c it can vary considerably from positive to negative values, according to the variation of $\ddot{\psi}$. That could generate a new braking force distribution fluctuating between 0 and 1 (braking force only on front wheel - braking force only on rear wheel), thus introducing a potential element of disturbance on the vehicle.

Therefore ρ_c has been limited to positive values by an output saturation to 1. Because of ρ_c is subtracted from ρ_x, the variation of the final force distribution can change only between the actual value and 0. That criterion was chosen according to several simulations and following the indication obtained from the investigation of ABS and C-ABS performances. The test outcomes highlighted that the combined braking + anti-lock function was more efficient to reduce the influence on vehicle yaw and roll oscillations than the single anti-lock function. Moreover, the percentages revealed that between the single anti-lock function actuated on the front wheel and the single anti-lock function actuated on rear wheel, the rear braking case turned out to be the least efficient. The latter evaluation is true in particular for the Super Sports Motorbike (do not completely apply for the Beverly) where the single anti-lock function actuated on front wheel turned out to be more efficient than anti-lock function actuated on rear wheel.

According to the aforementioned considerations, the variation of the new force distribution within the actual value and 0 (Figure 6.9) was considered safer than the variation of the force distribution within the actual value and 1.

It is worth noting that the correction of the actual braking force distribution becomes fundamental in case of combined braking applied by the rider. Looking again at the analysis of ABS and C-ABS performances it is clear that for emergency situations the ABS guaranteed better braking performances than C-ABS (concerning the vehicle oscillation). That points out the necessity, for the specified maneuver indicated, to modulate the C-ABS braking distribution to achieve the braking performances offered by the simple ABS.

[4]It is fundamental to remind the activation of the alert as function of $RISK_{4.i}$ is subjected to the concurrent activation of $RISK_{4.0}$, $RISK_{4.1}$ and $RISK_{4.2}$

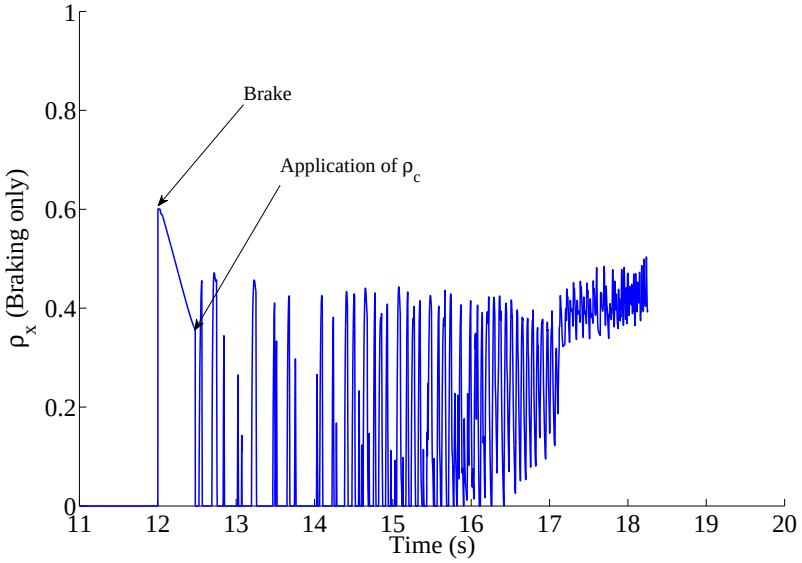

Figure 6.9: Example of the variation of ρ_x after the application of ρ_c

6.5 ABC vs ABS vs C-ABS

The new braking modulation function has been evaluated on the same simulations described in §6.3. The investigation has been conducted using the same mean of comparisons described for the ABS and C-ABS. In addition, to refine the analysis, the study of the Power Spectral Density (PSD) of $\dot{\delta}$ was introduced to evaluate the effort of the rider to control the vehicle in different braking conditions.

The Power Spectral Density is commonly used for statistical signal processing, and it is also used in the automotive field to consider the effort made by a system to control the process of some variables [91]. For the activity purpose, the system under investigation is the rider that operates the control over the steering bar. Therefore the evaluation of PSD of the steering rate defines the effort the rider does to control the vehicle, thus reveling the new system introduce an addition disturbance to the steering control that the rider must counterbalance.

The power of a signal $x(t)$ is computed according to the following time average:

$$P = \lim_{T\to\infty} \frac{1}{2T} \int_{-T}^{T} x(t)^2 dt \tag{6.15}$$

Considering the frequency domain of the signal with a Fourier transform $\hat{x}(\omega)$, the PSD can be derived as follows:

$$PSD = \lim_{T\to\infty} \mathbf{E}[|\hat{x}(\omega)|^2] \tag{6.16}$$

For some signal it is not possible to derive the Fourier transform, thus the truncated form of the transform is adopted $\hat{x}_T(\omega)$, where the signal is integrated only over a finite interval [0, T].

More precisely, the steering effort of the rider has been analyzed by the computation of the area under the PSD curve in the frequency domain. The result is the power of the steering rate signal. Comparing two signals, in this case, the signals coming from different braking systems, it is possible to find out which braking system guarantees the highest attenuation of the signal. Considering P_{sr} as the power of the reference signal and P_{si} as the power of the signal under investigation, the comparison is:

$$R_{dB} = 10 \cdot log_{10}(\frac{P_{si}}{P_{sr}}) \tag{6.17}$$

Negative values mean that the investigated signal is more attenuated than the reference signal. Transposing these contents in terms of steering rate, high damping of the signals mean less effort to control the steer motion.

6.5.1 Results

Following the same investigation procedure adopted for the ABS and C-ABS, firstly the total number of *Safe Braking* maneuvers is addressed. In total, on 1296 run, the ABC system installed on the Beverly300 succeeded in performing a *Safe Braking* in the 66.6% of the cases. Recalling the values reported in §6.3 (58.9% for the ABS and 62.9% for the C-ABS) it is shown that the ABC guarantees a higher number of *Safe Braking*, while the other technologies cannot avoid the motorcycle fall in a higher number of cases. More in detail the differences is 47 cases compared to the C-ABS and 99 cases compared to the ABS.

Addressing the Sports Motorbike, the percentages again depict a higher effectiveness of the ABC (64.7%), but the percentages trend changes. At this time the C-ABS turned out to be the least effective: in absolute terms the ABC guaranteed 839 *Safe Braking* maneuvers, the ABS 788 and the C-ABS 724.

An example of the activation of the ABC, in comparisons with the C-ABS is depicted in Figure 6.10.

The comparison represents how the C-ABS and the ABC support the rider braking action. The time steps of the braking force application and the activation of the active control braking functions are reported. In the example the roll curve clearly points out that only the ABC guarantees a *Safe Braking* maneuver, while the C-ABS introduces an instability that the rider cannot control.

According to the analysis in §6.3 the comparison among the different braking systems is carried out considering one of the systems as the reference for the remaining ones. In this case the reference system is the ABC, therefore each consideration drawn hereafter is based on the results coming from the application of the ABC.

The analysis of the mean decelerations reached by the braking systems defines the capabilities of the systems to comply with one of the tasks: maximization of the deceleration. The comparison shows that the C-ABS leads the vehicle to a

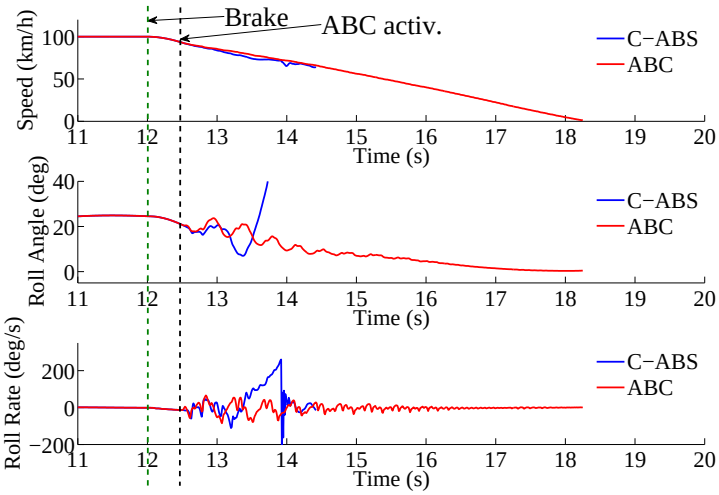

Figure 6.10: Comparison between the same braking maneuver, involving the ABC system (red line) and the C-ABS system (blue line). Running conditions: Speed 100 km/h, Braking force 100 N, Distribution Front and Rear, Wet asphalt, Curvature radius 200 m

mean deceleration higher than the ABS and ABC, however the percentages stay below 3.4% (C-ABS: Beverly 3.4%, Sports -1.4%, always referring to the ABC performances). Therefore, it possible to state that the decelerations obtained by the three systems are comparable and the differences are almost negligible.

That points out that the ABC system does not reduce the braking performances, in terms of deceleration, if compared to other standard systems. Moreover, in case the analysis is limited to the simulations in low-medium speeds, when the fusion of the *RISK* unit and the braking modulation unit is not limited, the deceleration gap between the ABC and the C-ABS is further reduced. Again the main part of the analysis focuses on the $\ddot{\psi}$ and $\ddot{\varphi}$[5].

Differently from the investigation of the ABS and C-ABS features, the running speed of the simulations is crucial for the results.

Starting from overall considerations on $\ddot{\psi}$ and $\ddot{\varphi}$, if only *Safe Braking* maneuvers for the three systems are considered, the results are reported in Table 6.5.

The results clearly show that looking at all the simulations leading to *Safe Braking* maneuvers, in case of Beverly, the C-ABS is sensibly more efficient to reduce the yaw and roll oscillations than the new modulation system. In addition, the ABS turned out to be more stable than the ABC. Instead, the Sports Motorbike shows a more stable behavior and the ABC systems turned out to be the most effective system in terms of mean oscillations.

[5]The mean of comparison is, again, the average of the mean values of the absolute terms of the parameters

Table 6.5: Average values of mean $\ddot{\varphi}$ and mean $\ddot{\psi}$, in case of run completed with a *Safe Braking* maneuver. The percentages refer to the ratios between mean values generated by the C-ABS and ABS and the mean values generated by the ABC system. Thus the ABC performances are the base of the comparison. A positive value means that the C-ABS or ABS generates a higher value of mean angular acceleration that represents worse performances

	ABS $\ddot{\varphi}$	ABS $\ddot{\psi}$	C-ABS $\ddot{\varphi}$	C-ABS $\ddot{\psi}$
Beverly	-9.1%	-13.0%	-38.4%	-43.4%
Sports Motorbike	3.0%	6.8%	20.1%	17.3%

Table 6.6: Average values of mean $\ddot{\varphi}$ and mean $\ddot{\psi}$, in case of run completed with a *Safe Braking* maneuver. The percentages refer to the ratios between mean values generated by the C-ABS and ABS and the mean values generated by the ABC system. Thus the ABC performances are the base of the comparison. A positive value means that the C-ABS or ABS generates a higher value of mean angular acceleration that represents worse performances. Subcase of analysis: running speed $\leq 100\ km/h$

	ABS $\ddot{\varphi}$	ABS $\ddot{\psi}$	C-ABS $\ddot{\varphi}$	C-ABS $\ddot{\psi}$
Beverly	17.57%	15.85%	0.55%	-1.29%
Sports Motorbike	6.61%	11.27%	23.89%	21.35%

Dividing the simulations by the running speed, $\leq 100\ km/h$ and $> 100\ km/h$ the results change drastically, especially for the Beverly300, Tables 6.6 and 6.7.

The data shows that the ABC introduces more oscillations on the vehicle at high speeds, in particular for the Beverly300. That can results in an uncomfortable feeling for the rider, during emergency maneuver and it is potentially dangerous due to the specific braking conditions under analysis (hard braking). That is clearly related to the ABC layout out for different speeds. As already specified in the model description, the current version of the active braking unit is totally matched with the $RISK$ unit only for low-medium speeds. For high speeds, the algorithm for the braking modulation is subjected to relevant limitations.

Therefore, the benefits of the complete ABC system can be observed mainly at low-medium speed, as the findings indicate.

Addressing the Sports Motorbike also at high speeds, the percentages do not show a big difference among the three systems and in general, the mean effects of the three systems on the motorcycle are similar.

The parameters described define the influence of different braking combinations on the roll and yaw movements of the vehicle. In order to address the influence on the steer control the PSD of the steer rate has been investigated. In particular the comparison among the R_{dB} (Eq.6.17) values generated by the C-ABS, ABS and ABC (again, taken as reference value) has been considered.

For the Beverly300, at high speeds, R_{dB} of the C-ABC turned out to be the best

Table 6.7: Average values of mean $\ddot{\varphi}$ and mean $\ddot{\psi}$, in case of run completed with a *Safe Braking* maneuver. The percentages refer to the ratios between mean values generated by the C-ABS and ABS and the mean values generated by the ABC system. Thus the ABC performances are the base of the comparison. A positive value means that the C-ABS or ABS generates a higher value of mean angular acceleration that represents worse performances. Subcase of analysis: running speed $> 100\ km/h$

	ABS $\ddot{\varphi}$	ABS $\ddot{\psi}$	C-ABS $\ddot{\varphi}$	C-ABS $\ddot{\psi}$
Beverly	-39.5%	-41.37%	-82.7%	-84.8%
Sports Motorbike	-12.03%	-11.92%	4.35%	0.61%

one (in terms of attenuation of disturb), -20.9 dB, then the ABS -12.6 dB. That means that at high speeds for the actual configurations of the braking algorithms the C-ABS (even the ABS) is preferable to the ABC, because the control effort is lower. Also for the Sports Motorbike the results are similar (even with ABS that is more efficient than ABC, -14 dB).

As stated before, this result was expected, in accordance with the layout out of the system. Decreasing the speed, the ABC control definitely increases his performances: for these conditions the ABC turn out to be the system less affecting the steering control (ABS Bev. +8.3 dB, ABS Spo. +0.1 dB, C-ABS Bev. +8.3 dB, C-ABS Spo. +1.6 dB).

The results of the steering rate are in accordance with the results addressing $\ddot{\varphi}$ and $\ddot{\psi}$, thus pointing out the correlation between the stability of the vehicle body and the steer stability, for this kind of braking maneuvers.

Finally, let us consider the influence of the other parameters like the tire-road friction condition or the braking intensity for low-medium speed where the algorithm demonstrated to have the best performances.

Addressing the braking force intensity, always with the *Safe Braking* maneuvers, the data shows that the ABC offers better performances than ABS and C-ABS, in particular in case of Beverly300. Neglecting the braking maneuvers involving the braking inputs of 50 N and 100 N on the brake levers, in case of panic braking close to the rider's limit braking potentials (in terms of force applicable on the levers), the Beverly300 and the Sports Motorbike lead to opposite conclusions. In case of Beverly300, the differences of yaw acceleration and roll acceleration among the systems are small, within the 3%, while for the Sport Motorbike those differences come to the 15.7% (roll acceleration, C-ABS) in favor of the ABC.

Including also the road condition as mean of comparison, it is possible to find common relations between the two vehicles and the corresponding application of the active braking system. For high adherence, both vehicles show a low influence of ABS on the body oscillations, which turned out to be the best solution in those running conditions. On the contrary, as soon as the road condition changes into wet the ABS turned out to be the worst solution: the Sports Motorbike shows that the best stability results with the ABC (e.g. mean $\ddot{\varphi}$ lower by the 47.9% than ABS

and 5.1% than C-ABS); the Beverly300 shows the best results using the C-ABS (e.g. ABC mean $\ddot{\varphi}$ lower by the 28.0% than ABS and higher by the 18.6% than C-ABS.)

Together with the latter findings, the general indications obtained by this preliminary analysis reveal how the ABC could be useful for a vehicle like the Beverly300 that is more intrinsically unstable than a standard motorcycle. The ABC results show the potentialities of the system both for the motorcycle and for the scooter, but the best results are more evident on the vehicle with "lower" handling performances.

Efficiency of the ABC system

The ABC was investigated in detail, focusing the attention on the system efficiency in one specific road scenario: braking while cornering. It is clear that the aforementioned investigation in not exhaustive for a full understanding of the potentialities of the active braking function. However, the present study gives some precious indications and it can be addressed as a preliminary step for the development of the new braking force modulation concept.

According to the data analysis, it is possible to define the effectiveness range of the current configuration of the *Active Braking Control* system. The system's good qualities are grouped in four, according to the speed and the vehicle type.

- Beverly300

The strength points of the ABC for low-medium speeds ($\leq 100\ km/h$):

- Considering high tire-road adherence conditions the system has the same performances of the ABS and C-ABS. The number of *Safe Braking* maneuvers is almost equal. The influence produced on the vehicle control is lower than the other systems, considering the steering rate and it is lower also in terms of roll oscillations compared to the C-ABS (higher that ABS).

- Considering low friction, the performances of the ABC sensibly increases, and compared to ABS and C-ABS it turned out to be the best braking system. In terms of total *Safe Braking* maneuvers the ABC guarantees up to 10% more than the other systems. The high number of safe maneuvers is also significant for the running performances of the vehicle in terms of maximum roll angle reached (thus the sharpest curve to run). For hard braking maneuvers (over 100 N on the braking levers) the ABC gives the possibility to perform the maneuvers with a maximum roll angles from $\simeq 10°$to $\simeq 20°$larger than what ABS and C-ABS can do. That aspect is peculiar of the single front braking and single rear braking. In general, in the scenarios addressed, the ABC is the best solution for rider's safety or, at least, it has the same potentialities of ABS and CBS. Moreover, it turned out to be the best system also in terms of vehicle control and influence on vehicle oscillations.

For high speeds ($> 100\ km/h$):

- Considering high road adherence conditions the system has again better performances then the ABS and C-ABS, thus guaranteeing at least 4% of *Safe Braking* maneuvers (14 cases) more. The best performances were obtained for combined braking and rear braking. In the other braking condition, the performances in terms of maximum roll angles are similar to the standard braking systems.

- Considering low friction, the performances of the ABC is comparable with the performance of C-ABS, but definitely better then ABS, in terms of *Safe Braking* maneuvers. The limitations and the weakness points will be described in the paragraph §6.5.1.

- Super Sports Motorbike
The strength points of the ABC for low-medium speeds ($\leq 100\ km/h$):

- Considering high road adherence conditions the vehicle with the ABC has slight improvements in terms of braking performances. The difference in terms of *Safe Braking* maneuvers is not big, though positive (at least 1.5% more), therefore the effectiveness of the three systems is almost the same. Addressing the oscillations, the numbers demonstrated the better potentialities of the ABC system toward the C-ABS.

- Also for the Sports Motorbike, in low friction conditions the ABC system offers the best braking modulation. In terms of vehicle control and oscillation the differences with the other systems are relevant, e.g. for the mean roll acceleration the benefits increases until 50% more than the ABS. The number of *Safe Braking* maneuvers is slightly bigger respect to ABS and C-ABS, however that positive results still guarantees from 5°to 15°of roll angle more than the other systems, in some running scenario (front and combined braking).

For high speeds ($> 100\ km/h$):

- Considering high road adherence conditions the system has better performances then the ABS and C-ABS, guaranteeing at least 6% more of *Safe Braking* maneuvers (19 cases). The best performances were obtained for combined braking. In the other braking conditions, the performances in terms of maximum roll angles are similar to ABS and C-ABS.

- Considering low friction the performances of the ABC remains better then ABS and C-ABS in terms of *Safe Braking* maneuvers. The limitations and the weakness points will be described in the paragraph §6.5.1.

It is worth noting that the ABC system is characterized by a homogeneous behavior. Hence if the vehicle is effective for specified running conditions, decreasing the complexity of the maneuver (e.g. for increasing curvature radii) the system is always effective, without inconsistencies. On the other side, in some scenario the ABS or the C-ABS turned out to be effective for some running condition but not for the following easier scenario.

Limitations and possible improvements

The general limitations of the current version of the ABC algorithm have been shown by the results reported and they are similar for the Beverly and the Super Sports Motorbike (even if they are more evident on the scooter). There is a big gap between the benefits offered by the system at low-medium speeds and at high speeds. As already reported, the continuous activation of the new braking modulation at high speeds reduces the effect of the optimal braking distribution. Since in those conditions the Active Braking function is always active, the force modulation is on also in those scenarios where the activation in not needed.

The general consequences of a less effective modulation at high speed affect mainly the vehicle oscillations and the steering control. E.g. at high speeds and high friction coefficients the ABC introduces relevant oscillations on roll acceleration and yaw acceleration, compared to the ABS and C-ABS (at least 50% more, data from Beverly300 simulations). In addition, the steering control performance decreases as well. That means that the rider should make more effort on the vehicle control, due to an extra disturbs introduced by the braking modulation.

Finally in some running condition at high speed, the standard active braking systems, in particular the C-ABS during combined braking, guaranteed a number of *Safe Braking* maneuvers with higher roll angles (up to 5°more).

6.6 Discussion

The algorithm presented for the new braking modulation gave positive results and all the information gathered from the simulation campaign revealed the potentialities of the new system.

In all the 2592 simulations, involving a Piaggio Beverly300 and a Super Sports Motorbike, the ABC system allowed a number of *Safe Braking* maneuvers higher than a simple ABS and C-ABS. Basically the positive results turned out to be confirmed in all the running scenario addressed, for different speeds, for different braking forces and distributions, for different road conditions and for different set of curves.

The simulations showed how much the system reduces the instability generated by the braking maneuvers, in case of critical conditions, that means high deceleration matched with dangerous oscillation of the vehicle body and of the steering bar. The system has been designed to be activated only in case the ABS or the C-ABS cannot provide a sufficient support to the stability of the vehicle.

The simulations showed that the ABC system, composed by an anti-lock function, a combined braking function and an active braking function (that provides the new braking forces modulation, supported by the fall detection unit), has better performances than the standard ABS and C-ABS, thus giving the system the possibility to perform a higher number of *Safe Braking* maneuvers, at higher roll angles. That strongly influences the possibility to perform emergency braking maneuvers. Accordingly, the rider is able (supported by the ABC system) to enhance his braking performances, thus controlling the vehicle in critical braking scenarios, where the ABS and C-ABS cannot intervene with positive results.

The active braking function together with the fall detection function was able to comply with the main safety tasks imposed as goals for the virtual experiments: the maximization of the deceleration and the enhancement of the vehicle stability and control.

The effectiveness of the system was addressed mainly in emergency braking conditions, characterized by intense braking, close to the tire-road friction limit. The normal decelerations were not investigated in detail, considering that for those braking conditions, the increase of the deceleration performances is demanded to the riders training [92] and not to advanced riding assistance systems.

The simulations clearly showed that for low-medium speeds, in no maneuvers the ABC turned out to have lower performances than ABS or C-ABS. At the same time, the simulations showed that the algorithm should be further improved for high-speed running. Concerning the latter condition the partial decoupling of active braking function and the $RISK$ unit badly affects the ABC performances, limiting the number of *Safe Braking* maneuvers and the vehicle control and stability. Over 100 km/h the ABC, even permitting a higher number of *Safe Braking* maneuvers, disturbs the vehicle control more than the other braking systems.

That points out the necessity to update the ABC algorithm, in order to guarantee an optimal activation of the system in every running condition without limitations. In particular, it will be necessary further evaluations on the interaction between the fall detection algorithm and the new modulation criteria.

Concluding, even if the optimization and development of the ABC requires more intensive simulation tests and analyses, the preliminary results obtained during this activity showed the potentialities of the system and they are encouraging for further developments and for the application on real vehicles.

Chapter 7

Conclusions

The aim of the present work is the definition of the criteria to design an innovative braking system able to support the rider maneuvers in case of emergency braking in different running scenarios.

To address this goal it is fundamental to have a clear view of the aspects correlated to PTW braking dynamics. The investigation of braking dynamics from different points of view gives the possibility to evaluate the influence of the manoeuver on the vehicle stability, the riders control and the deceleration performances. Accordingly, the vibration behavior of a motorcycle under hard braking was addressed for different running conditions and scenarios.

The vehicle modal analysis in case of braking shows the importance of the modes associated to the motorcycle itself, like *Wobble* and *Weave*, and the structural modes like *Chatter*. Special attention was given to the *Chatter* phenomena, related to the interaction between the transmission components and the rear frame assembly. Even if it is a mode mainly observed in super sports motorcycles, the effect of the unstable *Chatter* posed a serious issue to investigate, due to its potentiality to decrease the running performances and the stability.

In case of hard braking the instability of the *Chatter* oscillation arises as function of rear braking intensity, coupled with the presence of the engine brake. As the braking torque increases, the fluctuations induced by the transmissions components on the rear assembly (swingarm and suspensions) can reach accelerations over 10 g with a vibration frequency around 20 Hz. For some running conditions those vibrations turn into not-damped oscillations for the whole duration of the braking manoeuver. Addressing cornering brake the *Chatter* behaviors change for different running conditions, pointing out that despite the swingarm acceleration decreases for increasing roll angles, the presence of *Chatter* can excite other modes like *Weave*, thus introducing unstable critical oscillations on the vehicle.

Moreover, looking at the general stability of the vehicle during braking it is important to highlight that this vibrating mode can influence the vehicle braking performances and stability whether the road surface has irregularities or the motorcycle tire faces a sudden change of road friction condition (e.g. passing from dry to wet road surface).

It is worth noting that the vibration mode due to the transmission interaction is only a subcase of the complex general phenomenon, generally named motorcycle

Chatter. The investigation addressed only a part of the potential effects of *Chatter* on motorcycle dynamics, that it is expected to be influenced also by structural properties of the chassis and the other parts of the vehicle assembly.

Having continuous and accurate information of the PTW dynamics gives the possibility to detect critical events generated by the evolution of instable chattering or by any other unsteady phenomenon related to (hard) braking.

For the estimation of PTW braking dynamics, a simple motorcycle model has been proposed. The set of equations derived, rely on the signals coming from standard sensors for PTW application, used to estimate the highest number of parameters to monitor the evolution of the maneuvers. The most challenging aspect of dynamics monitoring is the evaluation of the vehicle speed and the real-time tire-road adherence. The methodology proposed for the speed estimation is based on the observation of the vehicle status (acceleration, braking, constant speed) and the generation of the speed value according to the front and rear wheels speeds and vehicle acceleration. The evaluation of the method by virtual simulations revealed the effectiveness of the algorithm and the best performances turned out to be under rear braking. The necessity to adopt a back-propagation strategy to derive the vehicle speed in case of combined braking or front braking reduced the performances of the estimator, anyhow guaranteeing always an absolute error, in terms of the speed evaluation, below 5%.

Those results can be considered satisfactory looking further at the application of this method for the computation of the tires longitudinal slip, to be used within the real-time estimation of the tire-road friction. The accuracy of the inputs to the friction estimator has a relevant influence on the estimation, in particular considering the theoretical implementation of the proposed algorithms inside the logic control of an active braking system. The friction estimator designed within this research activity estimates the maximum friction coefficients, during a braking manoeuver, by a non-linear regression of the real-time friction coefficients and longitudinal slips, acquired during the manoeuver. The applicability of the method has been verified by simulations, reproducing real scenarios and real vehicle functionalities (e.g. sensors noise). The estimator turned out to be effective to predict, with a good accuracy, the value of the maximum friction coefficient (in case of emergency braking leading the wheel to lock up), some time steps before the tire could reach it while decelerating. The potentialities of the methodology were demonstrated in different running scenarios: straight braking, cornering brake, dry and wet road surfaces.

The constant monitoring of the PTW dynamics gives the possibility to detect dangerous situations for the rider and motorcycle safety, also addressing the oscillation of the vehicle and the pitch dynamics, related to the braking intensity. Starting from the study of state of the art of motorcycle fall dynamics, and then using a number of simulations of different motorcycle falls, a fall detection algorithm was derived. The fall detection algorithm aims to detect every event, critical for the PTW stability and safety, which can lead, potentially, the vehicle to fall. The expected applicability of the fall detection algorithm was proved by simulations reproducing hard, but safe, braking maneuvers and hard braking maneuvers leading the PTW to fall. The algorithm derived was calibrated by virtual and experimental

data, thus optimizing the equations and reducing the possibility of false triggering of the detection process. The results of virtual simulations demonstrated the applicability of the algorithm in the situations tested. No false-positive detections were found in those simulations addressing not critical braking and all the braking maneuvers leading the PTW to fall were detected as dangerous events. Concerning the application of the fall detector on real data, the method turned out to be reliable, reporting only 2 false positive detections on 31 *potential falls* detected.

The proposed fall detection algorithm is a fundamental support to the active braking system described in the last part of the thesis, which aims to correct the PTW stability in case of hard braking maneuvers that can compromise the vehicle safety. The innovative braking system proposed, named *Active Braking Control* (ABC), provides a proper braking force modulation, supporting the action of the wheel anti-lock function and the combined braking function, when the vehicle movements become critical for the rider safety.

The ABC system poses itself as the evolution of a standard braking system implementing the functionalities of standard ABS and CBS. The system should not be considered as a brand new device, due to the strict correlation to the current braking systems, but it can be addressed as a *cornering C-ABS*. The first layout of the ABC system turned out to be in general more effective than a standard ABS and C-ABS. The additional braking force modulation function supported by the fall detection algorithm provided a number of safe braking maneuvers higher than those ones provided by the other braking systems analyzed.

Therefore, the vehicles equipped with the ABC were able to perform emergency braking on sharper curves, completing the maneuvers in safe conditions. Moreover, the system turned out to reduce the yaw, roll and steer movements and limit the effort spent by the rider to control the vehicle.

Despite the general good findings from the ABC testing on virtual scenarios, the performances of the new braking force modulation are still lacking for high speeds. Over 100 km/h the system, still providing a higher number of *Safe Braking* maneuvers, introduces additional disturbs to the vehicle control in non-critical braking maneuvers. That decreases the general positive evaluation of the braking performances offered by the new system. Accordingly, the general algorithm for the system control requires additional tests and tuning, in order to wider the effectiveness of the system over high vehicle speeds.

Further research is recommended to evaluate the applicability of the ABC in road scenarios different from those ones investigated within the activity. The ABC system has been verified only in case of emergency braking on steady cornering, notwithstanding it is fundamental to address the interaction of the new braking force modulation with unsteady and fast movements of the riders. The tests should perform other maneuvers potentially critical for the riders, such as a combination of braking and fast swerving or hard braking at curve entry, thus including a more detailed rider model. This will give the possibility to go more in detail in understanding the rider's reaction to the ABC system activation. Moreover, it will be interesting to evaluate the influence of the system in complex scenarios, e.g. in the urban traffic, where the rider's maneuvers are usually performed at slow speeds but with large steering angles and fast movements.

In addition, concerning the simulations, a more detailed PTW should be addressed, thus including the transmission system and the chassis flexibility properties, to investigate in depth the influence of the concurrent effects coming from the activation of the anti-lock function and the excitation of structural modes. The analysis of *Chatter* showed how much the combination of emergency braking and cornering can affect the vehicle stability, therefore an additional perturbation of the vehicle structure given by the ABC activation should be investigated to enhance the overall performances of the active safety system and of the vehicle in general.

Further updates and optimizations of the system will set up the basis for the implementation of the algorithms and methodologies proposed in the thesis on real powered two-wheelers. The main aspect to prove will be the applicability of the estimators of the vehicle speed and the tire-road friction conditions. The estimation errors and the delays introduced by the filtering process of real input signals will be the first issues to address, thus verifying the robustness and reliability of the estimation techniques adopted.

Finally, the farthest target to address is the evaluation of the effectiveness of the ABC system's algorithms on a real vehicle. That goal is really challenging, not due to the implementation of the model, the equations or the methods on a real PTW, but due to the definition of the test protocol. As a matter of fact, the rider safety is always the main issue to address also during experimental tests. That introduces serious problems to solve in order to set up, at the same time, safe and accurate emergency braking tests, able to provide realistic and reliable outcomes.

Bibliography

[1] G. Yannis, P. Evgenikos, P. Papantoniou, J. Broughton, C. Brandstatter, N. Candappa, M. Christoph, K. van Duijvenvoorde, and M. Vis. Basic Fact Sheet "Motorcycles and Mopeds", Deliverable D3.9 of the EC FP7 project DaCoTA. Technical Report 2010, 2010.

[2] V. Cossalter, R. Lot, and F. Maggio. On the braking behavior of motorcycles. *SAE paper 2004-32*, 18(1), 2004.

[3] D.J.N. Limebeer, R.S. Sharp, and S. Evangelou. The stability of motorcycles under acceleration and braking. *Proceedings of the Institution of Mechanical Engineers, Part C: Journal of Mechanical Engineering Science*, 215(9):1095–1109, September 2001.

[4] M. Corno, S.M. Savaresi, M. Tanelli, and L. Fabbri. On optimal motorcycle braking. *Control Engineering Practice*, 16(6):644–657, June 2008.

[5] V. Cossalter. *Motorcycle dynamics*. Lulu.com, 2006.

[6] T. Tsuchida, Y. Nishimoto, and Thiem M. Advanced brake systems for powered two wheelers: CBS, ABS and future directions. In *Proceeding of 4th International Motorcycle Conference, IFZ Institute for Motorcycle Safety*, Munich, 2002.

[7] C.K. Huang and M.C. Shih. Design of a hydraulic anti-lock braking system (ABS) for a motorcycle. *Journal of Mechanical Science and Technology*, 24(5):1141–1149, May 2010.

[8] R. Grant, R. Frampton, G. Savino, and M. Pierini. PISa – Powered two-wheeler Integrated Safety . Project objectives , achievements and remaining activities. In *Proceeding of 7th International Motorcycle Conference, IFZ Institute for Motorcycle Safety*, Cologne, 2008.

[9] G. Savino, M. Pierini, R. Grant, R. Frampton, R. Talbot, S. Peldschus, E. Schuller, A. Oudenhuijzen, J. Pauwelussen, B. Scheepers, A. Teerhuis, K. Venkata, R. Babu, B. Roessler, M. Nanetti, and R. Guggia. PISa – Powered two-wheeler Integrated Safety. Development, implementation and testing of PTW integrated safety systems. In *Proceeding of 8th International Motorcycle Conference, IFZ Institute for Motorcycle Safety*, number October, pages 1–16, Cologne, 2010.

[10] G. Savino. *Development of the Autonomous Braking for Powered Two Wheeler Application*. PhD thesis, Università degli Studi di Firenze, 2009.

[11] G. Savino, M. Pierini, and N. Baldanzini. Decision logic of an active braking system for powered two wheelers. *Proceedings of the Institution of Mechanical Engineers, Part D: Journal of Automobile Engineering*, 226(8):1026–1036, February 2012.

[12] G. Savino, A. Penumaka, M. Pierini, and N. Baldanzini. Design of the decision logic for a PTW integrated safety system. In *Proceedings of the 21st ESV conference*, Stuttgart, 2009. U. S. Department of Transportation, 1200 New Jersey Avenue SE Washington DC 20590 USA.

[13] F. Giovannini. *Studio della Manovra Evasiva d'Emergenza nello Sviluppo di un Sistema di Frenata Automatica per Veicoli a Due Ruote*. PhD thesis, Università degli Studi di Firenze, 2010.

[14] F. Giovannini, G. Savino, and M. Pierini. Influence of the minimum swerving distance on the development of powered two wheeler active braking. In *Proceedings of the 22nd International Technical Conference on the Enhanced Safety of Vehicles*, Washington D.C., 2011.

[15] F. Giovannini, G. Savino, M. Pierini, and N. Baldanzini. Analysis of the minimum swerving distance for the development of a motorcycle autonomous braking system. *Accident Analysis and Prevention*, 59C(031360):170–184, May 2013.

[16] K. Schröter, J. Bunthoff, F. Fernandes, T. Schröder, H. Winner, P. Seiniger, K. Tani, and O. Fuchs. Brake Steer Torque Optimized Corner Braking of Motorcycles. In *Proceeding of 8th International Motorcycle Conference, IFZ Institute for Motorcycle Safety*, pages 396–422, Cologne, 2010.

[17] M. Tanelli, M. Corno, and I. Boniolo. Active braking control of two-wheeled vehicles on curves. *International Journal of Vehicle Autonomous Systems*, 7(3):243–269, 2009.

[18] P. De Filippi, M. Tanelli, M. Corno, S.M. Savaresi, and L. Fabbri. Semi-Active Steering Damper Control in Two-Wheeled Vehicles. *Control Systems Technology, IEEE Transactions on*, 19(5):1003–1020, September 2011.

[19] Y. Marumo and N. Katagiri. Control effects of steer-by-wire system for motorcycles on lane-keeping performance. *Vehicle System Dynamics*, 49(8):1283–1298, August 2011.

[20] Y. Marumo and R. Nomiyama. Collision Avoidance System for Motorcycles Using Model Predictive Control. In *11th International Symposium on Advanced Vehicle Control*, Seul, 2012.

[21] M.A. Elliott, C.J. Baughan, J. Broughton, B. Chinn, G.B. Grayson, J. Knowles, L.R. Smith, and H. Simpson. *Motorcycle safety: a scoping study*, volume 581. Crowthorne, England: TRL Limited, 2003.

[22] M.A. Elliott, C.J. Baughan, and B.F. Sexton. Errors and violations in relation to motorcyclists' crash risk. *Accident Analysis & Prevention*, 39(3):491–499, 2007.

[23] K. Vavryn and M. Winkelbauer. *Bremskraftregelverhalten von Motorradfahrern.* Kuratorium fur Verkehrssicherheit, Abt. Fahrausbildung und Kfz-Technik, 1998.

[24] K. Vavryn and M. Winkelbauer. Braking performance of experienced and novice motorcycle riders - Results of a field study. In *4th International Conference on Traffic and Transport Psychology*, volume 1, Washington D.C., 2004.

[25] E.R. Teoh. Effectiveness of antilock braking systems in reducing motorcycle fatal crash rates. *Traffic injury prevention*, 12(2):169–73, April 2011.

[26] M. Rizzi, J. Strandroth, and C. Tingvall. The effectiveness of antilock brake systems on motorcycles in reducing real-life crashes and injuries. *Traffic injury prevention*, 10(5):479–87, October 2009.

[27] M. Tanelli, S.M. Savaresi, and C. Cantoni. Longitudinal Vehicle Speed Estimation for Traction and Braking Control Systems. *Computer Aided Control System Design, 2006 IEEE International Conference on Control Applications, 2006 IEEE International Symposium on Intelligent Control*, pages 2790–2795, October 2006.

[28] M. Tanelli, L. Piroddi, and S.M. Savaresi. Real-time identification of tire–road friction conditions. *IET Control Theory & Applications*, 3(7):891–906, 2009.

[29] P. De Filippi, M. Tanelli, M. Corno, and S.M. Savaresi. Enhancing active safety of two-wheeled vehicles via electronic stability control. *Proceeding of the18th IFAC World Congress Autom. Control*, pages 638–643, 2011.

[30] P. De Filippi, M. Tanelli, M. Corno, and S.M. Savaresi. Electronic Stability Control for Powered Two-Wheelers. *Control Systems Technology, IEEE Transactions on*, 2013.

[31] P. De Filippi, M. Tanelli, M. Corno, and S.M. Savaresi. Towards electronic stability control for two-wheeled vehicles: a preliminary study. In *Proceedings of the 10th ASME Dynamic Systems and Control Conference (DSCC)*, 2010.

[32] P. Seiniger and H. Winner. Potential of Active Suspension Systems for Vehicle Stabilization. In *Proceeding of 7th International Motorcycle Conference, IFZ Institute for Motorcycle Safety*, Cologne, 2008.

[33] P. Seiniger. *Erkennbarkeit und Vermeidbarkeit von ungebremsten.* PhD thesis, Technischen Universität Darmstadt, 2009.

[34] P. Seiniger, K. Schröter, and J. Gail. Perspectives for motorcycle stability control systems. *Accident Analysis and Prevention Prevention*, 44(1):74–81, January 2012.

[35] J. Gail, J. Funke, and P. Seiniger. Anti Lock Braking And Vehicle Stability Control For Motorcycles- Why Or Why Not? In *Proceedings of the 21st ESV Conference*, Stuttgart, 2009.

[36] A. Doria, R. Lot, and V. Cossalter. Optimum Suspension Design for Motorcycle Braking. *Vehicle System Dynamics*, 34(3):175–198, September 2000.

[37] C. Spelta, S.M. Savaresi, and L. Fabbri. Experimental analysis of a motorcycle semi-active rear suspension. *Control Engineering Practice*, 18(11):1239–1250, November 2010.

[38] D. Barbani. *Sicurezza nei motoveicoli: Analisi e sviluppo di sistemi di sicurezza passiva integrati su motoveicolo.* PhD thesis, Università degli Studi di Firenze, 2012.

[39] A. Sporner and T. Kramlich. Motorcycle braking and its influence on severity of injury. In *Gesamtverband d. Dt. Versicherungswirtschaft e. V., GDV, Inst. f. Fahrzeugsicherheit.*, pages 1–7. Gesamtverband d. Dt. Versicherungswirtschaft e. V., GDV, Inst. f. Fahrzeugsicherheit, 2001.

[40] A. Sporner. Most recent accident research results of the German car insurance companies association with the focus of interest on the braking of motorcycles. In *IfZ Motorcycle Conference*, 2002.

[41] G. Roll, O. Hoffmann, and J. König. Effectiveness evaluation of antilock brake systems (ABS) for motorcycles in real-world accident scenarios. In *Proceedings of the 21st International Technical Conference on the Enhanced Safety of Vehicles*, Washington D.C., 2009. U. S. Department of Transportation, 1200 New Jersey Avenue SE Washington DC 20590 USA.

[42] R. Grant, R. Frampton, M. Pierini, G. Savino, S. Peldschus, E. Schuller, V. StClair, M. Mccarthy, R. Babu, and C. Halewood. Use of In-depth Crash Studies to Identify and Prioritise the Functions of an Integrated Safety System for Motor Cycles. In *52nd AAAM Annual Conference*, pages 0–1, San Diego, CA, 2008. PISa Project.

[43] G. Savino, F. Giovannini, N. Baldanzini, M. Pierini, and M. Rizzi. Assessing the potential benefits of the motorcycle autonomous emergency braking using detailed crash reconstructions. *Traffic injury prevention*, 14 S.(August 2013):S40–9, January 2013.

[44] G. Savino, M. Pierini, M. Rizzi, and R. Frampton. Evaluation of an autonomous braking system in real-world PTW crashes. *Traffic injury prevention*, 14(5):532–43, January 2013.

[45] T. Kishi, T. Uchiyama, and S. Fujii. Relation between the weave mode in low speed range and slalom running of motorcycles. *SAE International Journal of Passenger Cars-Mechanical Systems*, 5(4):1316–1323, 2012.

[46] R.S. Sharp. A motorcycle model for stability and control analysis. *Multibody System Dynamics*, 6(2):123–142, 2001.

[47] R.S. Sharp and D.J.N. Limebeer. On steering wobble oscillations of motorcycles. *Proceedings of the Institution of Mechanical Engineers, Part C: Journal of Mechanical Engineering Science*, 218(12):1449–1456, December 2004.

[48] V. Cossalter, R. Lot, and M. Massaro. The chatter of racing motorcycles. *Vehicle System Dynamics*, 46(4):339–353, April 2008.

[49] M. Massaro, R. Lot, and V. Cossalter. On engine-to-slip modelling for motorcycle traction control design. *Proceedings of the Institution of Mechanical Engineers, Part D: Journal of Automobile Engineering*, 225(1):15–27, January 2011.

[50] M. Massaro, R. Sartori, and R. Lot. Numerical investigation of engine-to-slip dynamics for motorcycle traction control applications. *Vehicle System Dynamics*, 49(3):419–432, March 2011.

[51] V. Cossalter, R. Lot, and M. Massaro. The Significance of Powertrain Characteristics on the Chatter of Racing Motorcycles. *ASME 2012 11th Biennial Conference on Engineering Systems Design and Analysis*, 3:607–6013, 2012.

[52] R.S. Sharp and Y. Watanabe. Chatter vibrations of high-performance motorcycles. *Vehicle System Dynamics*, (April 2013):37–41, 2013.

[53] M. Massaro, V. Cossalter, R. Lot, and A. Croce. The Motorcycle Chatter. In *Bicycle and Motorcycle Dynamics 2013*, number November, pages 11–13, Narashino, 2013.

[54] S. Fujii, S. Shiozawa, A. Shinagawa, and T. Kishi. Investigation of steady-state cornering characteristics of motorcycles based on tire slip angle measurement. *SAE Technical Paper*, 2010.

[55] A.P. Teerhuis and S.T.H. Jansen. Motorcycle state estimation for lateral dynamics. *Vehicle System Dynamics*, 50(8):1261–1276, 2012.

[56] T. Kishi. Measuring Tire Forces and Moments of Motorcycles. In *Bicycle and Motorcycle Dynamics 2013*, number November, pages 11–13, 2013.

[57] S. Fujii, S. Shiozawa, and A. Shinagawa. Steering characteristics of motorcycles. *Vehicle System Dynamics*, 55(8):1277–1295, 2012.

[58] J.G. Ziegler and N.B. Nichols. Optimum Settings for Automatic Controllers. *ASME*, 64(11):759–765, 1942.

[59] L. Xu, Y. Yang, Z. Chang, and J. Liu. Dynamic modeling of a roller chain drive system considering the flexibility of input shaft. *Chinese Journal of Mechanical Engineering*, 3(23):367–374, 2010.

[60] H.B. Pacejka. *Tyre and vehicle dynamics*. Butterworth-Heinemann Ltd, 2005.

[61] M. Burckhardt. ABS und ASR, Sicherheitsreleuantes, Radschlupf-Regel System. *Lecture Scriptum, University of Braunschweig, Germany*, 1987.

[62] U. Kiencke and A. Daiß. Observation of lateral vehicle dynamics. *Control Engineering Practice*, 5(8):1145–1150, 1997.

[63] C. Canudas de Wit and P. Tsiotras. Dynamic tire friction models for vehicle traction control. In *Proceedings of the 38th IEEE Conference on Decision and Control*, volume 4, pages 3746–3751. IEEE, 1999.

[64] C. Canudas de Wit, P. Tsiotras, E. Velenis, M. Basset, and G. Gissinger. Dynamic friction models for road/tire longitudinal interaction. *Vehicle System Dynamics*, 39(3):189–226, 2003.

[65] G. Savino, F. Giovannini, N. Baldanzini, and M. Pierini. Training System for Optimal Braking on a Powered Two Wheeler. In *5th International Conference on Driver Behaviour and Training*, Paris, 2011.

[66] A. Bellati, V. Cossalter, R. Lot, and A. Ambrogi. Preliminary investigation on the dynamics of motorcycle fall behavior: influence of a simple airbag jacket system on rider safety. In *Proceeding of 6th International Motorcycle Conference, IFZ Institute for Motorcycle Safety, Cologne*, pages 9–10, Cologne, 2006.

[67] G. Savino, F. Giovannini, N. Baldanzini, and M. Pierini. Real-time estimation of road–tyre adherence for motorcycles. *Vehicle System Dynamics*, (October 2013):1–14, September 2013.

[68] R.S. Sharp. The stability and control of motorcycles. *: Journal of Mechanical Engineering Science 1959*, 13(5):316–329, October 1971.

[69] R.S. Sharp. Stability, control and steering responses of motorcycles. *Vehicle System Dynamics*, 35(4-5):291–318, March 2001.

[70] R.S. Sharp, S. Evangelou, and D.J.N. Limebeer. Advances in the modelling of motorcycle dynamics. *Multibody System Dynamics*, 12(3):251–283, October 2004.

[71] R.S. Sharp. Motorcycle steering control by road preview. *Journal of dynamic systems, measurement, and control*, 129(4):373, 2007.

[72] G. Baffet, A. Charara, and J. Stéphant. Sideslip angle, lateral tire force and road friction estimation in simulations and experiments. In *Proceedings of the 2006 IEEE International Conference on Control Applications*, pages 903–908, October 2006.

[73] G. Baffet, A. Charara, and D. Lechner. Estimation of vehicle sideslip, tire force and wheel cornering stiffness. *Control Engineering Practice*, 17(11):1255–1264, 2009.

[74] L. Haffner, M. Kozek, J. Shi, and H.P. Jorgl. Estimation of the maximum friction coefficient for a passenger vehicle using the instantaneous cornering stiffness. In *American Control Conference*, pages 4591–4596. IEEE, 2008.

[75] R. Rajamani, N. Piyabongkarn, and J. Lew. Tire-Road Friction-Coefficient Estimation. *Control Systems*, 30(4):54–69, 2010.

[76] R. Rajamani, G. Phanomchoeng, D. Piyabongkarn, and J. Y. Lew. Algorithms for Real-Time Estimation of Individual Wheel Tire-Road Friction Coefficients. *IEEE/ASME Transactions on Mechatronics*, 17(6):1183–1195, December 2012.

[77] G.A.F Seber. Nonlinear Regression. In *Hoboken, NJ: Wiley-Interscience*. 2003.

[78] S. Laporte and S. Espié. 2BeSafe project - Project final report. Technical Report 0, 2012.

[79] L. Zhao, Z. Liu, and H. Chen. Design of a Nonlinear Observer for Vehicle Velocity Estimation and Experiments. *IEEE Transactions on Control Systems Technology*, 19(3):664–672, 2011.

[80] Y. Gao, Y. Feng, and L. Xiong. Vehicle Longitudinal Velocity Estimation with Adaptive Kalman Filter. In *Proceedings of the FISITA 2012 World Automotive Congress*, pages 415–423, 2012.

[81] A. Bellati, V. Cafaggi, and V. Cossalter. Exploratory Study of the Dynamic Behaviour of Motorcycle-Rider During Incipient Fall Events. In *19th International Technical Conference on the Enhanced Safety of Vehicles Conference (ESV)*, pages 1–8, Washington D.C., 2005.

[82] V Cossalter, R Berritta, and G Cocco. Analysis of the dynamic behaviour of motorcycles in dangerous manoeuvres using the multi-body code MSC Working Model. *Proceeding of the 1999*, pages 1–10, 1999.

[83] V. Cossalter, A. Aguggiaro, D. Debus, A. Bellati, and A. Ambrogi. Real Cases Motorcycle and Rider Race Data Investigation: Fall Behavior Analysis. In *Proc. of 20th Enhanced Safety of Vehicles Conference, Innovations for Safety Oppotunities and Challenges*, pages 1–7, Lyon, 2007.

[84] A. Ambrogi, Al. Bellati, V. Cossalter, and R. Lot. Method and device for the prediction of a fall of a person from a vehicle or the like, 2010.

[85] A. Boubezoul, S. Espié, B. Larnaudie, and S. Bouaziz. A simple fall detection algorithm for powered two wheelers. *Control Engineering Practice*, 21(3):286–297, March 2013.

[86] A. Erke. Effects of electronic stability control (ESC) on accidents: a review of empirical evidence. *Accident Analysis and Prevention Prevention*, 40(1):167–173, 2008.

[87] A. Lie, C. Tingvall, M. Krafft, and A. Kullgren. The effectiveness of electronic stability control (ESC) in reducing real life crashes and injuries. *Traffic Injury Prevention*, 7(1):38–43, 2006.

[88] M. Nuessle, R. Rutz, and M. Leucht. Objective test methods to assess active safety benefits of ESP. In *20th Int. Technical Conf. on the Enhanced Safety of Vehicles (ESV)*, pages 1–8, Lyon, 2007.

[89] S. Mammar, S. Espié, and C. Honvo. Motorcycle modelling and roll motion stabilization by rider leaning and steering torque. In *Proceedings of 2005 IEEE Conference on Control Applications, 2005. CCA 2005.*, pages 1421–1426. Ieee, 2005.

[90] M. Gerard, W. Pasillas-Lépine, E. de Vries, and M. Verhaegen. Improvements to a five-phase ABS algorithm for experimental validation. *Vehicle System Dynamics*, 50(10):1585–1611, October 2012.

[91] A.L. Schwab and N. Appleman. Dynamics and Control of a Steer-by-Wire Bicycle. In *Bicycle and Motorcycle Dynamics 2013*, pages 11–13, Narashino, 2013.

[92] G. Savino, F. Giovannini, N. Baldanzini, and M. Pierini. Development of a Motorcycle Braking Trainer System. In *11th International Symposium on Advanced Vehicle Control*, Seul, 2012.

Acknowledgements

I would like to thank Professor Marco Pierini for believing in me and in my capabilities. His esteem and his continuous support have been fundamental for my work and they have given me the possibility to achieve valuable results.

I am deeply grateful to Dr. Giovanni Savino for all he has done for me. He guided my professional and personal growth by putting his trust in me. For me he is a model of professionalism, integrity and dedication to the job as well as an example of enthusiasm and passion for life.

I would like also to thank Professor Niccolò Baldanzini, his remarks, suggestions and support to my research have been very important to me, to achieve my goals.

I am grateful to Professor Sergio Matthew Savaresi, from Politecnico di Milano, for his professionalism and attention in the review of my thesis. Because of his great experience in the research area I dealt with, his analysis and his reflections added great value to my work.

My acknowledgment goes to the entire working group CISAP, to all friends and colleagues for their cooperation and their support to my activity.

I would like to thank also Eng. Hitoshi Watanabe, Kenji Seto, Shigeru Fujii, Tomoaki Kishi, all the colleagues and friends from the Research and Development department of Yamaha Motor Company and Eng. Andrea Borin from Yamaha Motor Research & Development Europe for having given me the opportunity to join their research group and work on challenging topics.

Above all, my deepest and sincere gratitude goes to my Parents Guglielmo and Grazia and to my Brother Riccardo. Without them, I might have done only a small part of the steps that I have done so far. My success is their success because they never left me without their love, not even for a moment, and their support, during these years, has been essential to me to achieve my goals. I could not wish for a family better than this.

Special thanks go to my Grandmothers. To my Grandma Maria, who loved me till the end, who greeted me with a smile. I will always keep her in my heart. To my Grandma Angela, for whom her grandchildren are always the best in the world. She never misses a chance to give me her very great love and her presence makes me full of joy every time.

I am also grateful to my Uncles, my Aunts and my Cousins, they have always been close to me. I really like to remember their Skype calls, to keep me company when I was in Japan.

Finally, special thanks go to my best friends, in particular to Luca, Matteo, Francesco, Davide, Iacopo, Roberto, Lorenzo, Matteo (Ralloz), Fabrizio, Andrea, Paolo, Giulia F., Giulia G., Giulia P., Elena, Chiara and Annachiara, for the moments and laughs together, for the *sentences of the week*, and, above all, for the great friendship they have always given me.

(Translation in Italian)

Desidero ringraziare il Professor Marco Pierini per aver creduto in me e nelle mie potenzialità. La sua stima nei miei confronti e il suo continuo sostegno sono stati imprescindibili per la mia attività e mi hanno permesso di raggiungere risultati importanti.

Sono profondamente riconoscente a Giovanni Savino per tutto quello che ha fatto per me. Ha accompagnato la mia crescita professionale e personale riponendo in me sempre una grande stima. È per me un modello di professionalità, integrità e dedizione al lavoro nonché un esempio di entusiasmo e passione per la vita.

Vorrei ringraziare anche il Professor Niccolò Baldanzini, il cui supporto al mio lavoro, i consigli e le considerazioni sulla mia ricerca sono stati fondamentali per il conseguimento dei miei obiettivi.

Ringrazio il Professor Sergio Matteo Savaresi del Politecnico di Milano per la professionalità e la cura nella revisione della mia Tesi. Data la sua grande esperienza nella materia da me trattata, la sua analisi e i suoi commenti aggiungono grande valore al mio lavoro.

I miei ringraziamenti vanno a tutto il gruppo di lavoro CISAP, a tutti gli amici e i colleghi per la loro collaborazione e per il loro supporto alla mia attività.

Vorrei ringraziare gli Ingegneri Hitoshi Watanabe, Kenji Seto, Shigeru Fujii, Tomoaki Kishi, tutti i colleghi e gli amici della sezione di Ricerca e Sviluppo di Yamaha Motor Company e l'Ingegner Andrea Borin di Yamaha Motor Research & Development Europe per avermi dato l'opportunità di unirmi al loro gruppo di ricerca e lavorare su temi stimolanti.

Il mio ringraziamento più grande va ai miei Genitori Guglielmo e Grazia e a mio Fratello Riccardo. Senza di loro forse avrei fatto solo piccolissima parte dei passi che ho fatto fino ad oggi. Il mio successo è il loro successo perché non mi hanno mai lasciato senza il loro amore, neppure per un istante, e il loro sostegno durante questi anni è stato essenziale per il raggiungimento dei miei obiettivi. Non potrei desiderare una famiglia migliore di questa.

Un enorme grazie va alle mie Nonne. A mia Nonna Maria, che mi ha amato fino all'ultimo, che mi ha salutato con un sorriso. La porterò sempre con grandissimo affetto nel mio cuore. A mia Nonna Angela, per la quale i suoi nipoti sono sempre i migliori al mondo. Non perde mai occasione per regalarmi il suo sconfinato affetto e la sua presenza mi riempie ogni volta il cuore di gioia.

Ringrazio anche i miei Zii, le mie Zie e i miei Cugini che mi sono sempre stati vicino e mi hanno sempre dimostrato il loro affetto. Ricordo con piacere le loro chiamate via Skype, per tenermi compagnia quando ero in Giappone.

Infine un grazie speciale va ai miei amici più cari, in particolare a Luca, Matteo, Francesco, Davide, Iacopo, Roberto, Lorenzo, Matteo (Ralloz), Fabrizio, Andrea, Paolo, Giulia F., Giulia G., Giulia P., Elena, Chiara e Annachiara, per i momenti e le risate insieme, per le *frasi della settimana* e soprattutto per la grande amicizia che mi hanno sempre dimostrato.

Firenze, December 2013